Université de Liège
Faculté des Sciences
Département de Physique

Study of the birth, the growth and the life of a dynamical cluster under microgravity conditions

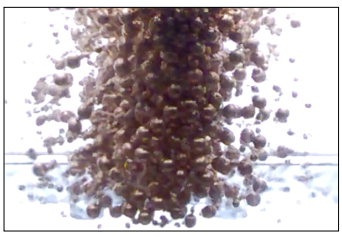
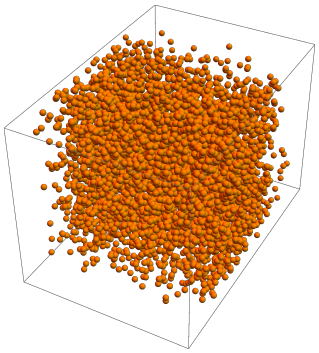
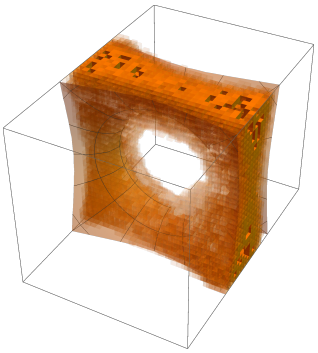

Dissertation présentée par
Martial Noirhomme
en vue de l'obtention du grade de
Docteur en Sciences

Année académique 2017-2018

Remerciements

En premier lieu, je tiens à remercier mon promoteur, Nicolas Vandewalle, qui m'a fait confiance dès 2011 lorsque j'ai commencé mon mémoire au GRASP. Merci de m'avoir ensuite engagé comme assistant malgré le flegme ardennais qui m'habite.

Merci au baron Eric vonOpsomerkraut et à François Ludewig, compagnons de bureau de mes débuts, de m'avoir encadré, encouragé, aiguillé. Ce n'aurait pas été pareil sans vous. Tant que je suis au 3.50, merci à Alexis Skatdeux pour ses développements mathématiques de haut vol. Maintenant que j'ai fini, je peux le dire, je n'ai pas toujours tout compris, et puis merci à Vincent Timelapipe et Salvapoutre Pilipili. C'était drôle.

Merci à tous les autres membres du GRASP pour l'ambiance au labo. J'ai découvert grâce à eux que de travailler dans la bonne humeur faisait partie de mes petits plaisirs. Merci à Julien-Pierre deSchockmeulatre (dit, "la Science"), à Smegmastien Bontempi (dit "le vieux daim"), au boulanger qui pétrit la farine dans son joli pétrin pour faire du bon pain, à Floriane (j'aurais pu écrire le Chinois de dos mais elle n'aime pas), à Martin, à Sofiene, à Bob, à Boris leFilou, à Maximouze, à Mr deMetzmachère, à Sébastien Mawet c'est clair, à Med et à Tamia (surtout sur Wolf), à Michel, à Chouaib. Merci à tous les autres, qui n'ont pas reçu de surnom. Et finalement, merci à l'open space du mois de mai 2018 car c'est vraiment là que les petits plaisirs se créent.

Merci à la fédération Wallonie-Bruxelles pour la bourse d'études et merci à papa d'avoir rempli les papiers pour la bourse d'études. Merci à maman et Virgoule aussi parce que si je remercie papa et pas eux, ils vont être jaloux. Merci à Violette et Bastien, qui ne comprendront pas pourquoi quand ils seront en âge de comprendre, ou alors qui comprendront un truc que je ne serai plus en âge de leur expliquer.

Merci au ministre Marcourt car si, à mon avis, son décret n'est pas terrible (c'est un euphémisme), la partie qui dit que les membre du personnel de l'ULiège ne payent pas de droits d'inscription quand ils font un doctorat m'a été bien utile. Merci aussi à la dame du service des inscriptions qui avait eu vent de cette partie du décret. Ses collègues, par contre, feraient bien de prendre exemple sur elle.

Merci aux Lyonnais, la Meuse est belle chez vous! Merci aussi aux Bordelais, c'est le Picon qui est beu chez vous, euh bu... beau! Merci aux Novespaciens, la scopolamine c'est une tuerie. Merci la France quoi!

Merci à mon étudiante biologue. Grâce à elle je suis désormais en mesure de faire la différence entre une buse variable et un milan royal, entre une vieille huitre et une jeune moule. J'ai encore beaucoup à apprendre en biologie (et elle en physique, purée ça tombe bien, c'est carrément un échange du coup, ça doit être un signe) mais merci.

Merci aux Forces Spéciales de protéger la Belgique en dehors de ses frontières (c'est une dédicace secrète adressée au colonel).

Finalement, et puis après j'arrête parce que je n'ai vraiment pas le temps, merci une seconde fois à Eric MrChoucroute, ainsi qu'à Charlotte, pour leur travail de relecture et merci au jury pour son travail de lecture.

Martial Puissance Souplesse Subtilité Délicatesse Modestie Grand-Schtroumpf Noirhomme

PS: et bonjour à ta femme!

Abstract

Granular materials can produce spectacular phenomena due to the dissipation that occurs when the grains collide. In microgravity environments, a granular material can adopt different behaviors, mainly depending on the packing fraction of the system and the intensity of the energy that is injected into the system. By regulating the packing fraction, a granular gas or a dense and slow aggregate can be observed. These aggregates are called "clusters" and their emergence has been studied both theoretically and numerically in the last decades. In addition, the parameters triggering the gas-cluster transition were highlighted during these studies. Nevertheless, these theoretical and numerical considerations have never been verified experimentally and the cluster, which always coexist with granular gases in the case of excited systems, requires still a lot of attention. That's why the SpaceGrains project has been launched by the European Space Agency (ESA). This project contributes to the study of granular phenomena in microgravity thanks to the development of the VIP-Gran-PF instrument, containing of a cell in which bronze beads can be excited by two oscillating pistons. The cell can be quasi-two or three dimensional. The instrument was developed for parabolic flights and the first part of this work has consisted in verifying experimentally the gas-cluster transition and to observe some dynamics which have been predicted by numerical simulations. These simulations constitute the second part of our work.

Perfect knowledge of the capabilities and performance of the VIP-Gran-PF instrument as well as advanced training were required before starting to use it in parabolic flights. Our experimental work began with the study of the instrument itself. Once the handling of the VIP-Gran-PF device acquired, we focused on several topics. The first concerned the experimental verification of the gas-cluster transition. This study required a large number of parabolic flight campaigns (5 to be exact) since it was necessary to explore an entire phase diagram, that was derived from numerical simulations. Granular gases and clusters, as well as an unexpected "bouncing aggregate" regime, have been observed during these campaigns. By developing an original image processing, we have been able to reconstruct the distributions of the three dimensional positions of the particles in the VIP-Gran cell on the basis of two dimensional pictures. Adapting an existing model, we also predicted the possibility of emergence of the "bouncing aggregate" regime.

In parallel with this study, we performed numerical simulations in order to determine the mechanism of birth and growth of clusters within the instrument. By sorting the grains as gaseous or clustered with a local criterion, we have discovered that the cluster was born in the corners near the lateral walls of the cell, as far as possible from the oscillating pistons. We also show that the cluster grows because the gas has to keep a critical packing fraction. Other numerical simulations allowed us to identify a specific dynamic of the cluster. By asymmetrically exciting the particles, it is possible to displace the position of the center of mass of the sys-

tem. Moreover, a natural oscillation of the cluster, linked to its size, the asymmetry and the driving frequency, has been highlighted. Finally, we were interested in the structure of clusters in the case of a mixture of two different types of particles. As a function of their difference in mass and/or in volume, we showed that different structures are observed and that a phase segregation could take place in the system.

Finally, we realized experiments in order to validate all of our numerical simulations, except for the growth of the clusters, which is impossible to observe in the current configuration of the VIP-Gran-PF instrument. We also investigated the clustering of elongated particles, the behavior of intruders in a granular gas, such granular osmosis by using a semi permeable wall and the behavior of a mobile wall placed in between both pistons. At this point, the data of these studies still has to be analyzed.

Résumé

Les matériaux granulaires peuvent produire des phénomènes spectaculaires en raison de la dissipation d'énergie qui a lieu lorsque des grains entrent en collision. Sous microgravité, un matériau granulaire peut adopter différents comportements dynamiques, principalement en fonction du remplissage du système et de l'intensité et de la manière avec laquelle l'énergie est injectée dans le système. En jouant sur ce remplissage, un gaz granulaire ou la formation d'agrégats denses et lents peuvent être observés. Ces agrégats sont appelés "clusters" et leur émergence a été étudiée aussi bien théoriquement que numériquement au cours des dernières décennies. De plus, les paramètres à faire varier pour déclencher la transition gaz-cluster ont été mis en évidence lors de ces études. Néanmoins, ces considérations théoriques et numériques n'ont jamais été vérifiées expérimentalement et la dynamique des clusters, qui coexistent toujours avec un gaz granulaire dans le cas de systèmes excités, nécessite encore beaucoup d'attention. C'est pourquoi le projet SpaceGrains a été lancé par l'Agence Spatiale Européenne (ESA). Ce projet contribue à l'étude des phénomènes granulaires en microgravité grâce au développement, pour les vols paraboliques, de l'instrument VIP-Gran-PF. Cet instrument est principalement composé d'une cellule, quasi-bidimensionnelle ou tridimensionnelle, dans laquelle des billes de bronze peuvent être excitées à l'aide de deux pistons oscillants. La première partie de ce travail a consisté à vérifier expérimentalement la transition gaz-cluster lors de campagnes de vols paraboliques et à observer certaines dynamiques prédites par des simulations numériques. Ces simulations numériques constituent la deuxième partie du présent travail.

Une connaissance parfaite des capacités et des performances de l'instrument VIP-Gran-PF ainsi qu'un entraînement poussé étaient nécessaires avant de commencer à utiliser l'instrument en vols paraboliques. Notre travail expérimental a donc commencé avec l'étude de l'instrument en lui-même. Une fois la manipulation de l'outil acquise, nous nous sommes concentrés sur plusieurs sujets. Le premier concernait la vérification expérimentale de la transition gaz-cluster. Cette étude nécessitait un grand nombre de vols paraboliques (114 pour être exact) car il était nécessaire de couvrir tout un diagramme de phase établi au préalable sur base de simulations numériques. Des gaz granulaires et des clusters, ainsi qu'un mode de "bouncing aggregate" inattendu, ont été observés au cours de ces vols. En développant un traitement d'image original, nous avons pu reconstruire les distributions tridimensionnelles des positions des particules dans la cellule VIP-Gran à partir d'images à deux dimensions. En adaptant un modèle pré-existant, nous avons également pu prédire la possibilité d'une éventuelle émergence de l'état de "bouncing aggregate".

Parallèlement à cette étude, nous avons effectué des simulations numériques afin de déterminer le mécanisme de naissance et de croissance des clusters. En triant les grains, appartenant au gaz ou au cluster, à l'aide d'un critère de compacité local, nous avons découvert que le cluster naissait systématiquement dans les coins et sur

les parois latérales de la cellule, au plus loin des pistons oscillants. Nous avons également montré que le cluster grandissait de manière à ce que le gaz conserve sa densité critique. Ce comportement rappelle la condensation d'une phase gazeuse classique une fois que la pression dépasse la pression de vapeur saturante dudit gaz. Une autre campagne de simulations numériques nous a permis d'identifier une dynamique spécifique du cluster. En excitant les particules de manière asymétrique, il a été possible de déplacer la position moyenne du centre de masse du système, que nous avons définie comme la position d'équilibre du cluster. De plus, une oscillation naturelle du cluster, liée à sa taille, à l'asymétrie et à la fréquence de l'excitation, a été mise en évidence. Enfin, nous nous sommes intéressés (encore une fois numériquement) à la structure des clusters dans le cas d'un mélange de deux types de particules différentes. En fonction de leur différence de masse et/ou de volume, nous avons montré que différentes structures étaient observées et qu'un phénomène de ségrégation de phase pouvait avoir lieu.

Enfin, nous avons réalisé des expériences afin de valider toutes nos simulations numériques, à l'exception de celles concernant la croissance des clusters. Pour cette étude, il est en effet impossible d'observer la structure d'un cluster tridimensionnel ou de prendre les mesures adéquates dans la configuration actuelle de l'instrument VIP-Gran-PF. Nous avons également étudié le clustering de particules allongées, le comportement d'intrus dans un gaz granulaire, l'osmose granulaire en utilisant un mur semi-perméable ainsi que le comportement d'une paroi mobile placée entre les deux pistons, qui est excité sur ses deux faces par deux gaz de différentes densités. À ce jour, toutes les données de ces études doivent encore être analysées.

Preamble

This work consists in a collection of articles written during my six years of assistantship, which gave me the chance to realize my PhD thesis. The manuscript begins with an introduction that summarizes the state of the art about granular materials in general and a description of the SpaceGrains project. My personal contributions to the project are listed at the end of the introduction. In the second part of the thesis, five articles, which highlight the work accomplished during the last six years, are presented. For each of them, an introduction as well as the main results are given. An offprint of he articles can be found at the end of each chapter. Finally, the conclusion and perspectives of this work are given at the end of the manuscript.

List of Publications

- *Hysteretic behavior in three-dimensional soap film rearrangements.* N. Vandewalle, M. Noirhomme, J. Schockmel, E. Mersch, G. Lumay, D. Terwagne and S. Dorbolo, Phys. Rev. E **83**, 021403 (2011).

- *How dynamical clustering triggers Maxwell's demon in microgravity.* E. Opsomer, M. Noirhomme, N. Vandewalle, and F. Ludewig, Phys. Rev. E **88**, 012202 (2013).

- *Clustering and segregation in driven granular fluids* E. Opsomer, N. Vandewalle, M. Noirhomme, and F. Ludewig, Eur. Phys. J. E **37**, 115 (2014).

- *Granular transport in driven granular gas.* M. Noirhomme, E. Opsomer, N. Vandewalle and F. Ludewig, Eur. Phys. J. E, **38** 9 (2015).

- *On the coarsening dynamics of a granular lattice gas.* E. Opsomer, M. Noirhomme, F. Ludewig and N. Vandewalle, Eur. Phys. J. E **39**, 62 (2016).

- *Segregation and pattern formation in dilute granular media under microgravity conditions.* E. Opsomer, M. Noirhomme, N. Vandewalle, S. Merminod, and E. Falcon, NPJ Microgravity **3**, 1 (2017).

- *Cluster growth in driven granular gases.* M. Noirhomme, F. Ludewig, N. Vandewalle and E. Opsomer, Phys. Rev. E **95**, 022905 (2017).

- *An instrument for studying granular media in low-gravity environment.* S. Aumaître, R. P. Behringer, A. Cazaubiel, E. Clément, J. Crassous, D. J. Durian, E. Falcon, S. Fauve, D. Fischer, A. Garcimartín, Y. Garrabos, M. Hou, X. Jia, C. Lecoutre, S. Luding, D. Maza, M. Noirhomme, E. Opsomer, F. Palencia, T. Pöschel, J. Schockmel, M. Sperl, R. Stannarius, N. Vandewalle and P. Yu, Rev. Sci. Instrum. **89**, 075103 (2018).

- *Threshold of gas-like to clustering transition in driven granular media in low-gravity environment.* M. Noirhomme, A. Cazaubiel, A. Darras, E. Falcon, D. Fischer, Y. Garrabos, C. Lecoutre, S. Merminod, E. Opsomer, F. Palencia, J. Schockmel, R. Stannarius and N. Vandewalle, EPL, **123**, 14003 (2018).

- *Thermalization of beads in a granular gas.* M. Noirhomme, A. Cazaubiel, A. Darras, E. Falcon, D. Fischer, Y. Garrabos, C. Lecoutre, E. Opsomer, F. Palencia, U. Petrone, J. Schockmel, R. Stannarius and N. Vandewalle, (2018) in preparation.

Contents

Part I

Introduction

Chapter 1

State of the art

At all times, humans have been fascinated by the usefulness of granular materials. During antiquity, Egyptians, Aztecs and Mayans built monumental stable granular piles using big stone blocs, forming that way the first pyramids. The transport of granite was realized by the workers which were able to excavate huge granules from the mountains. Later, the hourglass appeared, helping men to measure time intervals based on the flow of grains of sand. Without knowing it, the inventor of this device had taken advantage of the Janssen effect [1]. This effect permits to keep a constant pressure at the place where the grains of sand fall, giving in this way a relatively constant velocity to the flow. Even though men had already found some use for granular materials, long before Science replaces superstitions in the world, their behaviors were not necessarily understood. Indeed, "Dust Devils", these swirls of sand that appear in the desert when the sun insulates the air near the surface causing ascending spiral flows, have long been associated with evil spirits. Actually, they are an example of inoffensive granular gases [2]. Usefulness, fear or the limitless human curiosity are all reasons that have prompted the desire to better understand granular materials.

(a) (b) (c)

Figure 1.1: Common examples of the three granular states. (a) The pyramid of Kukulcán in Mexico made of huge particles. (b) Sugar pouring in my coffee cup. (c) Dust devil in Eloy, Arizona [2]

From a more economical point of view, granular materials represent no less than eighty percent of the materials used in sectors such as pharmaceutics, mining, construction and food. In addition, companies such as Deep Space Industries or Planetary Resources [3, 4] have in mind to industrialize the harvest of rare earths metals from asteroids. Above all financial and economical implications, scientific research concerning granular materials still has a lot to reveal, as you will see in the following sections.

1.1 Granular Matter

The definition of granular matter may vary from one author to another, but everyone agrees that the constituent particles must be macroscopic. The latter implies that thermal fluctuations (in other words, molecular interactions) must be negligible [5]. Size matters in this definition, as much as the interactions between particles. The size of the constituents can vary from micrometers, for powders, to up to several meters, for natural phenomena such as landslides in mountains. The macroscopic size of the grains induces energy losses by friction and/or inelastic collisions. Although other forces (magnetic, electrostatic, hydrodynamic...) can induce some interesting effects, it is actually the dissipative forces that grant their complexity to granular materials. If required, the negligible thermal agitation can be replaced by another external agitation in the granular media. However, given the dissipative nature of the interactions, this external excitation has to be maintained in order to observe a stationary state in the system. According to this external solicitation, the media can behave like a solid, a liquid, or a gas, in the classical sense of the terms. A non-exhaustive collection of solid, liquid and gaseous granular behaviors is presented below.

1.1.1 Granular solids

A granular material is abusively called "solid" if its composing particles do not move with regards to their neighborhood. In this case, the contacts between grains are permanent. Strange similarities can appear between granular and classical solids. For example, Pacheco-Vázquez *et al.* [6] have discovered a kind of metastable state in a quasi two dimensional system composed of metal grains of 3.15 mm diameter. Their setup consists of a horizontal hexagonal lattice whose size is a multiple of the diameter of the grains. In this configuration, they were able to create a hexagonal close packed monolayer. By vibrating this lattice vertically with a strong agitation (the frequency f and the amplitude A of oscillation of the lattice have been varied until 100 Hz and 0.4 mm), they observed that the crystal could remain in the solid state for a long time then abruptly sublimate into the gaseous state (see Fig. 1.2). They have been able to make an analogy with the state of classic superheating [6]. Several non intuitive properties can result from the particulate nature of the material. Among others, one can cite the capacity of a granular solid to increase its volume when submitted to an increasing external pressure (this effect is called the Reynolds dilatancy [7]). This is obviously not the case for classical solids.

One of the most remarkable property of a solid assembly composed of granular particles is the ability of the grains to deflect the vertical forces. This effect was discovered in 1895 (at a time when engineering and science were serving the same cause) by Henri Adelbert Janssen, a German engineer. Janssen's experiment, illustrated in Fig. 1.3, was conceived to measure the weight G of a granular pile contained in a silo and to report this measurement as a function of the real weight of the pile, noted W. The result of the experiment is the following: for small amounts of

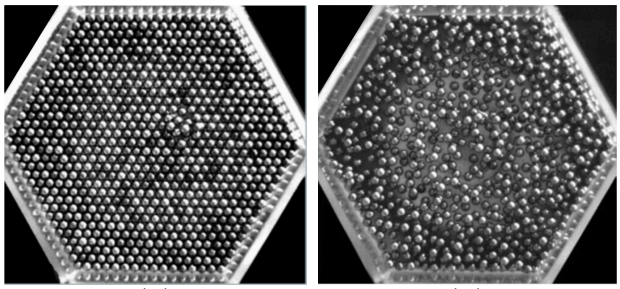

(a) (b)

Figure 1.2: From [6]. (a) Close packed monolayer of 3.15 mm diameter metal grains in a horizontal hexagonal lattice. The packing can be seen as a granular solid. (b) The same monolayer after ~ 0.5 s of vertical sinusoidal shaking. The parameters of excitation of the container are $f = 60$ Hz and $A = 0.12$ mm.

grains in the silo, G increases linearly with W and thus with the height h of the pile since $W = \rho A h$ (where ρ is the density of the granular media and A is the surface of the horizontal section of the silo). On the the other hand, having passed a critical height, G begins to saturate with increasing W (see Fig. 1.4). These observations indicate that the gravitational forces acting on each of the constituents of the pile are deflected towards the walls, where a static friction acts on the peripheral grains, helping the scale to sustain the pile.

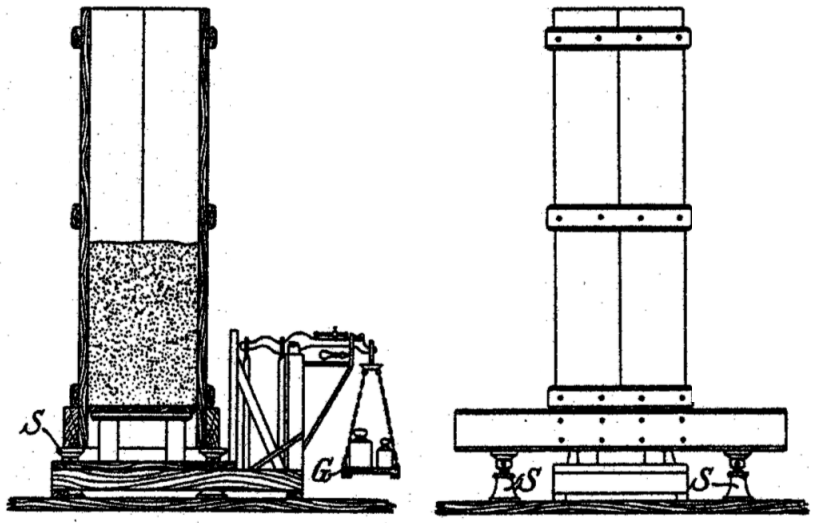

Figure 1.3: From [1]. Front and side views of the original experiment, designed by Janssen himself. A silo contains a given amount of grains placed on a scale. The horizontality of the system is adjusted thanks to four screws S. The weight of the column of grains is balanced by a counterweight G.

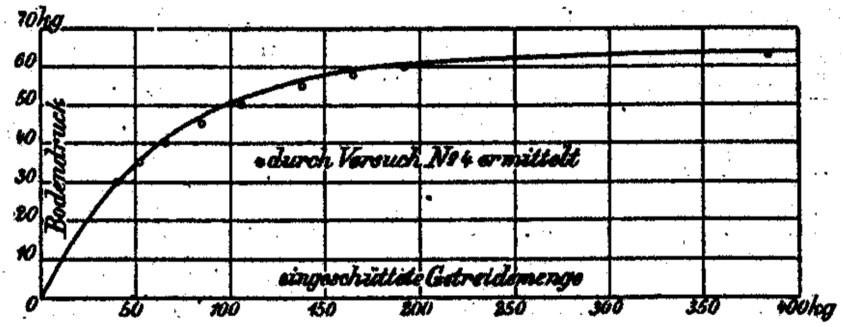

Figure 1.4: From [1]. Ground pressure (*Bodendruck*) as a function of the amount of grain poured in the silo (*eingeschüttete Getreidemenge*), expressed in kg. Past an amount of ~ 150 kg of grains in the silo, the measured mass, related to the pressure on ground, saturates at ~ 65 kg.

Mathematically, Janssen made only one hypothesis. He assumed that each vertical pressure p_v exerted in the grain pile could be deflected to the walls of the silo and generate a horizontal pressure $p_h = Kp_v$ directly proportional to p_v. Note that the constant K is *a priori* unknown and could depend on the section of the silo. This horizontal pressure, which induces a static friction along the walls of the silo, helps to carry the weight of the grain column. By expressing a balance of the forces acting on a grain slice of surface A and perimeter P, perpendicular to gravity, the equation that gives the evolution of the vertical pressure p_v in a granular medium according to the grain height h in the silo. One finds

$$p_v = \frac{\rho g A}{P K \mu_s} \left[1 - \exp\left(-K\mu_s \frac{P}{A} h\right)\right], \tag{1.1}$$

where μ_s is the static friction coefficient between the grains and the silo. The curve of Fig. 1.4 fits perfectly the measurements of Janssen. For small values of h, the well-known hydrostatic law $p_v \sim \rho g h$ is found. On the other hand, for higher values of h, the vertical pressure saturates at $p_v = \frac{\rho g A}{P K \mu_s}$. This saturation pressure value enabled Janssen, through a handmade adjustment of its measurements, to determine the constant $K \approx 0.22$ for 4 silos of different sections.

1.1.2 Granular liquids

In Janssen's experiment described above, a pile of *static* grains enclosed in a silo was studied. If the silo is opened at its base, the grains, subject to gravitational attraction, will begin to fall. Depending on the size of the opening, the flow rate will vary and arches, accompanied by density fluctuations, can be observed [8]. Despite its apparent simplicity, this particular flow is still studied nowadays [9, 10]. Many other granular flows, among which shear flow (in diverse geometries), avalanches on inclined plane, heap flows or rotating drums (see Fig. 1.5), have been studied during the previous decades [11]. If in some cases an analogy can be made with the classical flows of fluids. However, there is still not a unique theory to govern

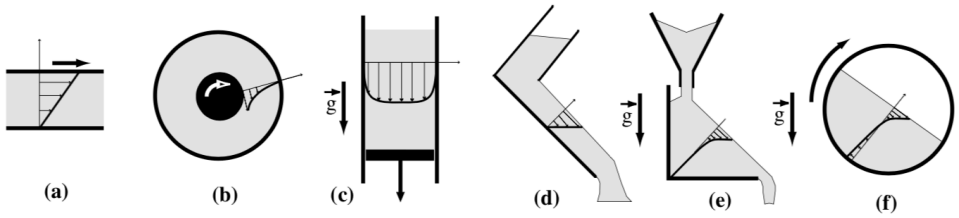

Figure 1.5: From [13]. The six most studied granular flows: (a) plane shear, (b) annular shear, (c) vertical-chute flows, (d) inclined plane, (e) heap flow, (f) rotating drum.

all the observed dynamics. The study of such flows is of great importance in earth sciences and geophysics. Many questions remain open today, some of which are of almost vital importance: the detection of geophysical flows, their understanding and the prevention of the dangers they may cause could certainly save lives, especially in tsunami-prone areas [12]. Unfortunately, laboratory experiments and related theoretical developments do not often stick with geophysical observations because of a drastic change in scale [13].

In fluid mechanics, motions can occur in the liquid through pressure exerted on it or because of the gravitational attraction to which it is subjected. Other types of movements can also be observed in the fluid if a temperature gradient is applied to it. For example, heating water can lead to the emergence of convection rolls. This effect is mainly due to the fact that raising the temperature of a fluid is accompanied by a decrease of its density. Thanks to buoyancy forces, motions of hot fluid rising in a colder liquid can arise when the fluid is heated from the bottom. However, in granular materials, a rise in temperature through one of the surfaces of the container enclosing the grains will have no visible effect on the density of the material. In order to mimic a temperature gradient in a granular medium, the system can be vibrated in order to mechanically raise the speed of a few grains (close to the vibrating wall). The experiment of vibrating a granular system has been reproduced over the past years, in different geometries and with materials of all kinds and sizes, highlighting many interesting effects such as convection or pattern formations [14–16]. Depending on the intensity of the mechanical excitation, characterized by a reduced acceleration $\Gamma = A\omega^2/g$, where A and ω are the amplitude and the pulsation of the excitation, the granular medium can form different patterns (see Fig. 1.6) and adopt a gaseous behavior, as explained in the next section.

1.1.3 Granular gases

Because of the inherent inelasticity of the grains and their relatively large size (we will consider in this work that a material is granular if its size is at least one micrometer), energy is lost during collisions, even in dilute granular systems. The most commonly known granular gas is the Dust Devil, which is composed of sand grains stirred by swirling winds. An example of Dust Devil is given in Fig. 1.1c. The dy-

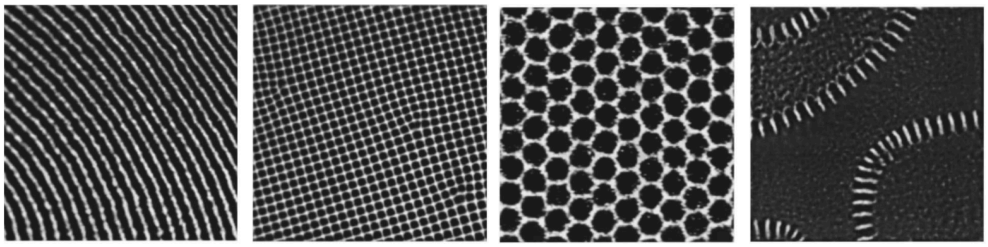

Figure 1.6: From [15]. Top view of a typical experiment of vibrating a granular system. The sinusoidal mechanical excitation is characterized by a reduced acceleration Γ. From left to right (with an increasing Γ), different patterns, reminiscent of convection rolls, are observed.

namics of granular gases composed of spherical particles has been extensively studied over the last decades. The same observation has been made for many different geometries and many different shaking: the velocity distribution in the gas does not follow the Maxwell-Boltzmann distribution but presents high velocity tails [17–29]. A general expression of this kind of distribution is given by Rouyer [22]:

$$P(v_x) = C \exp\left[-\beta \left(\frac{|v_x|}{\sigma_x}\right)^{\alpha}\right], \tag{1.2}$$

where $\sigma_x^2 = \langle v_x^2 \rangle$, $\alpha \approx 1.5$ and β and C are two fitted parameters.

One might think that the velocity distributions are different depending on the material or the shape of the particles, but this is not the case, as it was shown by a team of German researchers in 2013. Indeed, Harth *et al.* have studied a granular gas composed of dissipative rods. As they explain in [30], the elongated shape of their particles allowed them to calculate the translational as well as rotational velocities within their system. The main result of this study is that both the translational and the rotational velocity distribute according to Eq. (1.2) and are non Gaussian. Another remarkable thing to note is that the equipartition of energy is not verified in the case of such particles. However, a few months ago, Harth *et al.* were able to show through a similar experiment that equipartition is found as long as the rod gas cooled freely [31]. In addition, the decrease of the energy of the system during a cooling process follows Haff's law [32], which states that the energy of the system decreases with time as

$$E(t) = \frac{E_0}{(1 + t/\tau_H)^2}, \tag{1.3}$$

where E_0 is the initial energy of the system and τ_H is its typical relaxation time. The expression of τ_H is given in Sec. 1.2.3 as a function of the key parameters of the system.

To conclude, it should be noted that Rouyer's distribution and Haff's law seem to derive from the dissipative character of granular systems, and not from their geometry nor from the nature or the shape of the particles. The coefficient of restitution of the particles ε, which is nothing more than the velocity of the grain

after a collision divided by the velocity it had before, is thus a key parameter in the dynamics of granular media [33]. The size of the container as well as the grain density can influence the state of the system, as explained in the next section. Indeed, depending on the number of dissipative particles in a given box, one can observe either a granular gas, as presented above, or a cluster, or both of them.

1.2 Clustering

A cluster is defined as a granular bulk whose constituents are of a lower velocity than the gas surrounding it. It can be in two different regimes, a cooling regime and a dynamical regime. In one case, the energy of the system decreases over time [32] and in the other, the energy is kept constant thanks to a mechanical injection that compensates the loss during collisions. The study of these dynamical clusters represents the basis of this work.

1.2.1 From a granular gas to a cluster

If you want to keep grains in the state of gas, that is to say with a relatively large average free path and erratic motions, some restrictions have to be fulfilled. Many authors have studied the question. In 1997, Episov and Pöschel studied analytically and numerically a system consisting of a tube of length L and section d^{D-1} (where D is the number of dimensions of the system) filled with inelastic particles of diameter d. The packing fraction of the system is noted $\Phi = \eta V$, where η is the particle density of the system and $V = \pi d^3/6$ is the volume of a single spherical grain. The inelasticity of the grains is included in their restitution coefficient ε. This definition makes it possible to deduce the loss of energy in the system after each collision. This loss is equal to $1-\varepsilon^2$. Episov and Pöschel demonstrated that the state of their granular system could be kept gaseous as long as the condition $(1-\varepsilon)\left(\eta L d^{D-1}\right)^2 < 1$ is fulfilled [34]. The inversion of this equation gives a simple condition for keeping a granular system in the gaseous state in the classical sense of the term, i.e. with Gaussian distributed velocities. One finds

$$\frac{L}{d} < \frac{1}{\Phi}\frac{\pi}{6\left(1-\varepsilon\right)^{1/2}}. \tag{1.4}$$

A few years later, Aumaître *et al.* deduced another criterion similar to that of Episov and Pöschel, based on other hypotheses [35]. They theoretically and numerically studied a strongly excited system. Their study consists of a two dimensional square box of length L that is filled with disks of diameter d. The external excitation is given by a side of the square which is moving with a saw tooth motion. If the dissipation is taken into account during particles binary collisions, the interaction with the walls are purely elastic. In this case, it is possible to find classical behaviors of the kinetic theory of gases (Gaussian distributed velocities) if following Aumaître's criterion of

the form $(1-\varepsilon^2)(\eta L d^{D-1})^2 < 1$, or, for spherical grains,

$$\frac{L}{d} < \frac{1}{\Phi}\frac{\pi}{6\left(1-\varepsilon^2\right)^{1/2}}. \tag{1.5}$$

The difference between both models is small although the assumptions are different. In the first case, Episov studied a system which cools freely while in the second case, Aumaître studied an excited system that reached a stationary state. Despite this difference, as long as the quasi-elastic limit is not exceeded (i.e. as long as the condition (1.4) or (1.5) is fulfilled), the granular gas behaves almost as a classical gas. Past this limit, the gas condenses in both cases.

Finally, Opsomer *et al.* deduced in 2012 another criterion. They studied the transition from a gaseous-like state to a clustered state by varying the number of spherical grains in the VIP-Gran cell, which will be described in the next chapter. In this case, the cooling as well as the external excitation were taken into account, without however focusing on the distributions of the velocity of the grains in the system. They deduced the following frontier [36]

$$\frac{\delta}{d} < \frac{\ln\left[1+\frac{C_0}{\varepsilon(1+\varepsilon)(1-6\Phi)}\right]}{6\Phi\ln\left(1/\varepsilon\right)} \tag{1.6}$$

where V is the volume of a single grain, δ is the typical length of the system which is approximatively equal to L if the container is thin enough and C_0 is a free parameter. The mathematical development of this frontier is done in section 3.2. This theoretical frontier is of major importance for this work since a part of this thesis consisted of experimentally verifying it. The three equations (1.4), (1.5) and (1.6) predicting the transition from a gaseous to a clustered state are presented in Fig. 1.7 for a system composed of spherical grains enclosed in a box of dimensions Ll^2. The different lines correspond to two different restitution coefficients equal to 0.7 (dashed lines) and 0.9 (plain lines) and the value of the coefficient C_0 was found equal to ~ 1 with the help of numerical simulations (see Sec. 3.2.1 for more details). The different curves are interesting and even if the models come from different hypotheses, (cooling, excitation or both), the same behaviors are observed. Effectively, regardless of the model, the gas-cluster transition will always occur at lower packing fraction if the system is extended ($L/d \gg 1$). Moreover, at fixed L, the more the dissipation is important ($\varepsilon = 0.7$), the earlier the transition takes place (see the dashed curve and the solid curve for a fixed color). The quasi-elastic limit is reached more quickly if the system is more dissipative, which is in perfect agreement with the numerical observations and theoretical developments.

In summary, several models make it possible to predict whether a granular system is in a gas state or rather transits into a condensed phase, called a cluster. If the models of Episov and Aumaître have proven their robustness, Opsomer's model, developed in the framework of the SpaceGrain project (described in detail below) still has its proofs to make. At this point, an experimental check is required.

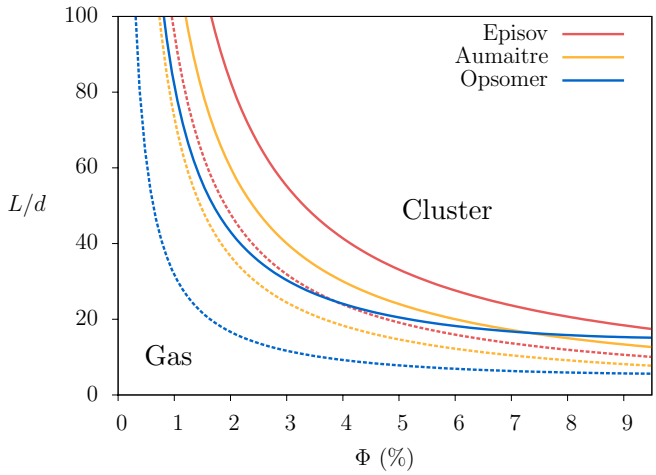

Figure 1.7: Confrontation of the models of Episov (red), Aumaître (orange) and Opsomer (blue). The curves are given by Eqs. (1.4), (1.5) and (1.6) for two different restitution coefficients $\varepsilon = 0.7$ (dashed lines) and $\varepsilon = 0.9$ (plain lines). The larger the dissipation, the earlier the transition.

1.2.2 Clustering on Earth

Clustering has been extensively studied since the late nineties. A famous experiment which allowed to highlight the clustering was conducted by Kudrolli *et al.* in 1997 [37]. They studied the gas-cluster transition in a horizontal quasi-2D system composed of N spherical stainless steel particles of 3.2 mm diameter. These particles are excited by a vibrating wall and thus able to roll on the horizontal surface. Depending on the filling of the box, they observed a granular gas or a cluster [see Fig. 1.8 (b) and (c)]. In addition, the system was designed to be able to be tilted with respect to the horizontal by an angle θ [see Fig. 1.8 (a)] Depending on this angle, the cluster is formed more or less far from the piston, as shown in Fig. 1.8 (c) and (d).

In 2013, Luu *et al.* studied clustering in a similar geometry. They also succeeded in describing the structure of the observed cluster and in deducing classical fluidic parameters such as surface tension. This is quite remarkable for a granular material. Luu's experiment, which constitutes the starting point of a part of this work, is described in more details at the beginning of Sec. 4.1.

Falcon *et al.* performed the same kind of experiment as Kudrolli in a 3D cylindrical system [38]. This time, the agitation was given vertically (which corresponds to an angle $\theta = 90°$ in Kudrolli's experiment). They observed a granular gas at low filling or a cluster at high filling. Eshuis *et al.* pushed Falcon's experiment even further by varying the dimensions of the experimental cell and its filling as well as the excitation parameters of the particles [39]. They were able to deduce a complete phase diagram showing all the observed regimes. The granular gas was part of it, as

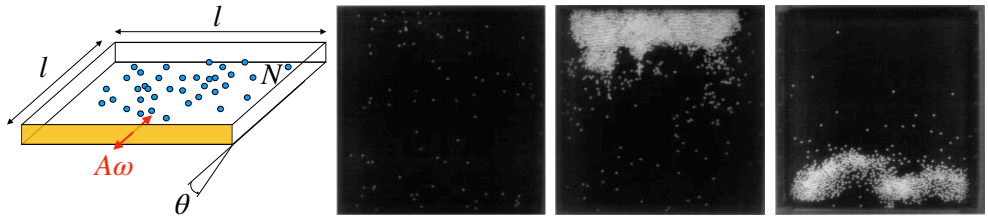

Figure 1.8: (a) Sketch of Kudrolli's experiment. N particles of 3.2 mm diameter are enclosed in a quasi-2D square box of dimensions 30 × 30 mm^2. The particles are driven by a vibrating wall. The parameters of excitation are the amplitude A and the pulsation ω. The whole system can be tilted from an angle θ. (b), (c) and (d) Observation of a granular gas, a cluster far from the piston for $\theta = 0°$ and a cluster near the piston for $\theta = 0.22°$. Images (b), (c) and (d) are taken from [37].

well as the cluster. Once the clustering appeared, they identified 4 different states according to the filling and the excitation of the system: "Bouncing bed" where all the particles adopt a collective vertical motion, "Undulations" where the grains form a pattern similar to a stationary wave on the surface of the vibrating plate, "Leidenfrost" where an excited cluster is kept away from the excitation by gaseous grains and "Convection" where the particles have a rotational motion in the vertical plane (see Figure Fig; 1.9). These observations show once again the complexity of a granular system when clustering takes place. Eshuis' experiments were numerically reproduced and confirmed by Rivas et al. [40].

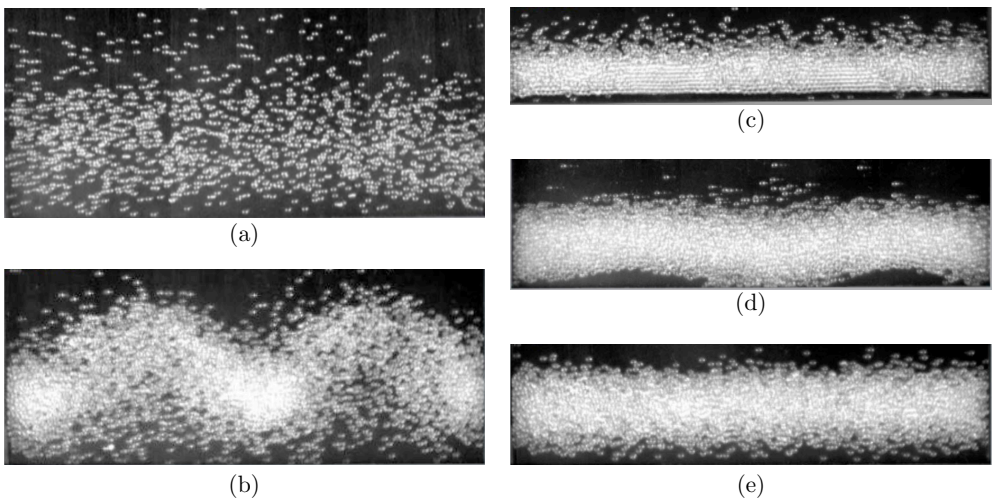

Figure 1.9: From [39]. Five granular states observed when a granular material is shaken. Depending on the filling and the excitation of the system, a granular gas is observed (a), or a cluster emerges and many different states can result: "Convection" (b), "Bouncing bed" (c), "Undulations" (d) and "Leidenfrost" (e).

1.2.3 Clustering in microgravity

As Eshuis' experiment shows, different dynamics are observed, principally depending on the intensity of the excitation provided to the system. This excitation is actually always in competition with the gravitational acceleration, which thus plays a crucial role in the clustering process. What happens if gravity is removed? Theoretical developments and numerical simulations have shown that the dissipative character of granular materials can lead to a gas-cluster transition (see Sec. 1.2.1). Experimentally, this transition has been observed, both when the system is excited and when it is allowed to cool. The clusters are similar in the case of an excited system and in the case of cooling. Effectively, both consist in a dissipative bulk where the kinetic energy is lost but from the point of view of the entire system, there is a fundamental difference. In the case of dynamical clusters, the total energy of the system is kept constant by the external agitation while not in the case of cooling clusters. Moreover, phase coexistence is observed in the system, i.e. a dynamical cluster is always surrounded by an excited granular gas. Anyway, both dynamical and cooling clusters are due to dissipative collisions and are observable, as shown in the following.

The question of the cooling of a granular gas motivated a lot of research and a lot of results were obtained, predicting the emergence of the cooling cluster [33, 41–43]. A successful experiment that allowed the observation of a cooling cluster in microgravity was conducted by Maaß *et al.* in 2008 [44]. Their system is composed of diamagnetic grains subjected to a force, provided by a suitable magnetic field, that counterbalances their weight. The levitating grains are then agitated by external excitation and a granular gas is observed (see Fig. 1.10, left). After stopping the agitation, the particles collide, loose kinetic energy and finally form a cluster by cooling (see Fig. 1.10, right). Maaß *et al.* not only observed the cooling, but also described the decrease of the mean velocity in the system by expressing Haff's law [32]. They found

$$\langle v(t) \rangle = \frac{v_0}{1 + t/\tau_H}, \tag{1.7}$$

where v_0 is the typical velocity of a grain and τ_H is given by

$$\tau_H = \frac{2}{v_0(1-\varepsilon^2)\eta\sigma}. \tag{1.8}$$

In this last equation, ε, η and σ are respectively the restitution coefficient of the particles, the number density of the system and the cross section of a particle. The Haff time τ_H gives the system relaxation time scale. Note that this model is only valid for dissipative particles since it diverges for $\varepsilon \to 1$. Moreover, the value of τ_H is smaller if η and σ are large. This implies that the system will cool rapidly if it is dense and if the particles are large.

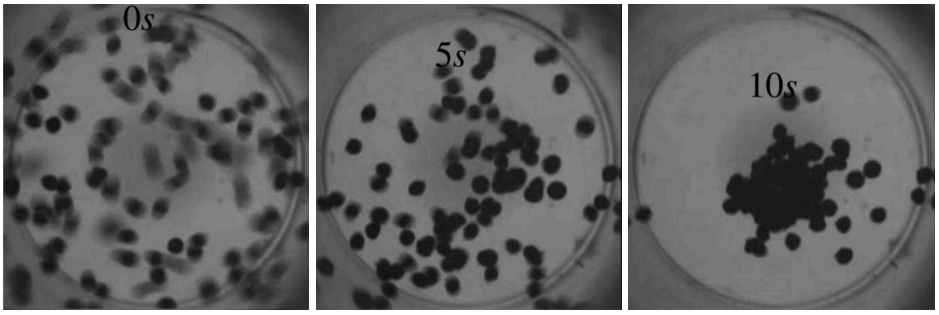

Figure 1.10: From [44]. Three snapshots of the Maaß experiment. After stopping the external agitation ($t = 0$ s, left image), the average energy decreases in the system due to dissipation during the collisions and the grains gather by cooling to form a cluster ($t = 10$ s, right image).

In continuity of his own work conducted on Earth, Falcon *et al.* realized their dynamical clustering experiment (described in the previous section) in microgravity [45]. In this experiment, they replaced the cylindrical container by three cubic cells filled with three different numbers of particles. The whole system, composed by these three boxes, can be externally excited and was launched in a sounding rocket. Falcon *et al.* observed two different regimes in the system: a granular gas or a dynamical cluster surrounded by gaseous particles. Just like on Earth, the experiment showed the appearance of a dynamical cluster for a sufficient filling of the cell. This experiment, which had never been done before, showed that dissipation is the key parameter of clustering, even when gravitational acceleration is suppressed and even the system is continuously externally excited. This experiment is also the basis of a part of this work and is more detailed at the beginning of Chap. 3.

In summary, this brief state of the art shows that the dissipation and the packing fraction of the considered granular system play a key role in the clustering process. If a lot of experiments have been performed on Earth, there is a clear lack of experimental research in microgravity, due to the difficulty and the cost to reproduce the required conditions. The SpaceGrains project tries to fill this lack of experiments, as we explain in the following chapter.

Chapter 2

The SpaceGrains project

Launched in the late nineties, the SpaceGrains project (SG) is an international project that brings together 24 researchers from 7 different countries. It is supervised and funded by the European Space Agency (ESA). The scientific goal of the project is to study the dynamics and statistical behavior of granular materials that are not subject to any gravitational field. The collective motions of dissipative grains and the phenomena that can appear due to this dissipation are indeed still poorly understood. Given the wide variety of involved studies, the project was divided into 4 Work Packages (WP). The thematics and the aim of each of them are described in Sec. 2.2. A first prototype of the VIP-Gran-PF (for Vibration Induced Phenoma in Granular materials in Parabolic Flights) instrument has been developed. This instrument as well as both cells used during this thesis are described in Sec. 2.1 and the parabolic flight technique is exposed in Sec. 2.3. Unfortunately, although the microgravity levels achieved in such flights are quite good during a relatively long time ($\sim$ 22 s), some objectives require a much better microgravity and an observation time much larger. ESA has therefore decided to develop a new instrument adapted to the International Space Station (ISS). This instrument is currently under development.

2.1 The VIP-Gran-PF instrument

The main part of the VIP-Gran-PF instrument is composed of an experimental cell enclosing N dissipative particles. The driving mechanism that injects mechanical energy into the cell consists in two motors whose role is to move two facing walls of the cell. The pistons and the motors are linked by two magnetic joints so that an experimental cell can be exchanged with another one. The motions of each piston, which enable the injection of energy in the cell, can be totally independent of each other. The key parameters of the experiment are the distance between the pistons at rest L, the amplitudes A_1, A_2 and the frequencies f_1, f_2 of piston oscillations and the number of particles N in the system. If the first parameters can be easily changed, the variation of the number of particles in the container requires an additional tool. For this purpose, a bead feeder has been developed and added to the system. This device consists of 8 slots that can be filled with at most 1000 grains of 1 mm diameter. Each slot can be emptied into the cell using an injection piston. The engineering, design, development and construction of the instruments and project-related cells were entrusted to DTM Technologies™ (Modena, Italy). The recorded data consist in uncolored pictures of the cell taken by two high speed cameras. Pictures are

taken from the bottom and from the front of the system with the help of mirrors. Two accelerometers as well as an impact sensor have been added to the pistons in order to check their real motions. Currently, only two experimental cells (over the six proposed) have been developed. The dimensions and the functionality of these two containers are described in Secs. 2.1.2 and 2.1.1.

2.1.1 The 3D cell

The 3D cell is composed by a container of width and depth $l = 30$ mm. The length L of the container is controlled by the position of the two pistons and cannot exceed the maximal value of 50 mm (see Fig. 2.1). This container is dedicated to WP 1, WP 3, WP 4(a) and 4(c).

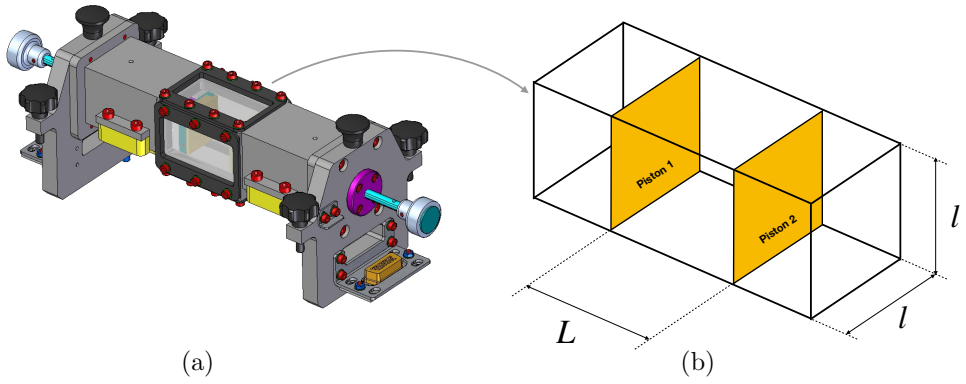

Figure 2.1: (a) 3D view of the entire 3D cell (with the authorization of DTM Technologies™). The magnets connecting the pistons to motors are again colored in green. (b) Sketch of the 3D cell. The dimensions of the width and depth are $l = 30$ mm and the length between the square vibrating pistons L is once again the tunable parameter.

2.1.2 The quasi-2D cell

Given the acquisition process of the data (the cameras take pictures of the shadow created by the particles), it is very difficult to track grains in three dimensions. For this reason, the VIP-Gran Topical Team decided to develop a quasi-2D cell, that allows to realize experiments (for example the one concerning the segregation) in which the particles have to be discriminated. The quasi-2D cell has been designed in the same way as the 3D cell, the only difference between both being the thickness. Effectively, the dimensions of the quasi-2D cell are $l \times h \times L$, where the width $l = 30$ mm and depth $h = 5$ mm are fixed and L is tunable (see Fig. 2.2). The main thematics addressed by this unit concern WP 3 and WP 4(b).

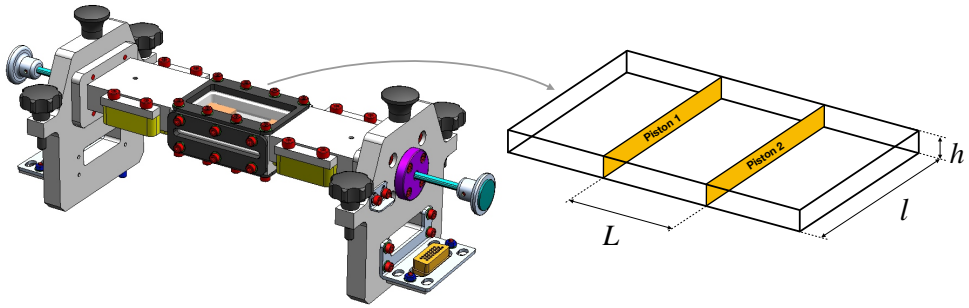

(a) (b)

Figure 2.2: (a) 3D view of the entire 2D cell (with the authorization of DTM Technologies™). The pistons are magnetically connected to the motors via the magnets colored in green. (b) Sketch of the 2D cell. The dimensions are $h = 5$ mm and $l = 30$ mm. The length between the vibrating pistons L is tunable.

The descriptions of the VIP-Gran-PF instrument are detailed in the article presented at the end of this chapter. Moreover, limitations and performances are given. In the next sections, the objectives of the SpaceGrains project, the various parabolic flight campaigns, and their related thematics are presented.

2.2 Objectives of the project

The thematics of the SG project are classified into 4 Work Packages described as follows:

1. Granular gas and liquid-gas transition.
   This work package is dedicated to the study of the phase transition in diluted granular media. In this kind of dissipative systems, the collisions between particles reduce the total energy of the system. A stationary state can however be maintained by continuously injecting mechanical energy into the system. For a low collision rate, the grains adopt a quasi-elastic behavior and a granular gas is created [35]. By increasing the collision rate (for example, by increasing the packing fraction) in the system, clustering can emerge. Our goal is to find and verify experimentally the gas-cluster phase transition conditions mentioned above and discussed in Sec. 1.2.1. This study was performed in the 3D cell, which is described in Sec. 2.1.1.

2. Dense systems.
   This WP covers two topics: the study of the compaction of granular assemblies and the response of a dense granular material to sonic pulses. To study these behaviors, a birefringent material is immersed in a liquid of the same refractive index and placed in a "wet" cell designed for this purpose. Unfortunately, it has not been tested yet.

3. Convection and transport.

   (a) Convection:
   The emergence of convection in a granular medium subjected to the Earth's gravitational field is directly related to the value of the gravitational acceleration. The latter creates a pressure gradient in the system which can be balanced by an external excitation [46]. If the gravity is removed, it is not known if convection can emerge. WP3 is devoted to study the possibility of creating convective flows in microgravity. To do this, the 2D and 3D cells are used and the necessary pressure gradient is mimicked by a difference in the excitation given by both vibrating pistons.

   (b) Granular transport:
   On Earth, Kudrolli *et al* have studied the possibility of creating a cluster and moving it through a simple 2D experiment. It involves placing a given number of spheres in a 2D box, which can be inclined relative to the horizontal, and one of the walls (the lowest) vibrates, thereby providing mechanical agitation to the system. It has been shown that the position of the cluster can be chosen by tilting the surface [37]. The position of the cluster is controlled by the competition between the mechanical excitation and the relative gravitational acceleration which is tuned by the orientation of the system. In the same way, we want to study in this work package if it is possible to move a cluster in microgravity by giving an asymmetric excitation to the system.

4. Maxwell's demon, segregation and aspherical particles.

   (a) Maxwell's demon:
   Originally, Maxwell's thought experiment consists of a demon that would be able to sort out particles of a gas without spending any energy. This experiment obviously violates the second law of thermodynamics since entropy is diminished. Since 1951, one has been able to find various approaches to elucidate the mystery [47, 48]. The use of a granular material, however, allows the creation on a macroscopic scale of such an experiment [49]. In this experiment, a container is divided into two compartments which communicate with each other through an aperture. The whole system is vertically vibrated and the trapping of the particles can be achieved by putting gravitational attraction in competition with external excitation. Depending on the intensity of the excitation, one observes a granular gas or a cluster located in a single compartment, the other being empty. In this part of WP4, we try to see if Maxwell's demon experiment is reproducible in microgravity. We tested this possibility numerically [50]. The experimental realization of Maxwell's demon using

the VIP-Gran-PF facility requires the development of a 3D cell add-on. It should be designed in the future.

(b) Segregation:
Segregation in a granular media composed of two different species is directly related to the shaking of the container, the friction between the walls and the grains and the acceleration of gravity [51]. In microgravity, the occurence of segregation as well as the parameters controlling the phenomenon are not known. In this part of WP4, we try to establish these parameters. Once again, we performed numerical simulations before conducting the experiment in parabolic flight. The numerical and experimental results have been published [52, 53] (see Sec. 5.4) recently.

(c) Non-spherical particles:
As explained in Sec. 3.2.1, the emergence of clustering in a granular medium is related to the collision rate between particles. This section of WP4 looks into the possibility of modifying the clustering conditions by changing the shape of the particles, thus varying the collision rate while maintaining a constant volume fraction in the system.

2.3 Parabolic Flight Campaigns

The parabolic flight is the only technique (except if the experiment is realized aboard the ISS) which allows to have a total control of the experiment. Researchers are actually constantly beside their equipment during the flight. Moreover, the parabolic flight technique allows to obtain relatively good microgravity conditions during a relatively long time. Indeed, the residual accelerations in the plane (called g-jitters) are of the order of $0.05g$. See Fig. 2.3 for a typical example of the achieved microgravity performance. In this figure, the measurements taken by the accelerometers onboard the aircraft are plotted against time. Other techniques provide a better level of microgravity. For instance, the g-jitters are of the order of $10^{-5}g$ when drop tower or sounding rocket are used [54] but in these cases, the onboard experiment has to be fully automated. As a consequence, the technique of parabolic flight was the most suitable for testing the instrument.

Obtaining microgravity is done by canceling all forces that apply to the Airbus A310 aircraft, with the sole exception of its own weight. For this purpose, the pilots have the difficult task of canceling the lift, the drag and the thrust of the engines acting on the plane. This can be done by following a parabolic trajectory, varying the altitude of the aircraft from 6 km to more or less 8.5 km. At this altitude, the length of the trajectory is more or less 8 km and the plane flies with a speed of approximately 350 km/h. The duration of micro-gravity aboard the aircraft can thus reach 22s. The only inconvenience for passengers is that in order to enter and exit the zero gravity phase, it is necessary to pitch the aircraft up to almost 45 degrees from the horizontal. The result for all occupants of the aircraft is an acceleration of $1.8g$, which is more or less the feeling of astronauts leaving for a

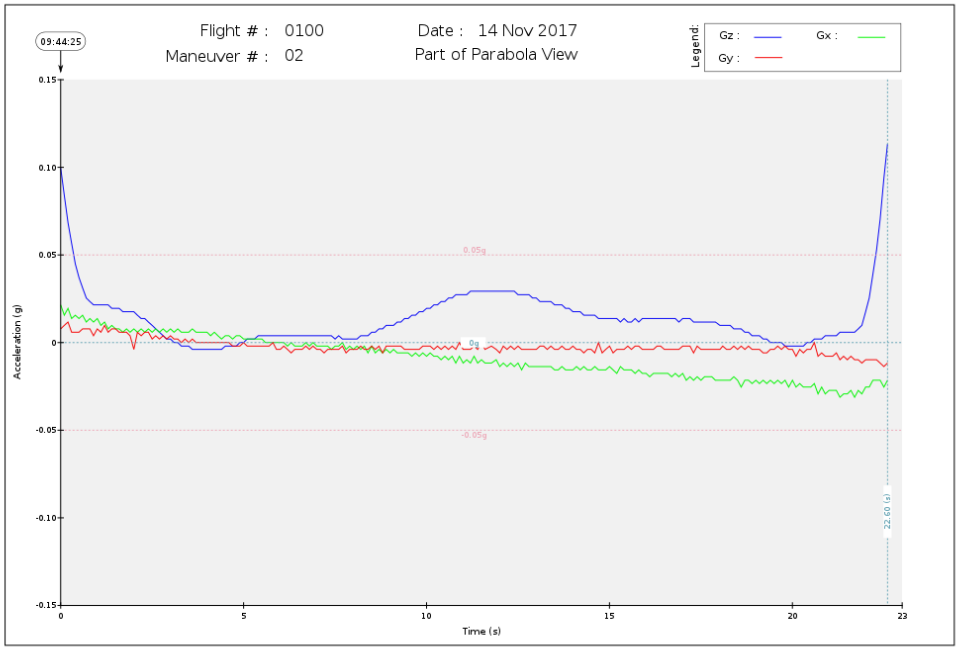

Figure 2.3: (With the authorization of Novespace) Typical values of the residual acceleration (called g-jitters) aboard the aircraft, projected on the three axes x, y and z. The g-jitters never exceed $0.05g$ during a parabola.

PFC / Thematic	63 2015	64 2016	65 2016	66 2017	67 2017	69 2018	Cell(s)
Technical tests ✔	×						2D/3D
Clustering ✔	×	×	×	×	×		3D
Cooling ✘		×					3D
Segregation ✔		×	×				2D
Convection ✘		×	×				2D/3D
Intruders ◷				×		×	2D
Rods ◷				×			3D
Mobile wall ◷					×		3D + wall
Osmosis ◷					×		3D + wall

Table 2.1: Summary of the thematics addressed during PFCs # 63 to 67. Some experiments led or will lead to publications (✔), others not (✘) because of strong g-jitters. The data concerning the four latter thematics has still to be analyzed (◷).

space mission. To compensate for these abrupt changes of gravity, each passenger can receive an injection of scopolamine, a powerful anti-vomitive. See Fig. 2.4 [55] for an example of parabolic trajectory.

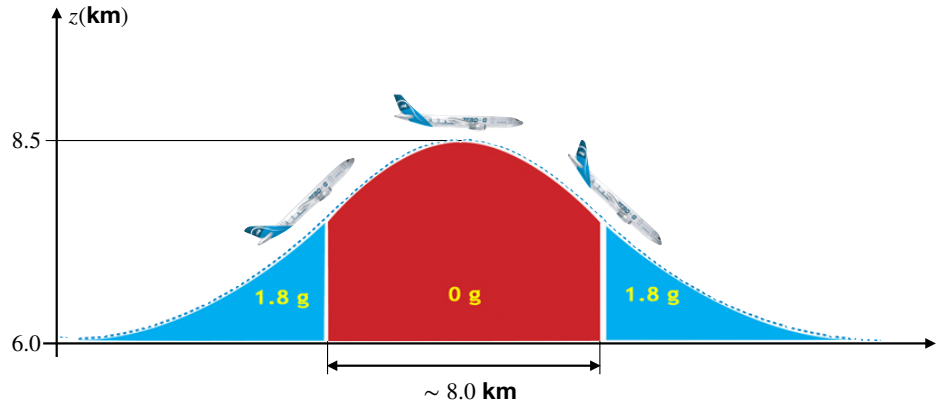

Figure 2.4: From [55]. Sketch of a typical trajectory of the airplane during a parabolic flight manoeuvre. The acceleration felt before and after the microgravity phase is worth 1.8 times the Earth's gravitational acceleration.

2.4 Summary

In this chapter, we detail the SpaceGrains project and the VIP-Gran-PF instrument for the study of granular materials in microgravity. The various thematics explored by the instrument were discussed and an overview of the obtained, processed and published results is given (the details of these results are given in the next chapters). The results concerning the observation of cooling and convection are not convincing enough. The level of microgravity reached during the PFCs is unfortunately not

sufficient. Nevertheless, these thematics will be the subject of future studies aboard the International Space Station. All performances and technical details of the VIP-Gran-PF instrument have been published in "Rev. Sci. Instrum.". The paper is given here after.

2.5 Personal contributions

The brief state of the art outlined above demonstrates the richness and diversity of observed behaviors in excited granular systems subject to gravitational attraction when clustering emerged. However, clustering in microgravity is still quite poorly understood. Although many numerical simulations have already been done, microgravity experiments are expensive and difficult to perform. The main objective of this work is to study clustering and the phenomena that can result from it. Our work is directly related to the work of Opsomer [36] and is divided into two main parts consisting of an experimental and a numerical one. The numerical part was used to prepare the experiments.

During the parabolic flight campaigns, we focused on several topics (listed in Tab. 2.1). The first objective was to experimentally verify the existence of the gas-cluster transition and to validate the Opsomer's model presented above (WP1). This experimental work led to scientific results published in *EPL*.

In a second step, we studied the segregation and the structure of clusters within mixtures of several species (WP4), both experimentally and numerically. This work led to further publications in *Eur. Phys. J. E* and *NPJ Microgravity*.

Experiments of cooling and convection (WP3) have also been performed. However, the obtained results were altered too much by the g-jitters. Longer campaigns will be launched aboard the ISS in the future.

Concerning the experiment of the intruders, the data have been partially processed and a brief example of what was observed was published in *Rev. Sci. Instrum.* with the description of the VIP-Gran-PF instrument. This study, which involves a mixture of two types of particles of different sizes, will lead to a publication in a near future.

We also collected a lot of data about the clustering of non-spherical particles (WP4) and about the possibility of creating granular osmosis. For this purpose, we 3D-printed in a semi-permeable wall (i. e., letting only small particles pass through) adapted to the 3D VIP-Gran-PF cell. This last theme was not planned at the start of the project and the data are also still to be treated.

Finally, we tested numerically (under perfect microgravity) the asymmetric excitation in the 3D cell. Once again, nothing could be concluded concerning a possible convective flow. Nevertheless, we obtained convincing results concerning the dynamics of the cluster and a possible granular transport, which have been published in *Eur. Phys. J. E*.

REVIEW OF SCIENTIFIC INSTRUMENTS **89**, 075103 (2018)

An instrument for studying granular media in low-gravity environment

S. Aumaître,[1,2] R. P. Behringer,[3] A. Cazaubiel,[4] E. Clément,[5] J. Crassous,[6] D. J. Durian,[7] E. Falcon,[4,a)] S. Fauve,[8] D. Fischer,[9] A. Garcimartín,[10] Y. Garrabos,[11] M. Hou,[12] X. Jia,[13] C. Lecoutre,[11] S. Luding,[14] D. Maza,[10] M. Noirhomme,[15] E. Opsomer,[15,b)] F. Palencia,[11] T. Pöschel,[16] J. Schockmel,[15] M. Sperl,[17] R. Stannarius,[9] N. Vandewalle,[15,c)] and P. Yu[14]
[1]*SPEC, DSM, CEA-Saclay, CNRS URA 2464, F-91191 Gif-sur-Yvette, France*
[2]*Laboratoire de Physique, ENS Lyon, UMR-CNRS 5672, F-69007 Lyon, France*
[3]*Department of Physics, Duke University, Durham, North Carolina 27708-0305, USA*
[4]*Université Paris Diderot, SPC, MSC, UMR 7057 CNRS, F-75013 Paris, France*
[5]*PMMH, ESPCI, UMR 7636 CNRS, F-75005 Paris, France*
[6]*Université Rennes 1, IPR, UMR 6251 CNRS, F-35042 Rennes, France*
[7]*University of Pennsylvania, Philadelphia, Pennsylvania 19104-6396, USA*
[8]*École Normale Supérieure, LPS, CNRS, UMR 8550, F-75005 Paris, France*
[9]*IEP, Otto von Guericke Universität, D-39106 Magdeburg, Germany*
[10]*DFMA, Universidad de Navarra, E-31080 Pamplona, Spain*
[11]*CNRS, ICMCB, Université de Bordeaux, UMR 5026, F-33600 Pessac, France*
[12]*Institute of Physics, Chinese Academy of Sciences, Beijing 100190, China*
[13]*Institut Langevin, ESPCI Paris, PSL, CNRS, F-75005 Paris, France*
[14]*MSM, University of Twente, 7500 AE Enschede, The Netherlands*
[15]*GRASP, Institute of Physics B5a, University of Liège, B-4000 Liège, Belgium*
[16]*Friedrich-Alexander Universität, IMS, D-91052 Erlangen, Germany*
[17]*Institut für Materialphysik im Weltraum, DLR, D-51170 Köln, Germany*

(Received 9 April 2018; accepted 12 June 2018; published online 5 July 2018)

A new experimental facility has been designed and constructed to study driven granular media in a low-gravity environment. This versatile instrument, fully automatized, with a modular design based on several interchangeable experimental cells, allows us to investigate research topics ranging from dilute to dense regimes of granular media such as granular gas, segregation, convection, sound propagation, jamming, and rheology—all without the disturbance by gravitational stresses active on Earth. Here, we present the main parameters, protocols, and performance characteristics of the instrument. The current scientific objectives are then briefly described and, as a proof of concept, some first selected results obtained in low gravity during parabolic flight campaigns are presented. *Published by AIP Publishing.* https://doi.org/10.1063/1.5034061

I. INTRODUCTION

Granular systems belong to a particular class of materials since grains may exhibit solid, fluid, or gaseous behaviors. Although nearly 80% of the products used in industry are powders and grains, many fundamental questions concerning their rheology and their dynamics are still unsolved.[1] Space exploration (such as regolith on asteroid surfaces, powder propellants of rockets, or planetary rings dynamics) and space exploitation (such as asteroid mining) will also face major challenges concerning the handling of granular materials in low-gravity environments.[2–4] For example, nobody knows how to perform a simple operation like sieving in space, whereas several month efforts failed to free NASA's Mars Exploration Rover Spirit from a Martian sand trap in 2010. Therefore, it is of primary interest to better understand the flow and the dynamics of granular media in low-gravity conditions.

On Earth, when granular matter is subjected to vibrations, liquid-like behavior occurs such as convective flow[5] or surface waves.[6] For strong enough forcing, gas-like behavior, with particular modes of momentum and energy transport,[7] arises where particles move erratically in response to the vibrations and the dissipative nature of collisions. When the density of particles increases within such a granular gas, the formation of a dense cluster of particles is observed due to inelastic collisions.[8–10] This cluster formation constitutes one of the most astonishing properties of granular matter under vibrations. When the forcing is stopped, numerical simulations have shown the formation of density gradients during the cooling (instability of the homogeneous cooling state)[11] as well as inelastic collapse (particles undergoing an infinite number of collisions in finite time).[12] However, several phenomena occurring on Earth (such as sedimentation, convection, and confinement pressure due to the weight of grains) disappear in low gravity, thus leading to strongly different behavior for granular matter.

Generally, ground based experiments are perturbed by anisotropy induced by gravity and by the friction force which acts on all the particles and which is far from being negligible. A low-gravity environment is, thus, needed for dilute regimes of vibrated granular medium because it is the only way to achieve an experimental situation in which inelastic collisions are the only interaction mechanism. First,

a)Electronic mail: eric.falcon@univ-paris-diderot.fr
b)Electronic mail: eric.opsomer@uliege.be
c)Electronic mail: nvandewalle@uliege.be

experiments investigating the dynamics of these granular gases were conducted in the late nineties on a MiniTexus sounding rocket.[9] More recently, gases of rod-shaped particles have been studied on a REXUS flight[13] and in the ZARM Drop Tower in Bremen.[14] For dense regimes, a low-gravity environment is also needed to better understand the rheology,[15] sound propagation,[16] and jamming transition[17] of dense granular media without confinement pressure of grains due to their own weight.

In order to address fundamental questions and potential applications regarding grains in a low-gravity environment, in 2011, the European Space Agency (ESA) created a Topical Team[18] on the subject. Its objective is to perform unique measurements on granular gas, convection, segregation, sound propagation, and jamming in granular materials subjected to vibrations without the symmetry breaking influence of gravity. In collaboration with DTM Technologies™ (Modena, Italy), the Topical Team designed the VIP-Gran-PF instrument (short for Vibration-Induced Phenomena in Granular Matter in Parabolic Flights) whose modular design allows us to investigate both dilute and dense granular regimes.

This paper is organized as follows. Section II describes the experimental instrument and its performance. Section III presents the current scientific objectives and, as a proof of concept, some selected results obtained with this facility during four ESA parabolic flight campaigns (PFCs) onboard a modified Airbus A310 Zero-G aircraft. Finally, we draw our conclusions and perspectives in Sec. IV.

II. INSTRUMENT DESCRIPTION AND PERFORMANCE

The setup of the VIP-Gran instrument is displayed in Fig. 1. The basic principle of the experiment consists of a closed cell containing particles, in which two opposite walls of the cell are pistons vibrating either in-phase or out-of-phase motions. Control parameters are the number of particles, the cell length (volume), the amplitude, and the frequency of vibrations. Different interchangeable cells can be used depending on the scientific objective. Accelerometers are screwed in the shaft of each vibrating piston. Impact sensors are also implemented to measure the collision statistics of particles impacting on the pistons. Two cameras allow quantitative measurements including particle tracking in dilute regimes and correlations between particle displacements.

We describe below in detail the five major components of the setup: (A) interchangeable experimental cells to be filled with granular material; (B) a bead feeder that allows adding particles into the cells during the experiment; (C) the driving mechanism that allows the energy injection, the control of the volume, and the confining pressure; (D) the accelerometers and impact sensors; and (E) two high resolution speed cameras to capture relevant data during the experiments and the illuminations.

A. Experimental cells

An experimental cell is a closed cuboidal container of $60 \times 30 \times h$ mm^3 that can be filled by granular material

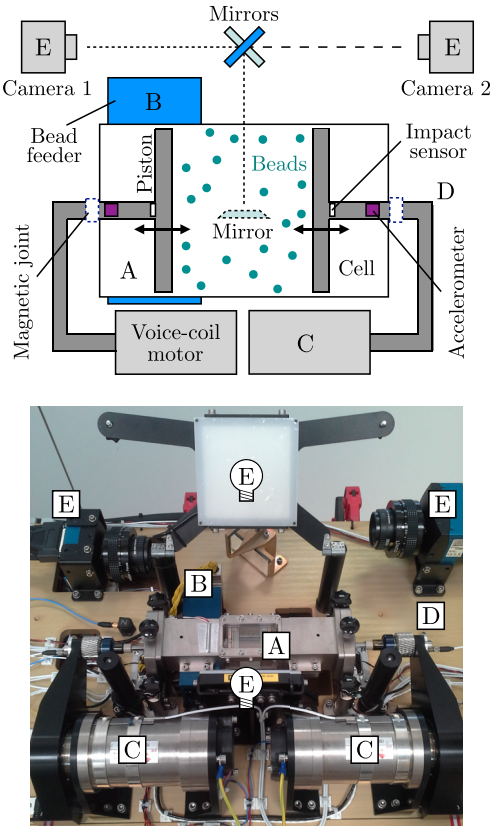

FIG. 1. For letters A, B, C, D, and E, refer to the main text. Top: Sketch (top view) of the VIP-Gran instrument. Two opposite walls, driven by voice coil motors, inject mechanical energy into the experimental cell containing a granular medium. Two cameras track grains or visualize the system from the bottom and from the side. Accelerometers and impact sensors are mounted on the shafts of the pistons respectively to control the energy injection in the system and to measure the collision statistics of the granular medium with the pistons. Bottom: Picture of the instrument built by DTM Technologies for parabolic flight experiments.

(spherical and/or aspherical particles). The top, bottom, and lateral sides of the cells are made of transparent polycarbonate, 8 mm in thickness. The two opposite walls of the cell are connected magnetically to linear voice-coil motors and act as pistons. The average distance, L, between the pistons can be adjusted in order to control the accessible volume of the system. Initially, a three-dimensional (3D) container ($h = 30$ mm) and a quasi two-dimensional (2D) container ($h = 5$ mm) were developed. A sketch describing these cells is given in Figs. 2(a) and 2(b). Different modifications can be applied to the cells in order to conduct particular experiments. For instance, placing additional walls within the container, as in Figs. 2(c) and 2(d), to create compartments can lead to trapping. Changing the curvature, or the roughness, of the pistons as in Figs. 2(e) and 2(f) can modify the energy injection into the system. Different physical phenomena and properties can then be investigated in low gravity within specific interchangeable cells: the out-of equilibrium stationary states of diluted granular medium in cells (a) and (b), handling of grains in cells (c) and (d), rheology in a cell (e) or sound propagation in granular media under weak applied confinement in a modified cell (a), and behaviors of the rheology of wet grains in a sealed cell (f). Some cells, such as (e) and (f), are in development. Therefore, we limit

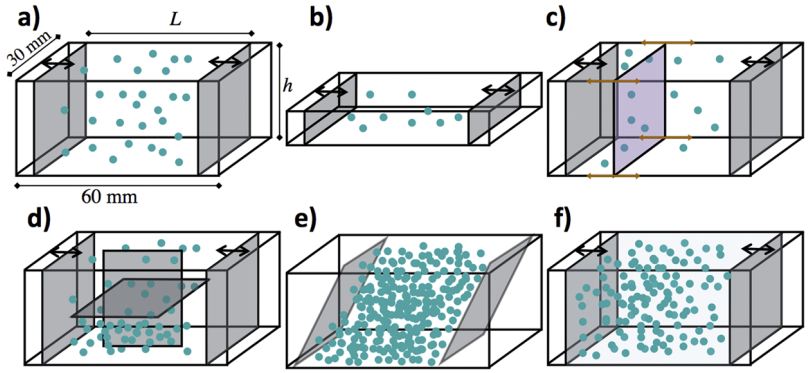

FIG. 2. Sketches of the experimental cells used in VIP-Gran-PF. Parameter L is tunable, thanks to the two mobile gray walls that act as pistons. The height h is 30 mm for 3D cells and 5 mm in the case of the quasi 2D cells: (a) 3D cell, (b) quasi-2D cell, (c) 3D cell with a free moving wall, (d) 3D partitioned cell, (e) 3D shear cell, and (f) 3D wet cell. Cells can easily be exchanged, thanks to a magnetic joint connection with the kinematic chain (see Fig. 1).

the discussion herein below to the use of the 3D cell (a) and the quasi 2D one (b).

B. Bead feeder

The experimental cells described in Sec. II A can be filled by spherical particles of different materials (bronze, steel, aluminum, glass, polyamide, etc.) and different diameters; see Table I. Moreover, cylindrical steel rods were also tested. Granular matter can either be placed directly into the cells before the experiment or be injected into them during the experimental runs using the bead feeder (see Fig. 3). The barrel of the bead feeder is divided into eight chambers, each able to contain either 1000 small (1 mm) or 250 large (2 mm) spherical particles. Thanks to a motorized linear rail slide system, each chamber can be positioned in front of the entry hole of the experimental cell. A piston then injects the particles. Note that the bead feeder does not allow extracting grains which means that, to start over again with new initial filling conditions, the cell has to be exchanged.

C. Driving mechanism

Two opposite walls of the cell are vibrating pistons (see Fig. 1). They are moved by using two linear voice-coil motors driven by a selected vibration stimulus (sine, single-pulse, quasi-static ramp, etc.). The forcing amplitude, A, of the piston is in the range [0.2, 25] mm (peak-to-peak), and its forcing frequency, f, in the range [1, 50] Hz. Note that the piston acceleration is limited to $5g$ (g being the acceleration of Earth gravity), meaning that some A, f combinations are not possible. For sine vibrations, pistons can oscillate either in-phase or out-of-phase. Both pistons are controlled in displacement with an accuracy of 10 μm at an acquisition rate of 1000 Hz. Since the vibrating walls of each cell are connected to the linear motors via magnetic joints mounted on both shafts (see Fig. 1), the cells can be changed on the instrument. A cooling fan is positioned on the back of each motor to keep the temperature constant.

D. Sensors and acquisition

Several sensors are installed in the instrument: accelerometers, impact sensors, linear positioning sensors, and temperature sensors. The two mono-axial accelerometers are screwed into the shaft of each vibrating piston to measure the piston's accelerations (8 kHz sampling frequency). One triaxial accelerometer is fixed on the breadboard, far away from the cell, in order to measure the ambient acceleration in response to the aircraft motions (1 kHz sampling rate). For 3D cells, the impact sensors are rectangular-shaped piezoelectric films mounted behind each vibrating piston, their axis being collinear with the vibration axis. Thanks to a 2 MHz sampling rate, each sensor is able to resolve the collision of a bead impacting on the piston wall. Such a contact lasts a few microseconds since the typical velocity of beads is of the order of few m/s at most. The two linear sensors for controlling the piston displacements are acquired at a 3 MHz sampling rate. Four temperature sensors are used to detect, at

TABLE I. Table of the experimental parameters of the VIP-Gran instrument. In each row, the description and the typical range of values are given for the different parameters. Note that L and h are defined in Fig. 2(a).

Symbol	Description	Value
N	Number of particles	...
R	Radius of the particles	1–5 mm
L	Distance between pistons	2–60 mm
h	Height of the cell	5 or 30 mm
V	Volume of the system	0.3–54 cm^3
ϕ	Packing fraction	0%–60%
A	Amplitudes of pistons	0–5 mm
f	Frequencies of pistons	0–50 Hz
φ	Phase shifts of pistons	0–π

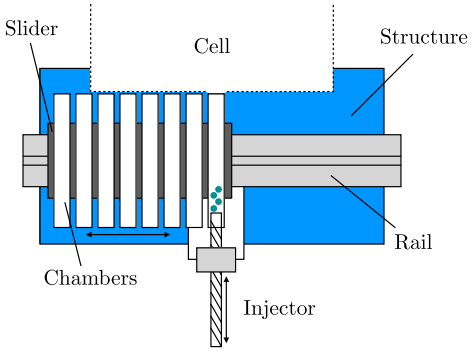

FIG. 3. Sketch of the bead feeder located below the cell. This device is used for the controlled injection of additional granular material into an experimental cell. It corresponds to letter B in Fig. 1.

a 1 Hz sampling rate, any abnormal overheating of the experiment cell, of each linear motors, and of the ambient air, to be able to promptly switch off the motors in order to cool them down. The onboard workstation, data acquisition system (interfaced by National Instruments cards), and electronics thus enable, for each parabola, high-frequency acquisitions of both video images and sensor signals as well as programming the required experiment profiles (piston frequency and amplitude and oscillation type). The time-tagging of acceleration data and impact force sensor data is synchronized with image acquisition and piston displacement (with a precision of 10^{-6} s).

E. Video cameras and illuminations

The instrument enables the observation of the experiment by means of two high-speed cameras of frame 1000 fps with a resolution of 1024 × 1024 pixels (Mikrotron EoSens 4CXP). The camera frame rate can be chosen down to 1 fps if low-speed acquisition is needed notably for experiments regarding dense regime. Observations are made in two perpendicular directions, perpendicular to the vibration axis. This corresponds to a bottom observation and a side-view observation in Fig. 1. The depth of field is selectable, whereas the field of view covers the full cell during vibrations. At full rates and resolution, 1.4 TBytes of video data are recorded by using both cameras during 31 parabolas (22 s each) of each flight. For each observation direction, the cell is illuminated from the back, corresponding to the two sides perpendicular to the field of view (see Figs. 1 and 4). Note that illuminator 2 on the top of Fig. 1 should be located on the top of the cell but has been turned over to enable the picture. In this open position, this illuminator masks the mirrors to obtain the required optical path between the cameras and the cell (see the top view of Fig. 1). Each illumination is individually switchable, and its intensity adjustable. The light from the light-emitting diode (LED) is diffused and uniform along all field of view. Straight light coming from outside the instrument, reflections on cell glass walls, and bright spots on particles are minimized. We can select which illumination and which camera should be activated (one of them or both).

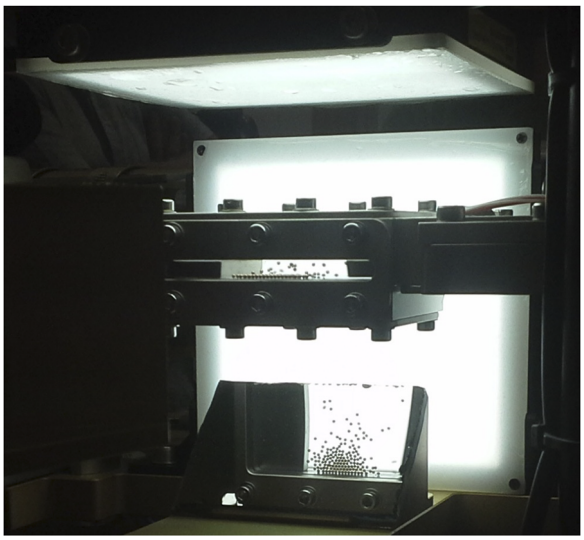

FIG. 4. Snapshot of the quasi-two-dimensional cell in front of the diffuse LED illumination (this image was taken on Earth). On the bottom, one can see the mirror enabling to take pictures from the bottom angle.

F. Experimental rack in the aircraft

A photo of the experimental rack mounted in the aircraft is displayed in Fig. 5. The rack is made of the Bosch Rexroth aluminum profiles, and the instrument baseplate is made of aluminum. The total mass of the experimental rack is 176 kg (100 kg for the payload, 76 kg for the structure). The rack dimensions are 1.1 m × 1 m and 0.67 m in height. Reinforcement bars of the rack in the aircraft main direction and in the perpendicular direction would resist in the case of a hard landing of $9g$ and $3g$, respectively.

G. Low-gravity conditions

The VIP-Gran-PF instrument was used during five ESA Parabolic Flight Campaigns (PFC63 to PFC67) from November 2015 to November 2017. The first PFC has been dedicated to the testing of the instrument and the other ones to scientific issues. A low-gravity environment (about $\pm 5 \times 10^{-2} g$) is repetitively achieved by flying with the specially modified

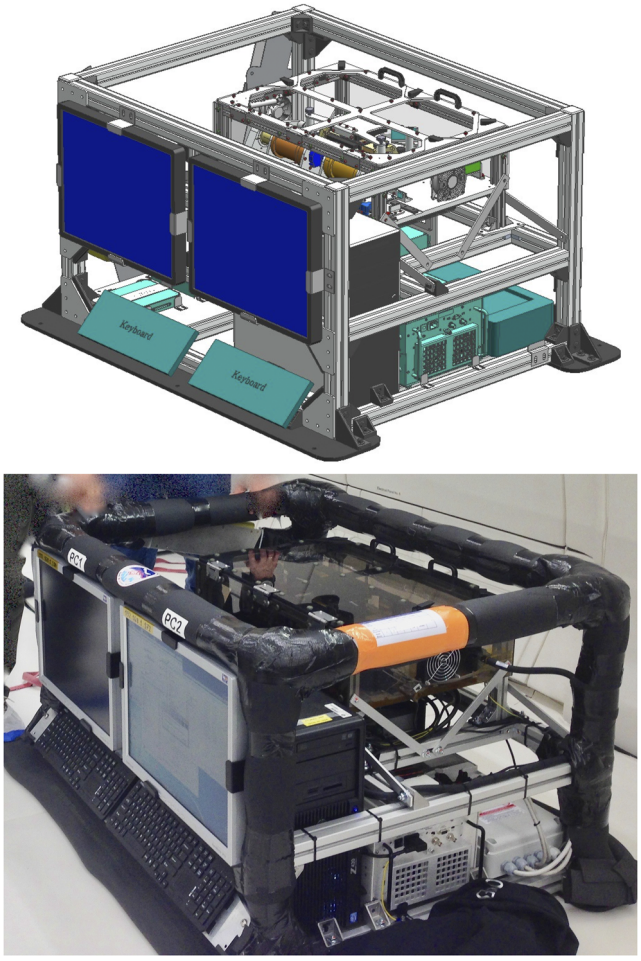

FIG. 5. Top: Drawing of the instrument rack by DTM Technologies. Bottom: Picture of the rack onboard the aircraft.

Airbus A310 Zero-G aircraft of Novespace[19] through a series of parabolic trajectories which result in low-gravity periods, each of 22 s. A flight campaign lasts 3 days with 31 low-gravity parabolas per day.

H. Experimental parameters

Different experiments are performed with various forcing parameters and filling (the number of beads and/or the type of bead). Since the grains cannot be removed automatically from the cell, the different experiments should be classified according to increasing filling parameters. An overview of all relevant experimental parameters for the performed experiments can be found in Table I.

III. SCIENTIFIC APPLICATIONS

The VIP-Gran-PF instrument is used since mid-2015. A wide variety of experimental situations can be studied in low-gravity conditions from dilute granular systems to dense assemblies. Several fundamental questions are notably addressed as follows:

(1) How a granular gas (which is intrinsically dissipative due to inelastic collisions) deviates from the elastic limit of an ideal gas when dissipation increases?
(2) What is the phase diagram of dynamical states of such an out-of-equilibrium dissipative gas?
(3) What is the segregation mechanism in granular media composed of two types of particle species in low gravity?
(4) What is the behavior of a granular medium near the jamming transition (transition from fluid to solid) without confinement pressure of grains due to their own weight?
(5) How does sound propagate in dense granular media under low confining pressure (i.e., lower than the one provided by gravity near unjamming)?
(6) Does a dense granular medium display large-scale convection-like dynamics, like on Earth, when subjected to a thermal gradient-like forcing (i.e., two vibrating walls with different velocities)?

Some of these questions have been addressed in numerical studies but never performed in experiments. Valuable experimental data will therefore be collected, for the first time ever, with the VIP-Gran instrument.

Since these open questions concern different experimental topics, numbers of particles, protocols, and time scales, different interchangeable cells are used to address them. As a proof of concept of the instrument, we will describe below some selected results obtained with this facility during ESA parabolic flight campaigns: (A) granular gas dynamics, (B) clustering, and (C) segregation, convection, and transport.

A. Granular gas dynamics

A granular gas displays striking properties compared to molecular gas: cluster formation at high enough density,[8,9] anomalous scalings of pressure[8] and collision frequency,[20] and non-Gaussian distribution of particle velocity.[10,21] These differences are mainly ascribed to the dissipation occurring during inelastic collisions between particles. Continuous injection of energy is thus necessary to sustain a stationary state in this dissipative out-of-equilibrium system. This is usually performed experimentally by vibrating a container wall or the whole container. For such a boundary-forced system, the particle velocity distribution is not Gaussian as for an ideal gas, but a stretched exponential, and is density dependent.[21] However, a spatially homogeneous forcing of a dilute granular gas leads to several major experimental differences (no cluster formation, exponential tail of the velocity distribution independent of the density).[22]

Here, we study with the VIP-Gran facility the analog of the dynamics of Brownian particles moving in thermalized fluids. To wit, we placed three large intruders in a driven granular gas of smaller beads that act as a surrounding fluid (see Fig. 6). Experiments were carried out in the quasi 2D cell in order to allow an easy tracking of the intruders by using the cameras. Thanks to image processing, we followed the

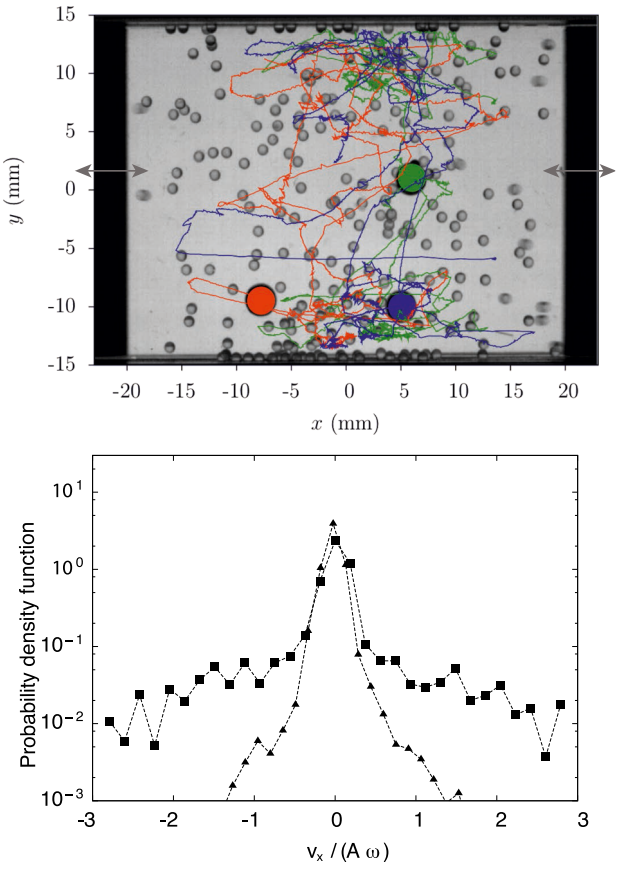

FIG. 6. Top: View of three large aluminum particles (5 mm in diameter, 176.6 mg in mass) immersed in a surrounding gas of thermalized small glass beads (1 mm in diameter, 4.08 mg in mass) in the quasi 2D cell. Both pistons (left and right black parts) vibrate sinusoidally in phase opposition. Each large particle is highlighted in a color (either orange, blue, or green), as well as its respective trajectories. Bottom: PDF of the normalized velocities (along the x axis) of the intruders for (■) low and (▲) high numbers of small particles ($N_s = 50$ and $N_s = 300$, respectively). Snapshot is taken from parabolic flight campaign ESA PFC66. Parameter range of the experiment: $f = 15$ Hz, $A = 5$ mm, packing fraction of small particles $\phi \in [1\%, 2.5\%]$, and $L = 45$ mm.

motion of the large particles for different numbers of small ones and different driving parameters. Figure 6 displays the trajectories of the three intruders obtained with our tracking. We then infer the mean square displacements of the intruders and the Probability Density Function (PDF) of their velocities v_x along the x axis normalized by the piston velocity $A\omega$ (with $\omega = 2\pi f$). We observe a non-Gaussian distribution with heavy tails for high velocities. This tail vanishes as the number of small particles increases due to the dynamical confinement of large particles by small ones. In another set of experiments, we experimentally study how a granular gas deviates from the quasi-elastic limit (ideal gas) when dissipation increases in the system. One way to do that is to increase the volume of the container at a constant particle density all things being equal, as it was shown numerically.[23] By varying some parameters of the experiment (particle number and volume of the cell), one observes how the granular system deviates or tends to the quasi-elastic limit (not shown here).

B. Granular clustering

The transition from a gaseous regime to a cluster of particles for a high enough density has been evidenced in a low-gravity experiment almost 20 years ago.[9] Numerical simulations have then reproduced this observation with the same parameters as in the experiment.[24] However, the parameters triggering this transition are far to be fully understood. By comparing the propagation time between two collisions and the relaxation time due to dissipative collisions, a 2D theoretical model based on an energetic approach predicts the marginal curve of the phase diagram separating gas- and solid-like regimes.[25] Here, with the VIP-Gran facility, we study the clustering transition in 3D to obtain the full experimental phase diagram and to compare it with the predictions. Control parameters are the number of beads N, the mean distance L between vibrating pistons, the amplitude A, and frequency f of the forcing. The packing fraction is then defined as $\phi = N\mathcal{V}_g/V \sim N/L$, where $\mathcal{V}_g$ is the volume of a single grain and V the cell volume. Different parabolic flight campaigns have been performed to cover the whole range of parameters. By means of the two perpendicular fields of view, and of image processing, the local density of particles and their velocities have been inferred in the 3D cell. As an example, Fig. 7 shows snapshots taken during PFC63 and PFC64. As one can see, starting from a gaseous regime, a cluster can be triggered by either increasing the packing fraction ϕ for a fixed volume (left column) or by increasing the volume for a fixed value of ϕ (right column). A regime of gas is discriminated from a cluster regime when the density distribution on both fields of view is found to be uniform (gas) or nonuniform (cluster). Moreover, from all the PFC data, we have obtained the full experimental phase diagram (not shown here). It is found to be well described by the model,[25] except for strongly diluted and dense cases where additional phenomena are observed. The corresponding data will be deeply described elsewhere.

Another set of experiments performed within our facility concerns aspherical particle dynamics. In a dilute regime, its dynamics has been already studied in low-gravity showing non-Gaussian velocity distributions and non-equipartition.[13] Here, we use granular materials composed of rods presenting an aspect ratio of about 5. By increasing the packing fraction, we observe for the first time in low-gravity the transition between a gas-like and a cluster regime of rods, as displayed in Fig. 8. The corresponding data will be deeply described elsewhere.

C. Granular segregation, convection, and transport

Here we give a few last examples of scientific applications that have been investigated with the VIP-Gran facility: Granular segregation, convection, and transport of particles in a partitioned cell under low gravity.

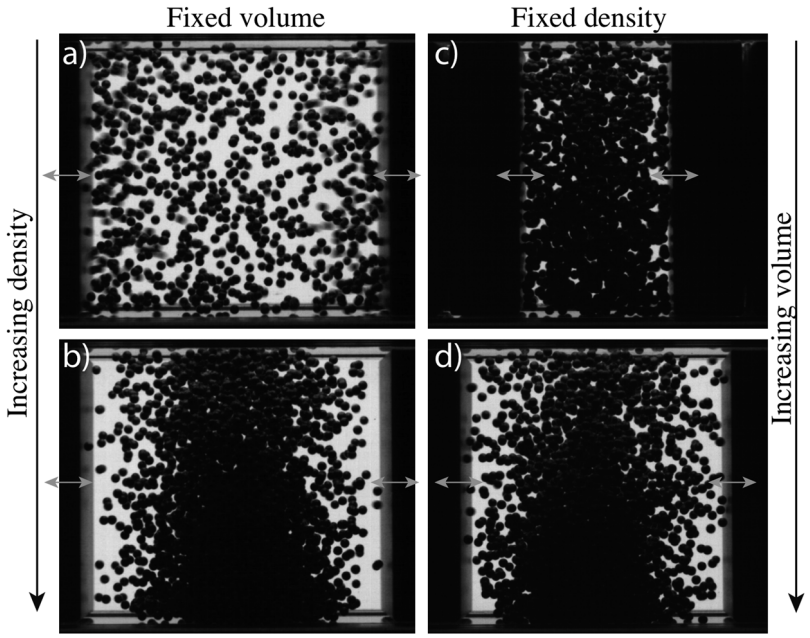

FIG. 7. Transition from a gas-like to a cluster regime of particles in low gravity in the 3D cell. Starting from a gaseous regime [(a) and (c)], a cluster can be obtained [(b) and (d)] by either (left row—PFC63) increasing the density ϕ = [1% (a) and 4% (b)] for a fixed volume (L = 40 mm) or by (right row—PFC64) increasing L = [12.5 mm (c) and 27.5 mm (d)] for a fixed value of ϕ = 6.5%. Both pistons (black parts) vibrate sinusoidally in phase opposition. Snapshots were taken during parabolic flight campaigns ESA PFC63 and PFC64 using the following forcing parameters: f = 20 Hz and A = 2 mm.

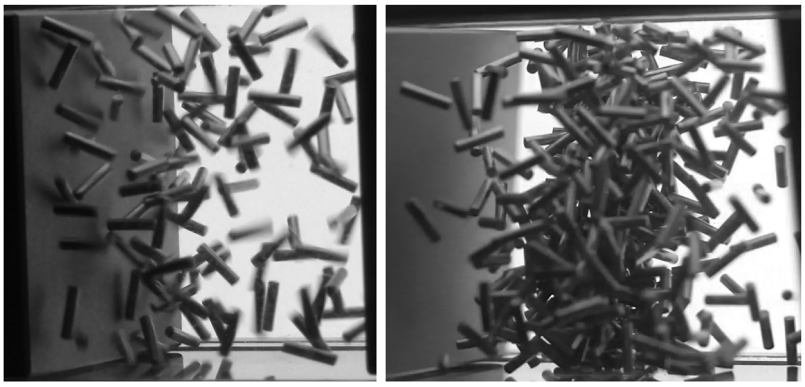

FIG. 8. Transition from a gas-like to a cluster regime of rods in low-gravity, when the packing fraction increases from 1% (left) to 3% (right). Experiments were performed in the 3D cell during the parabolic flight campaign ESA PFC66. Driving parameters and length in these snapshots are $f = 15$ Hz, $A = 5$ mm, and $L = 40$ mm. Stainless steel rods (issued from bearings) are 1 mm in diameter and 4.3 mm in length.

1. Segregation

On Earth, segregation of a granular medium composed of different particle species is well-known (and often called the Brazil nut effect) and is due to different mechanisms related to gravity, either convection by friction of particles on boundaries[26] or percolation of small particles beneath large ones.[27] In reduced gravity conditions, the segregation mechanism is unknown and the relevant control parameters are not yet established.[3] The origin of large-scale particle segregation observed on the asteroid regolith surfaces is a matter of intense debate.[28,29] Recently, collisional segregation has been proposed in this context[29] since a loose granular bed plays the role of impact absorbers either with gravity[30] or in the absence of gravity.[31]

Here, with the VIP-Gran facility, a mixture of small and large grains is subjected to vibrations in low gravity. Depending of the number N_s of small particles and the number N_l of large ones, different dynamics have been observed in the quasi 2D cell. In a dilute case, both particle types behave like gases homogeneously distributed [Fig. 9(a)]. When additional small beads are injected into the cell, large beads are then forced to the cluster in a strip in the center of the cell, thus leading to segregation [Fig. 9(b)]. This effect is due to the dissipative nature of collisions. For high enough fillings (of both particle types), we observed for the first time in low gravity a pattern in the center of the cell, constituted of alternative strips of small and large particles,[32] as it was predicted numerically[33,34] and theoretically.[35]

2. Convection

On Earth, convection in granular media is related to a spatial gradient of kinetic energy that, combined with gravity, produces a buoyancy-like force. When dissipation is large enough, this force can trigger the convection.[7,36] This mechanism should not be confused with air effect triggering convection rolls for submillimeter particles[5,37] or with convection induced by particle friction on boundaries for submillimetric particles.[3,26,38] In low-gravity conditions, with no boundary or air effect, convection has only been observed numerically.[33] With the VIP-Gran facility, one can apply different phases and velocities on each of the pistons to mimic a thermal-like gradient forcing. The corresponding cold and hot walls are expected to drive the system into a convective-like motion due to the generated spatial gradients of the kinetic energy.[39] Such large-scale convective motions have been observed in the 3D cell, during PFC experiments, within a mixture of large and small beads. However, the impact of the g-jitters on the phenomenon must still be clarified. This coarsening dynamics and the appearance of vortex-like structures will be further analyzed. In future, much longer experiments with a better level of low gravity will thus be performed in space (see Sec. III D).

3. Handling a granular medium in low gravity

On Earth, pouring a granular material is an easy way to handle it. In the absence of gravity, applying vibrations

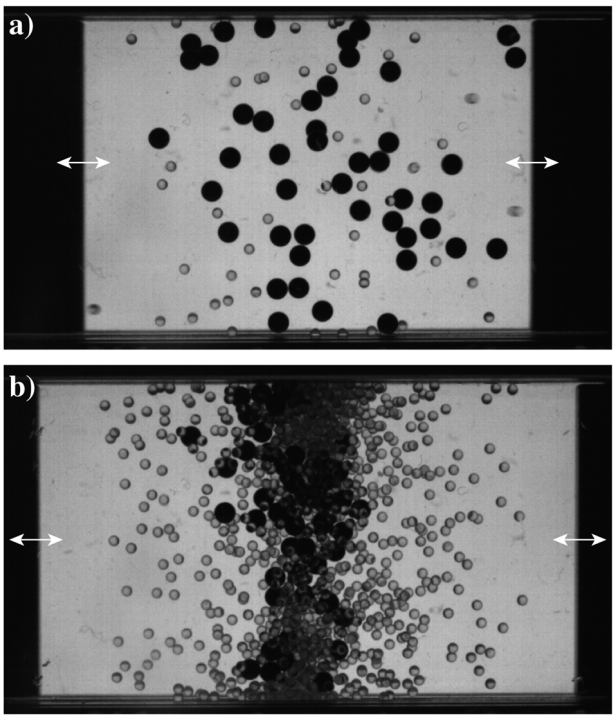

FIG. 9. Segregation of a mixture of large bronze and small glass beads in the 3D cell. In a dilute case ($N_L = 50$, $N_s = 50$), both particle types behave like a gas homogeneously distributed in the cell. (a) With additional small particles ($N_L = 50$, $N_s = 1000$), the latter force the large particles to accumulate in a stripe at the center of the cell, thus inducing segregation. (b) Both pistons (black parts) vibrates sinusoidally in phase opposition. Snapshots were taken during parabolic flight campaign ESA PFC65 with forcing parameters $f = 15$ Hz and $A = 5$ mm.

to the medium within partitioned cells with slits is a technique to manipulate it. However, the mechanisms leading to the exchange of particles between the compartments are poorly understood in the absence of gravity.[40–43] Within a box made of two connected compartments, the separation of a granular system into a cold and dense region on the one hand and a hot and dilute part on the other hand is usually called the Maxwell Demon experiment. On Earth, the apparent intrusion of a Maxwell Demon has been investigated theoretically,[44] experimentally,[45] and numerically.[46] The particle fluxes between compartments are related to the ratio between the gravitational potential energy of particles and the granular temperature both taken at the altitude of the slit.[40] In a low gravity, this control parameter of the phase separation does not hold up. Thus, investigations in low-gravity experiments involving compartmented systems are foreseen for next PFCs within the VIP-Gran facility. This study will be complementary to the Chinese SJ-10 satellite mission[47] and will be guided by previous numerical simulations with mono-disperse[42] or bi-disperse[43] particles in compartmented systems in the absence of gravity.

D. Future experiments in the International Space Station

The VIP-Gran facility was selected in early 2017 for flying on the International Space Station (ISS) in 2019. The ISS version of the instrument is currently in development. Excellent low-gravity conditions ($\sim 10^{-5} g$) are indeed needed to avoid g-jitters, as observed in previous PFC notably for cooling and convection experiments. Long time duration experiments ($\gg$22 s of PFC) are also needed to perform numerous iterative experiments to reach statistically convergent observations or for phenomena with long transients. Since the beginning of the project, the VIP-Gran instrument has been conceived for an ISS usage and, accordingly, its design was orientated toward versatility, full automatization, and modularity through interchangeable cells. Several experiments not discussed here are planned with the ISS version of the instrument, such as dynamics of granular cooling (when the forcing is stopped),[48] sound propagation, and rheology near the onset of jamming in dense granular media.

IV. CONCLUSION

To summarize, we have presented an experimental setup dedicated to the study of granular media in a low-gravity environment in three or two dimensions. This instrument is capable of conducting experiments over a large range of granular packing fractions from diluted to dense regimes (up to approximately 60%). The forcing mechanism is composed by two opposite walls of the cell driven by selected stimuli (sine, single-pulse, quasi-static ramp, etc.). The setup is instrumented by means of high-speed cameras in two perpendicular fields of view and accelerometers and impact sensors that allow us to infer quantitative measurements. The cell volume, the number of particles, and the amplitude, frequency, and phase of the driving are control parameters. Our preliminary results with modular geometries, based on different interchangeable cells, demonstrate the versatility of our setup. Our system thus provides a unique facility to perform experiments on granular media in reduced gravity conditions. Several open questions are currently investigated with this facility related to granular gases, segregation, convection, and transport of grains in a low gravity. Original scientific contributions as well as new applications for space exploration are thus expected.

An updated version of this facility is currently in development for the International Space Station to obtain excellent low-gravity conditions and a long duration of experimentations to study, notably, the cooling of a granular gas, convection, sound propagation in dense granular media under a ultra-low applied pressure, and rheology near the onset of the jamming transition without the confinement pressure of grains due to their weight.

ACKNOWLEDGMENTS

We thank M. Braibanti, O. Minster, and V. Köhne from ESA for fruitful discussions and for the flight opportunity. VIP-Gran-PF was built by DTM Technologies™ (Modena, Italy). We thank A. Pellegrini, L. Recanatesi, and D. Santachiara for their experimental support on PFC64. We thank the support of Novespace during parabolic flight campaigns (PFC64 to PFC67). E.O. thanks Prodex (Belspo) for financial support. Y.G., C.L., and F.P. thank P. Evesque for collaboration and thank CNES for both financial support and access to their PFC. This work was funded by ESA Topical Team No. 4000103461, CCN1, and CCN2.

[1] B. Andreotti, Y. Forterre, and O. Pouliquen, *Granular Media: Between Fluid and Solid* (Cambridge University Press, Cambridge, 2013); J. Duran, *Sands, Powders, and Grains* (Springer-Verlag, New York, 2000); P. Coussot, *Rheometry of Pastes, Suspensions, and Granular Materials: Applications in Industry and Environment* (John Wiley and Sons, 2005).
[2] F. Spahn, J. Schmidt, and M. Sremcevic, Lect. Notes Phys. **557**, 507 (2000).
[3] C. Güttler, I. von Borstel, R. Schräpler, and J. Blum, Phys. Rev. E **87**, 044201 (2013).
[4] See http://www.planetaryresources.com for Planetary Resources, Inc. (formerly Arkyd Astronautics) is an american start-up company aiming a profit-making mining of near earth asteroids.
[5] C. Laroche, S. Douady, and S. Fauve, J. Phys. **50**, 699 (1989).
[6] S. Fauve, S. Douady, and C. Laroche, J. Phys. Colloq. **50**, C3-187 (1989); F. Melo, P. Umbanhowar, and H. L. Swinney, Phys. Rev. Lett. **72**, 172 (1994).
[7] S. McNamara and S. Luding, Phys. Rev. E **58**, 813–822 (1998).
[8] E. Falcon, S. Fauve, and C. Laroche, Eur. Phys. J. B **9**, 183 (1999).
[9] E. Falcon, R. Wunenburger, P. Evesque, S. Fauve, C. Chabot, Y. Garrabos, and D. Beysens, Phys. Rev. Lett. **83**(2), 440 (1999).
[10] S. Luding, R. Cafiero, and H. J. Herrmann, "Driven granular gases," in *Granular Gas Dynamics*, Lecture Notes in Physics, Vol. 624, edited by T. Pöschel and N. Brillantov (Springer Verlag, Berlin, 2003).
[11] S. McNamara, Phys. Fluids A **5**, 3056 (1993); I. Goldhirsch and G. Zanetti, Phys. Rev. Lett. **70**, 1619 (1993); N. Brilliantov, C. Salueña, T. Schwager, and T. Pöschel, *ibid.* **93**, 134301 (2004); S. Luding and H. J. Herrmann, Chaos **9**(3), 673–681 (1999); S. Miller and S. Luding, Phys. Rev. E **69**(3), 031305 (2004); S. Gonzalez, A. R. Thornton, and S. Luding, Eur. Phys. J.: Spec. Top. **223**(11), 2205–2225 (2014).
[12] S. McNamara and W. R. Young, Phys. Fluids A **4**, 496 (1992); S. Luding and S. McNamara, Granular Matter **1**(3), 113–128 (1998).
[13] K. Harth, U. Kornek, T. Trittel, U. Strachauer, S. Höme, K. Will, and R. Stannarius, Phys. Rev. Lett. **110**, 144102 (2013); K. Harth, T. Trittel, K. May, S. Wegner, and R. Stannarius, Adv. Space Res. **55**, 1901 (2015).
[14] K. Harth, T. Trittel, S. Wegner, and R. Stannarius, Phys. Rev. Lett. **120**, 214301 (2018).

[15]G. Bossis, Y. Grasselli, and O. Volkova, J. Phys.: Condens. Matter **16**(18), 3279 (2004).
[16]C. H. Liu and S. R. Nagel, "Sound in sand," Phys. Rev. Lett. **68**, 2301 (1992); X. Jia, C. Caroli, and B. Velicky, *ibid.* **82**, 1863 (1999); B. Gilles and C. Coste, *ibid.* **90**, 174302 (2003); S. Wildenberg, Y. Yang, and X. Jia, Granular Matter **17**, 419 (2015); S. Wildenberg, A. Tourin, and X. Jia, Europhys. Lett. **115**, 34005 (2016); R. K. Shrivastava and S. Luding, Nonlin. Processes Geophys. **24**, 435–454 (2017); A. Merkel and S. Luding, Int. J. Solids Struct. **106-107**, 91–105 (2017); O. Mouraille and S. Luding, Ultrasonics **48**, 498–505 (2008).
[17]T. S. Majmudar and R. P. Behringer, Nature **435**, 1079 (2005); T. S. Majmudar, M. Sperl, S. Luding, and R. P. Behringer, Phys. Rev. Lett. **98**, 058001 (2007); R. Harich, T. Darnige, E. Kolb, and E. Clément, Europhys. Lett. **96**, 54003 (2011); D. Bi, J. Zhang, B. Chakraborty, and R. P. Behringer, Nature **480**, 355 (2011); J. Ren, J. A. Dijksman, and R. P. Behringer, Phys. Rev. Lett. **110**, 018302 (2013); H. Mizuno, L. E. Silbert, and M. Sperl, *ibid.* **116**, 068302 (2016); S. Luding, Nat. Phys. **12**, 531–532 (2016); N. Kumar and S. Luding, Granular Matter **18**, 58 (2016).
[18]See http://www.spacegrains.org for latest news on VIP-Gran.
[19]Airbus A310 Zero-G is managed and operated by the French company Novespace from the Bordeaux-Mérignac airport (France).
[20]E. Falcon, S. Aumaître, P. Evesque, F. Palencia, C. Lecoutre-Chabot, S. Fauve, D. Beysens, and Y. Garrabos, Europhys. Lett. **74**, 830 (2006).
[21]F. Rouyer and N. Menon, Phys. Rev. Lett. **85**, 3676 (2000); W. Losert, D. G. W. Cooper, J. Delour, A. Kudrolli, and J. P. Gollub, Chaos **9**, 682 (1999); J. S. Olafsen and J. S. Urbach, Phys. Rev. E **60**, R2468(R) (1999); A. Kudrolli and J. Henry, *ibid.* **62**, R1489 (2000); J. S. van Zon, J. Kreft, D. I. Goldman, D. Miracle, J. B. Swift, and H. L. Swinney, *ibid.* **70**, 040301(R) (2004); H.-Q. Wang, K. Feitosa, and N. Menon, *ibid.* **80**, 060304(R) (2009); S. Tatsumi, Y. Murayama, H. Hayakawa, and M. Sano, J. Fluid Mech. **641**, 521 (2009); S. E. Episov and T. Pöschel, J. Stat. Phys. **86**, 1385 (1997); C. Scholz and T. Pöschel, Phys. Rev. Lett. **118**, 198003 (2017).
[22]E. Falcon, J.-C. Bacri, and C. Laroche, Europhys. Lett. **103**, 64004 (2013); Phys. Rev. Fluids **2**, 102601(R) (2017).
[23]S. Aumaître, J. Farago, S. Fauve, and S. McNamara, Eur. Phys. J. B **42**, 255 (2004).
[24]E. Opsomer, F. Ludewig, and N. Vandewalle, Phys. Rev. E. **84**, 051306 (2011); J. Phys.: Conf. Ser. **327**, 012035 (2011).
[25]E. Opsomer, F. Ludewig, and N. Vandewalle, Europhys. Lett. **99**, 40001 (2012).
[26]J. B. Knight, H. M. Jaeger, and S. R. Nagel, Phys. Rev. Lett. **70**, 3728 (1993); R. Khosropour, J. Zirinsky, H. K. Pak, and R. P. Behringer, Phys. Rev. E **56**, 4467 (1997).
[27]J. C. Williams, Powder Technol. **52**, 245 (1976); A. Rosato, K. J. Strandburg, F. Prinz, and R. H. Swendsen, Phys. Rev. Lett. **58**, 1038 (1987); H. M. Jaeger, S. R. Nagel, and R. P. Behringer, Rev. Mod. Phys. **68**, 1259 (1996).
[28]N. Murdoch, P. Sánchez, S. R. Schwartz, and H. Miyamoto, in *Asteroids IV*, edited by M. Patrick, F. W. DeMeo, and W. F. Bottke (University of Arizona Press, Tucson, AZ, 2015), p. 767.
[29]T. Shinbrot, T. Sabuwala, T. Siu, M. Vivar Lazo, and P. Chakraborty, Phys. Rev. Lett. **118**, 111101 (2017).
[30]F. Pacheco Vázquez and S. Dorbolo, Sci. Rep. **3**, 2158 (2013).
[31]S. McNamara and E. Falcon, Powder Technol. **182**, 232 (2008).
[32]E. Opsomer, M. Noirhomme, N. Vandewalle, E. Falcon, and S. Merminod, npj Microgravity **3**, 1 (2017).
[33]S. Luding, O. Strauss, and S. McNamara, "Segregation of polydisperse granular media in the presence of a temperature gradient," in *IUTAM Symposion on Segregation in Granular Flows 297-303*, edited by A. D. Rosato and D. L. Blackmore (Kluwer Academic Publishers, 2000).
[34]E. Opsomer, N. Vandewalle, M. Noirhomme, and F. Ludewig, Eur. Phys. J. E **37**, 115 (2014).
[35]D. Serero, S. H. Noskowicz, M. L. Tan, and I. Goldhirsch, Eur. Phys. J.: Spec. Top. **179**, 221 (2009).
[36]R. Ramírez, D. Risso, and P. Cordero, Phys. Rev. Lett. **85**, 1230 (2000); R. D. Wildman, J. M. Huntley, and D. J. Parker, *ibid.* **86**, 3304 (2001); E. Khain and B. Meerson, Phys. Rev. E **67**, 021306 (2003); D. Paolotti, A. Barrat, U. Marini Bettolo Marconi, and A. Puglisi, *ibid.* **69**, 061304 (2004).
[37]H. K. Pak and R. P. Behringer, Phys. Rev. Lett. **71**, 1832 (1993); K. Kumar, E. Falcon, K. M. S. Bajaj, and S. Fauve, Physica A **270**, 97 (1999); A. Garcimartín, J. M. Pastor, R. Arévalo, and D. Maza, Eur. Phys. J.: Spec. Top. **146**, 331 (2007).
[38]N. Murdoch, B. Rozitis, K. Nordstrom, S. F. Green, P. Michel, T.-L. de Lophem, and W. Losert, Phys. Rev. Lett. **110**, 018307 (2013).
[39]P. Eshuis, K. van der Weele, M. Alam, H. J. van Gerner, M. van der Hoef, H. Kuipers, S. Luding, D. van der Meer, and D. Lohse, Granular Matter **15**(6), 893–911 (2013).
[40]N. Isert, C. C. Maaß, and C. M. Aegerter, Eur. Phys. J. E **28**, 205 (2009).
[41]J. J. Brey, F. Moreno, R. García-Rojo, and M. J. Ruiz-Montero, Phys. Rev. E **65**, 011305 (2001).
[42]Y. Li, M. Hou, and P. Evesque, J. Phys.: Conf. Ser. **327**, 012034 (2011); E. Opsomer, M. Noirhomme, N. Vandewalle, and F. Ludewig, Phys. Rev. E **88**, 012202 (2013); M. Noirhomme, E. Opsomer, N. Vandewalle, and F. Ludewig, Eur. Phys. J. E **38**, 9 (2015).
[43]W. Wang, Z. Zhou, J. Zong, and M.-Y. Hou, Chin. Phys. B **26**, 044501 (2017).
[44]J. Eggers, Phys. Rev. Lett. **83**, 5322 (1999).
[45]K. van der Weele, D. van der Meer, M. Versluis, and D. Lohse, Europhys. Lett. **53**, 328 (2001).
[46]A. Barrat and E. Trizac, Mol. Phys. **101**, 1713 (2003); M. Hou, H. Tu, R. Liu, Y. Li, K. Yu, P.-Y. Lai, and C. K. Chan, Phys. Rev. Lett. **100**, 068001 (2008); S. Shah, Y. C. Li, F. F. Cui, Q. Zhang, P. Evesque, and M. Hou, Chin. Phys. Lett. **29**, 034501 (2012).
[47]M. Hou, private communication (2018).
[48]C. C. Maaß, N. Isert, G. Maret, and C. M. Aegerter, Phys. Rev. Lett. **100**, 248001 (2008); Y. Grasselli, G. Bossis, and G. Goutallier, Europhys. Lett. **86**, 60007 (2009); S. Tatsumi, Y. Murayama, H. Hayakawa, and M. Sano, J. Fluid Mech. **641**, 521 (2009); D. Heißelmann, J. Blum, H. J. Fraser, and K. Wolling, Icarus **206**, 424 (2010); K. Harth, T. Trittel, S. Wegner, and R. Stannarius, EPJ Web Conf. **140**, 04008 (2017).

Part II

The life of a dynamical cluster

Chapter 3

Birth of the cluster

3.1 Introduction

As presented in Sec. 1.2, as a function of its packing fraction and the dimensions of the system in which it is enclosed, a granular medium can be either a granular gas or a cluster. In one case, the particles are uniformly distributed in the whole container and in the other, a slow and dense bulk, the cluster, is formed.

Our experimental work concerning the transition from a granular gas to a cluster is based on two main results. The first remarkable one consists in the very first observation of a dynamical cluster by Falcon *et al.* in 1999 [45]. In their experiment, they designed 3 cubic cells, of 1 cm^3 of volume, which can be vibrated sinusoidally. The cells were filled with 3 different numbers of 1 mm bronze beads and loaded in a sounding rocket. If these numbers of particles were arbitrary chosen, the results were outstanding. Indeed, as a function of the filling of the container, two different dynamical regimes were observed. In Fig. 3.1, these gaseous and cluster regimes are depicted. In the wake of this experiment, Opsomer *et al.* [36] have numerically studied the possibility of transition in the VIP-Gran cell. Calibrating their numerical model on Falcon's experiment, they have been able to deduce the mathematical frontier separating the gaseous state from the clustered state. This model is explained in detail in the next section.

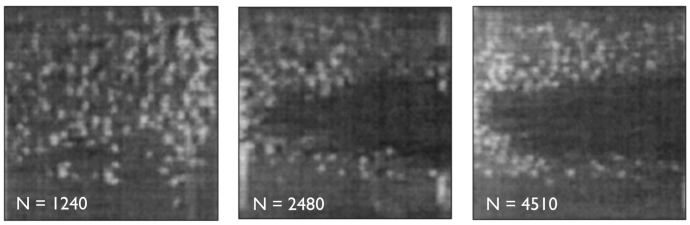

Figure 3.1: Three dynamical granular regimes observed during one Mini-Texus 5 experiment. As a function of the filling fraction of the container (from the left to the right), granular gas or clusters were observed. Taken from [45].

The questions arising from that are (i) how to find a routine which enables the detection of the granular gas (or the cluster) and (ii) how to verify experimentally the validity of the model derived here above. We attempt to give some answers in the publication presented at the end of this chapter.

3.2 Modeling the transition

3.2.1 Energetic approach

The conditions which have to be fulfilled to reach a clustered state can be established by considering N particles of diameter d and volume $V_{sph} = \pi d^3/6$, enclosed in the 3D version of the VIP-Gran cell described in Sec. 2.1. The volume of the cell is $V_c = (L + 2A)l^2$. Given these filling parameters, we can define the packing fraction of the system $\Phi = NV_{sph}/V_c$. The model is based on the following assumption: to create a cluster, the Haff time (the typical time needed by the system to decrease its mean velocity of a factor 2 [32]), denoted τ_H, has to be smaller than the propagation time, denoted τ_P. This latter is defined as the time needed to transmit the energy from one excited side of the container to the other. The condition $\tau_H \leq \tau_P$ reflects the fact that if the natural cooling of the system is the quickest phenomenon, the energy propagation is stopped by the cluster. In order to link the state of the system to its packing fraction, which is a key parameter, it is necessary to define both characteristic times cited above.

The Haff time is given by

$$\tau_H = \frac{C_0}{v_0(1-\varepsilon^2)\eta\sigma}, \tag{3.1}$$

where v_0, ε, $\eta = \Phi/V_{sph}$, $\sigma = \pi d^2$ and C_0 are respectively the typical velocity of a grain, the restitution coefficient of the particles, the number density of the system, the cross section of a particle and a calibration parameter.

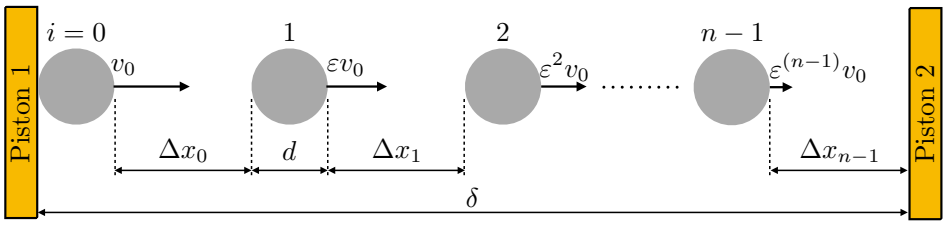

Figure 3.2: Sketch of the propagation mechanism of the information between both pistons. n particles are uniformly distributed along the mean distance δ separating both moving plates. The time needed to reach the next particle is $\Delta x_i/v_i$. After each collision, the velocity of the next particle is decreased by a factor ε and the distance d is instantaneously gained.

On the other hand, the propagation time can be calculated by adding the times needed for a particle i to reach the particle $i + 1$, at a distance Δx_i. After each collision, the velocity of the particle is decreased of a factor ε and a distance d is instantaneously gained (see Fig. 3.2). Starting this propagation chain from a piston with a particle of velocity v_0, the propagation time and the covered distance can be

respectively expressed by

$$\begin{aligned} \delta &= \sum_{i=0}^{n-1} \Delta x_i + nd \\ \tau_P &= \sum_{i=0}^{n-1} \Delta t_i = \sum_{i=0}^{n-1} \frac{\Delta x_i}{v_0 \varepsilon^i}, \end{aligned} \tag{3.2}$$

where δ is the mean distance between two points randomly located on the two pistons and n is the number of grains encountered by a particle coming from a piston over the distance δ. This number of particles is as a consequence equal to $n = \eta\delta\sigma$. Considering that the system is homogeneous, the distance separating a particle from its neighbor is always the same, noted Δx. We can express the latter as

$$\Delta x = \frac{\delta - dn}{n} = \frac{\delta}{n} - d. \tag{3.3}$$

The propagation time is finally given by

$$\tau_P = \frac{\Delta x}{v_0} \sum_{i=0}^{n-1} \frac{1}{\varepsilon^i}. \tag{3.4}$$

The transition from a gaseous to a clustered state is given by the balance of both characteristics times. One finds

$$\frac{C_0}{v_0(1-\varepsilon^2)\eta\sigma} = \frac{\delta/n - d}{v_0} \left(\frac{1-(1/\varepsilon)^n}{1-(1/\varepsilon)} \right). \tag{3.5}$$

We can finally invert this last relation by using the facts that $n = \eta\ \sigma\delta$ and $d = 2R$ in order to find the expression of δ/R as a function of Φ. One obtains

$$\frac{\delta}{R} = \frac{1}{3\Phi} \frac{\ln\left[1 + \frac{C_0}{\varepsilon(1+\varepsilon)(1-6\ \Phi)}\right]}{\ln(1/\varepsilon)}. \tag{3.6}$$

This model was calibrated with the help of numerical simulations in order to find the value of the constant C_0. The plot of δ/R as a function of Φ is presented in Fig. 3.6. In this figure, the points denote the transition from a gaseous to a clustered state for a wide range of numerical simulations. The transition was detected by performing a Kolmogorov-Smirnov test which will be described in Sec. 3.3.1.

3.3 Main results

In the following sections, the experimental work performed during five Parabolic Flight Campaigns is presented. Both, the image analysis of the collected data, as well as the statistical test which enables the detection of the clusters are detailed. We show that granular gases and dynamical clusters are observed and we compare the experimental results with the previously described model. We also observe another

PFC	Parabola	L(mm)	A(mm)	f(Hz)	N	Symbol
63	[0; 1; 2; 3; 4; 5] [6; 7; 8; 9; 10] [11; 12; 13; 14; 15] [16; 17; 18; 19; 20] [21; 22; 23; 24; 25]	40.0	[1.0; 1.4; 1.8; 2.0; 2.5; 3.0] [1.0; 1.4; 1.8; 2.0; 2.5]	20	250 750 1250 1750 2750	□
64	[6; 7; 8; 9; 10] [11; 12; 13; 14; 15] [21; 22; 23; 24; 25]	12.5 20.0 27.5	[0.5; 1.0; 1.5; 2.0; 2.5]	20	1611 2578 3545	△
65	[1; 2; 3; 4; 5] [6; 7; 8; 9; 10] [11; 12; 13; 14; 15]	30.0 35.0 40.0	[2.0; 2.5; 3.0; 3.5; 4.0]	15	2578 3008 3438	◇
66	[1; 2] [6; 7] [11; 12] [16; 17] [21; 22] [26; 27]	40.0	[5.0; 4.0]	15	2578 3438 4297 5157 6016 6875	○
67	[1; 2; 3; 4; 5] [6; 7; 8; 9; 10] [11; 12; 13; 14; 15] [16; 17; 18; 19; 20] [21; 22; 23; 24; 25] [26; 27; 28; 29; 30]	[20.0; 25.0; 30.0; 35.0; 40.0]	3.0	15	250 500 1000 1500 2000 2500	⬠

Table 3.1: Parameters that have been varied during the PFCs # 63 to 67. Each set of parameters has been determined in order to cover the entire phase diagram presented in Fig. 3.6.

state in the cell, where all the grains gather together to form a big cluster which moves periodically from one piston to the other. This regime, called "bouncing aggregate", is theoretically predictable, as developed in Sec. 5.1. These results have been compiled in a letter published in *EPL*. To close the discussion concerning the birth of the dynamical cluster, we show in Sec. 4.4 that the initial conditions of the system can affect the position of the theoretical frontier found in Sec. 3.2.

3.3.1 Image analysis

In order to determine experimentally the clustering conditions in terms of filling of the system, a large number of parabolic flights have been performed. As explained in the published article (at the end of this chapter), 114 parabolae were performed, during which the number of grains N as well as the dimension L of the cell were varied. See Tab. 3.1 for all the values of parameters that have been varied. Each parabola led to approximately 32000 pictures. Automated image processing was therefore required to process approximately $\sim 3.7\ 10^6$ images collected by the two high-speed cameras.

The routine first transforms the uncolored pictures (grey scale) to black-and-white images. From there on, we assume that black pixel reports the presence of one or more particles between the illuminator and the camera. Then, given the measured shadow profile, denoted $s(y)$ and given by the number N_y of black pixel in the projection of the slice over the considered axis divided by the total number of pixels in the projection (see for example Fig. 3.3), we were able to deduce the density profile of the system along the y-axis, denoted $\rho(y)/N$. The link between

the density and shadow profiles is given by

$$\frac{\rho(y)}{N} = \frac{dN_y}{LN} = \frac{d}{LN} \frac{\ln(1 - s(y))}{\ln(1 - (d/L))}. \tag{3.7}$$

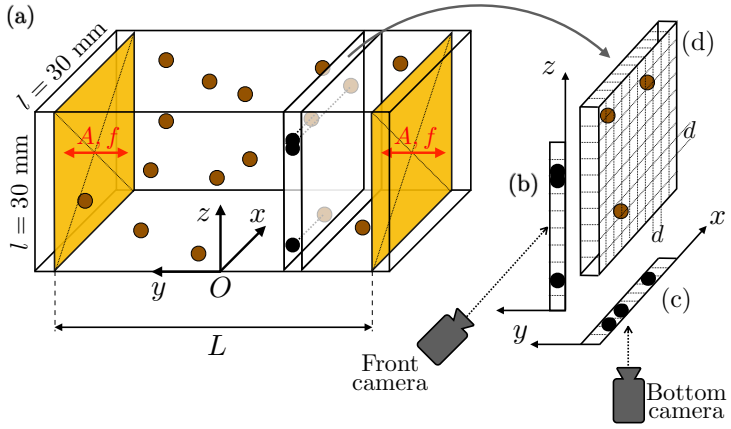

Figure 3.3: (a) Sketch of the 3D version of the VIP-Gran cell. N particles are enclosed in the container whose moving pistons are colored in grey. The images taken by the cameras can be divided along the y-axis in order to obtain two columns of dimensions dl in the (y, z)-plane (b) and in the (x, y)-plane (c). Given these measures, the distribution of the particles in the slice (d) can be reconstructed.

Based on the density profiles of all individual pictures, the averaged density profiles can be reconstructed for the whole experiment (i.e. for the whole parabola) and the 3D system can be numerically reconstructed (see Figs. 3.4 and 3.5 for two typical examples).

Finally, the cumulated distribution for the averaged density profile can be also found. The last task of the image analysis consists in comparing this cumulated distribution $F(y)$ to a cumulated uniform distribution $U(y)$, assuming that the latter corresponds to a gaseous state. This comparison is performed by using a Kolmogorov-Smirnov (short K-S) test, as for the numerical study of the frontier mentioned in Sec. 3.3. Mathematically, the test searches the maximal distance between the two cumulated distributions. This distance is given by

$$D = \sup_{|y| \leq L/2 - A} |F(y) - U(y)|. \tag{3.8}$$

If the distance D is less than a threshold $K_\alpha/\sqrt{k}$ (where α is the level of significance of the test and k is the number of classes characterizing the distributions), we can not state that $F(y)$ is non uniform. As a consequence, the state of the system is determined as gaseous. In contrario, if $D \geq K_\alpha/\sqrt{k}$, the system is not anymore gaseous and the presence of a cluster is likely. The full description of the image analysis is given here below in the article.

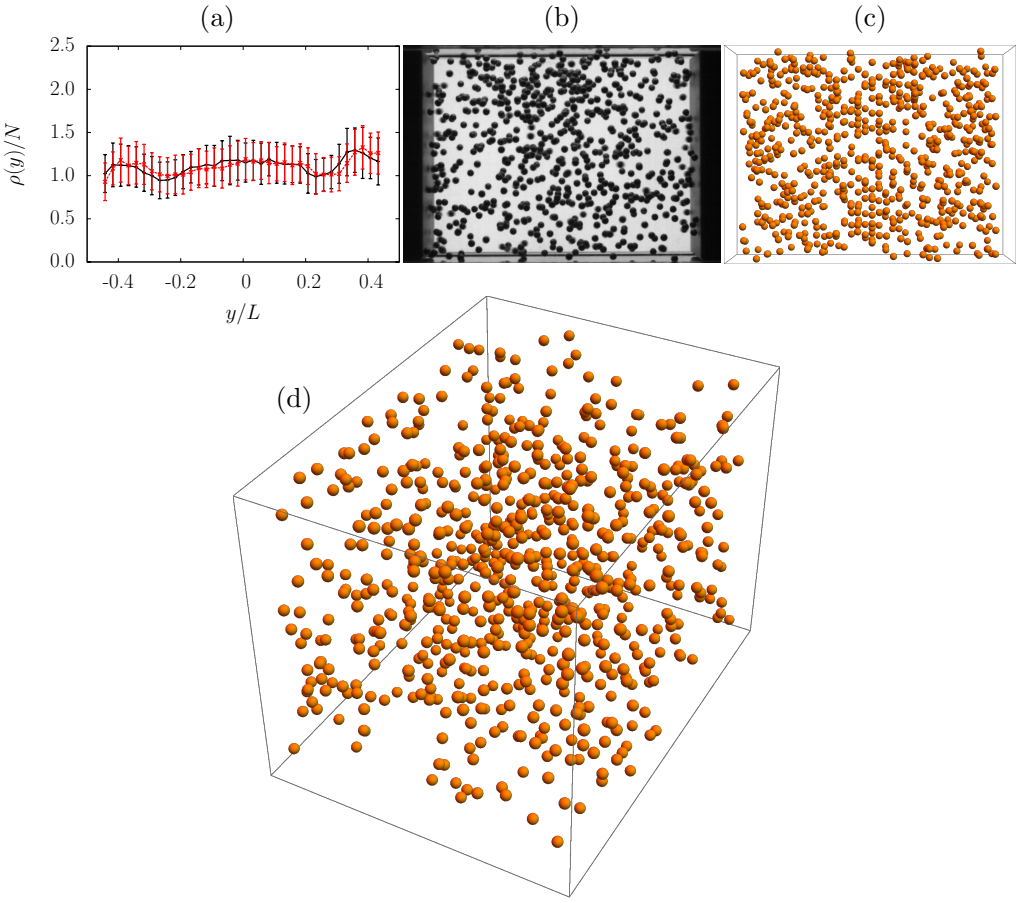

Figure 3.4: (a) Density profiles of the system evaluated with Eq. (3.7) on the basis of the pictures coming from both front (black line) and bottom (red line) cameras. The distributions seem to be uniform, reporting a gaseous state. (b) Typical picture taken by the front camera for a system with a low packing fraction. Front and 3D views of the numerical reconstruction of the system based on the averaged density profile. (a) and (b) are taken from [56]. The parameters of this experiment correspond to the parabola #8 of PFC #63 (see Tab. 3.1).

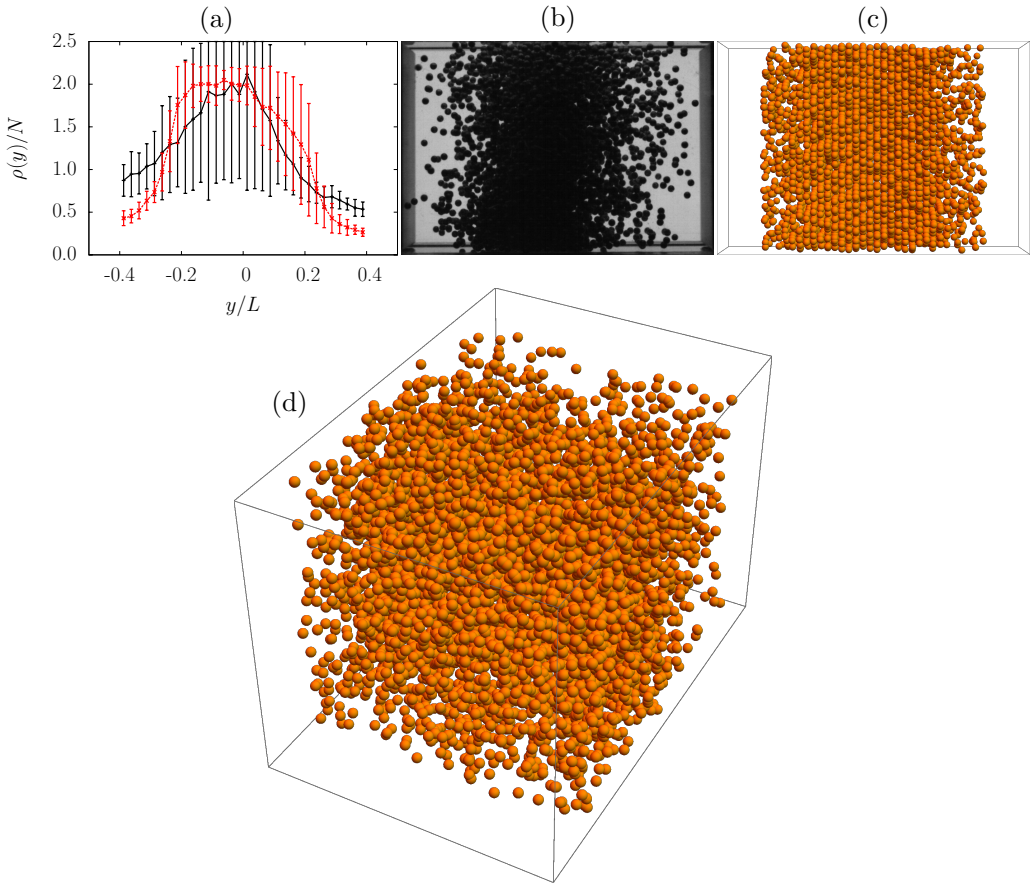

Figure 3.5: (a) Density profiles of the system evaluated with Eq. (3.7) on the basis of the pictures coming from both front (black line) and bottom (red line) cameras. The distributions are clearly non uniform, reporting no gaseous state in the system. (b) Typical picture taken by the front camera for a system with a high packing fraction. Front and 3D views of the numerical reconstruction of the system based on the averaged density profile. (a) and (b) are taken from [56]. The parameters of this experiment correspond to the parabola # 22 of PFC # 66 (see Tab. 3.1).

3.3.2 Phase diagram

The K-S test was applied to the 114 distributions in order to find the dynamical regime of each system. When a gas was detected, we colored the corresponding point in red in the $(\delta/R, \Phi)$ phase diagram. The presence of a cluster in the cell is depicted by a green point in this phase diagram. In Fig. 3.6, all the results have been reported, as well as the numerically determined transition points (see the black triangles) and the theoretical model derived in Sec. 3.2 (see the plain green curve). The results are in very good agreement, confirming the robustness of our model. Finally, we noted that a dynamical cluster cannot exist without the presence of a surrounding gas which transmits the energy from the plates to the cluster. This assumption has to be confirmed in future works on board of the ISS, with much better microgravity conditions.

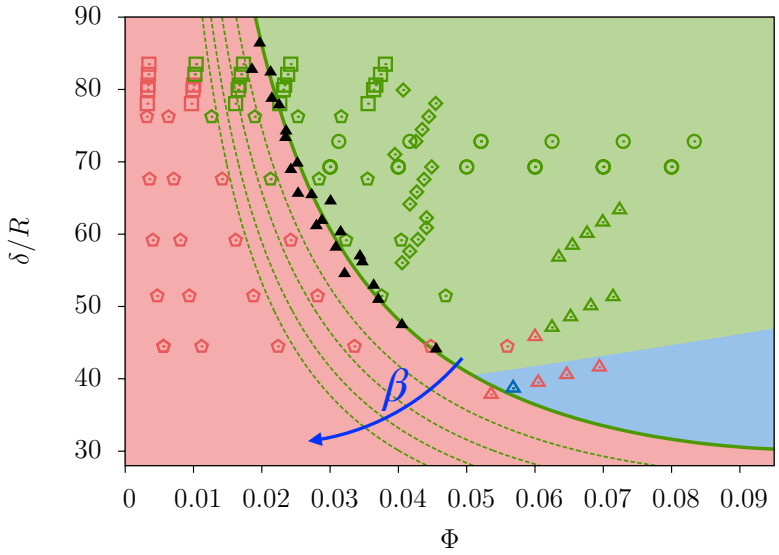

Figure 3.6: Phase diagram of the VIP-Gran cell. The dimension of the system normalized by the size of the particles δ/R is plotted as a function of the packing fraction of the system Φ. The points are colored in red when the system was determined as gaseous and in green when clusters were detected. The single blue point corresponds to the observation of a bouncing aggregate. See 5.1 for more details concerning this state. The shape of the points is linked to the parameters listed in Tab. 3.1. The different regions of the diagram are colored corresponding to the dynamical regimes observed. The separation of the gaseous and the clustered states is depicted by the plain green curve corresponding to Eq. (3.6) which has been calibrated with the help of numerical simulations. The black triangles correspond to these simulations. Finally, the dashed lines correspond to the transition curves for non uniform system, as explained in Sec. 3.4. At same number of particles in a given system, the clustered state is more rapidly reached if the particles are not uniformly distributed in the container, i.e. for increasing β.

3.4 Complementary measures

Our theoretical model predicting the phase transition is based on the hypothesis of uniformity in the distribution of the position of the particles. In this section, we show that if there is some inhomogeneity in the system, the transition will in any case occur for more dilute systems at fixed δ/R. Effectively, the propagation time is in that case longer than the homogeneous propagation time discussed in Sec. 3.2.1.

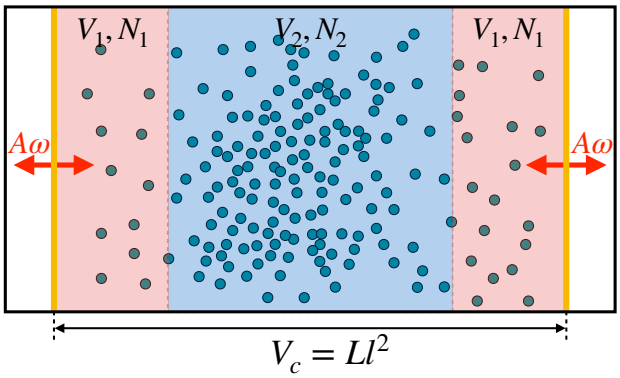

Figure 3.7: Front view of a sketch of the VIP-Gran 3D cell divided into a region of volume V_2 containing N_2 grains (blue area) and two other regions of volume V_1 each containing N_1 grains (red areas). The pistons are colored in orange and their excitation parameters are $A\omega$. The volume of the entire cell is $V_c = Ll^2 = 2V_1 + V_2$.

We consider the 3D VIP-Gran cell in which the N particles are separated into two populations. The densest population is composed of N_2 particles uniformly distributed in a region of volume V_2 centered at the middle of the cell. The other population is composed by the rest of the grains $N_1 = N - N_2$, uniformly distributed in between the latter region and the pistons, i.e. in both regions of volume $V_1/2 = (V_c - V_2)/2$. This separation, sketched in Fig. 3.7, is the simplest that can be imagined, given the symmetry of the system. We characterize the inhomogeneity with two parameters α and β with which the volume fractions, V_1 and V_2, and the number fractions, N_1 and N_2, of the populations can be expressed. One has

$$\begin{cases} V_1 = \dfrac{\alpha}{2} V_c \quad \text{and} \quad V_2 = (1-\alpha) V_c \\ N_1 = \dfrac{\beta}{2} N \quad \text{and} \quad N_2 = (1-\beta) N. \end{cases} \tag{3.9}$$

Given the parameters α and β, we can rewrite the propagation time with an inho-

mogeneity in the system, τ_P^{in}, using Eq. (3.2). One finds

$$\begin{aligned}\tau_P^{in} =& \frac{\delta_1/n_1 - d}{v_0}\left(\frac{1-(1/\varepsilon)^{n_1}}{1-(1/\varepsilon)}\right) \\ &+ \frac{\delta_2/n_2 - d}{v_0\varepsilon^{n_1}}\left(\frac{1-(1/\varepsilon)^{n_1}}{1-(1/\varepsilon)}\right) \\ &+ \frac{\delta_1/n_1 - d}{v_0\varepsilon^{n_1}\varepsilon^{n_2}}\left(\frac{1-(1/\varepsilon)^{n_1}}{1-(1/\varepsilon)}\right),\end{aligned} \tag{3.10}$$

where v_0 is the typical velocity given by the piston, δ_j is the typical distance to travel in the volume V_j and $n_j = \eta_j\delta_j\sigma$, with $\eta_j = N_j/V_j$ and $j = \{1, 2\}$. We consider that the inhomogeneity consists in a denser region in the middle of the cell, i.e. $\eta_2 > \eta$ and $\eta_1 < \eta$, since the pistons are the hot parts of the system. Both conditions lead to the same constraint $\beta < \alpha$.

Unfortunately, it is not possible to show that $\tau_P < \tau_P^{in}$, only based on their mathematical expressions. However, if we consider only 4 particles, we can easily be convinced that the quickest way to transmit the information through the system is realized in homogeneous conditions. In Fig. 3.8, a system composed of 4 homogeneously distributed particles (top) is depicted. The same system with inhomogeneously distributed particles (bottom) is also presented. In this figure, one sees that the time needed to cross the green zones is the same in both configurations since the same distance is covered at the same velocity. In the white zones, this is obviously not the case.

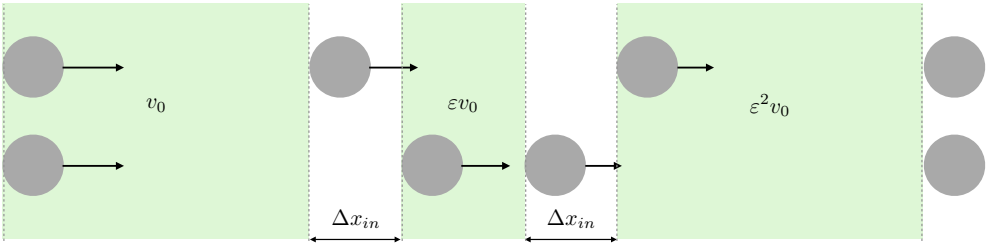

Figure 3.8: Same sketch as the one of Fig. 3.2 for 4 particles uniformly (top) and non-uniformly (bottom) distributed along the same distance. In both cases, the particles have the same velocities in the green regions and take as a consequence the same time to cover the same distance. In the white regions the time to cover the distances Δx_{in} is not the same in the uniform case as in the non-uniform. As demonstrated in the main text, the non-uniform distribution of the particles increases in any case the propagation time of the information.

The different times needed to travel the distance $2\Delta x_{in}$ in the homogeneous and inhomogeneous systems are respectively given by

$$\begin{aligned}t_h &= \frac{2\Delta x_{in}}{\varepsilon v_0} = \frac{\Delta x_{in}}{v_0}\frac{2}{\varepsilon}, \\ t_{in} &= \frac{\Delta x_{in}}{v_0} + \frac{\Delta x_{in}}{\varepsilon^2 v_0} = \frac{\Delta x_{in}}{v_0}\left(1 + \frac{1}{\varepsilon^2}\right).\end{aligned} \tag{3.11}$$

Dividing these two quantities leads to

$$\frac{t_{in}}{t_h} = \frac{1 + \frac{1}{\varepsilon^2}}{\frac{2}{\varepsilon}} = \frac{\varepsilon^2 + 1}{2\varepsilon} \geq 1. \tag{3.12}$$

The inequality in this last equation comes from the perfect square identity $\varepsilon^2 - 2\varepsilon + 1 = (\varepsilon - 1)^2 \geq 0$. The coefficient of restitution ε, which is one of the most important parameters of the clustering process, is always lesser than 1. If it was not the case, in a purely elastic system, where no energy is lost during the collisions, the propagation time would not be affected by any inhomogeneity. Therefore, for a constant distance needed to transmit the information from one piston to the other, as well as for a constant number of particles encountered over this distance, any inhomogeneity located near the middle of the cell will instantly increase the propagation time.

Finally, even though the balance of the Haff time τ_H and the inhomogeneous time τ_P^{in} has no analytical solution, we can solve the equation numerically in order to derive the frontier between gaseous and clustered systems in the presence of inhomogeneities. The corresponding curves are presented in Fig. 3.6. The green dashed lines in the diagram correspond to $\tau_H = \tau_P^{in}$ for different values of $\beta \in \{0.6, 0.7, 0.8, 0.9\}$ and $\alpha = 0.5$. As shown in this figure, the more important is the inhomogeneity, the sooner occurs the transition.

3.5 Summary

Thanks to this work, the transition from a gaseous to a clustered state in driven granular systems under microgravity conditions has been analyzed and compared with theory for the first time. Using simple arguments capturing the key parameters of the problem, we have shown that a phase transition can be predicted and that inhomogeneity in the cell can displace the frontier separating the gaseous phase from the clustered state. We have also developed an original image processing which allows to reconstruct three-dimensional density profiles of the system based on two-dimensional pictures.

A Letters Journal Exploring the Frontiers of Physics

July 2018

EPL, **123** (2018) 14003 www.epljournal.org
doi: 10.1209/0295-5075/123/14003

Threshold of gas-like to clustering transition in driven granular media in low-gravity environment

M. Noirhomme[1(a)], A. Cazaubiel[2], A. Darras[1], E. Falcon[2], D. Fischer[3], Y. Garrabos[4], C. Lecoutre-Chabot[4], S. Merminod[2], E. Opsomer[1], F. Palencia[4], J. Schockmel[1], R. Stannarius[3] and N. Vandewalle[1]

[1] *Group for Research and Applications in Statistical Physics (GRASP), CESAM Research Unit, Physics Department, B5a, University of Liège - B-4000 Liège, Belgium*
[2] *Université Paris Diderot, Sorbonne Paris Cité, MSC, UMR 7057 CNRS - F-75013 Paris, France*
[3] *Institute of Physics, Otto von Guericke University - D-39106 Magdeburg, Germany*
[4] *Institut de Chimie et de la Matière Condensée de Bordeaux (ICMCB)-UPR 9048 CNRS F-33608 Pessac, France*

received 30 May 2018; accepted in final form 17 July 2018
published online 13 August 2018

PACS 45.70.-n – Granular systems
PACS 45.70.Qj – Pattern formation

Abstract – Strongly driven granular media are known to undergo a transition from a gas-like to a cluster regime when the density of particles is increased. However, the main mechanism triggering this transition is not fully understood so far. Here, we investigate experimentally this transition within a 3D cell filled with beads that are driven by two face-to-face vibrating pistons in low gravity during parabolic flight campaigns. By varying large ranges of parameters, we obtain the full phase diagram of the dynamical regimes reached by the out-of-equilibrium system: gas, cluster or bouncing aggregate. The images of the cell recorded by two perpendicular cameras are processed to obtain the profiles of particle density along the vibration axis of the cell. A statistical test is then performed on these distributions to determinate which regime is reached by the system. The experimental results are found in very good agreement with theoretical models for the gas-cluster transition and for the emergence of the bouncing state. The transition is shown to occur when the typical propagation time needed to transmit the kinetic energy from one piston to the other is of the order of the relaxation time due to dissipative collisions.

Introduction. – When submitted to an external energy input, confined granular matter exhibits different dynamics depending on the filling and forcing conditions of the system [1]. These different dynamical regimes can be classified into three categories called "solid" [2–4], "liquid" [5] or "gas", in analogy to the classical counterpart. This letter is focused on very dilute systems with strong enough forcing, where particles can move erratically and have a gas-like behavior. However, such a granular gas displays properties strikingly different from those of a molecular gas: anomalous scalings of pressure [6] and collision frequency [7], and non-Gaussian distribution of particle velocity [8]. These differences are mainly attributed to the dissipation occurring during inelastic collisions between particles. Continuous injection of energy is thus necessary to sustain a stationary state in this dissipative out-of-equilibrium system. This is usually performed experimentally by vibrating a container wall or the whole container. When the forcing is stopped, numerical simulations have shown the formation of density gradients during the cooling (instability of the homogeneous cooling state) [9] as well as inelastic collapse (particles undergoing an infinite number of collisions in finite time) [10]. The predicted duration of the cooling phase [11] has been tested experimentally with success [12]. Due to the dissipative character of the collisions, increasing the density within a driven granular gas, and thus the number of collisions, will lead to an increase of the energy dissipation in the system. A cluster formation can then occur at high enough density despite the continuous energy injection. Such a transition from a gaseous regime to a cluster of particles when the density increases has been

(a) E-mail: mnoirhomme@uliege.be

established almost 20 years ago [6,13,14]. The parameters triggering this transition are far from being fully understood even though this observation has been reproduced numerically [15].

On Earth, experiments are biased by gravity-induced anisotropy and by the friction forces that act on all the particles composing the system. Low-gravity environment is thus needed for granular gases in order to obtain an experimental situation for which inelastic collisions are the only interaction mechanism between particles. For instance, the cluster formation was first observed experimentally on Earth in 3D [6] and 2D [13], and has then been more clearly demonstrated in low gravity in 3D [14]. More recently, a Topical Team of the European Space Agency (ESA) has designed an instrument called VIP-Gran (for Vibrated Induced Phenomena in Granular matter) [16]. It aims to study the dynamics and statistical mechanics of driven granular systems in low-gravity environment from dilute to dense regimes [17].

In this work, we study experimentally the transition from a granular gas to a clustered state in low gravity using the 3D VIP-Gran facility. The full experimental phase diagram is then obtained for large ranges of experimental parameters. These results are compared with numerical and theoretical work predicting the marginal curve of the phase diagram separating the gas- and liquid-like regimes [18]. Good agreement is found during this comparison showing that this transition is governed by the interplay between inertia (propagation time between collisions) and inelasticity (relaxation time due to dissipative collisions). This work follows the footsteps of Sack *et al.* [19] and Falcon *et al.* [14] where the authors have observed similar granular states in different geometries and for different excitations.

Setup. – The setup of the VIP-Gran instrument has been extensively described in [17]. We only recall here its main features regarding the experiments discussed in this work. As sketched in fig. 1, it consists of a cell of dimension $60 \times 30 \times 30$ mm where the energy is injected into the system by two oscillating pistons, separated by an average distance L. The latter can be tuned to control the accessible volume of the cell. The two opposite pistons, moved by linear voice-coil motors, are driven sinusoidally in phase opposition with the same frequency f and amplitude A. The vibration axis is perpendicular to the moving walls (see fig. 1). The cell is filled with N bronze beads of diameter $d = 1$ mm, either manually or automatically using a bead-feeding device [17]. Experimental data are acquired using two high-speed cameras of maximal frame rates $f_c = 1000$ fps with a resolution of 1024×900 pixels. Visualizations of the cell are obtained in the two directions perpendicular to the vibration axis (see fig. 1). During one period of vibration $T = 1/f$ (with a frequency f at most equal to 20 Hz), the number of recorded images is $f_c T$, that is 50 images at least. The control parameters are the number of beads N, the mean distance L between vibrating

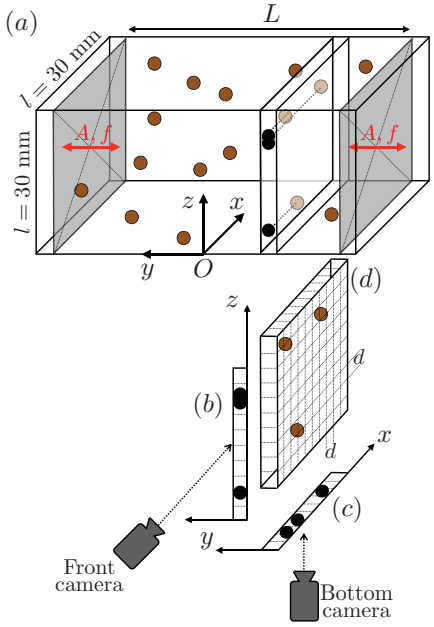

Fig. 1: (Color online) (a) Sketch of the experimental VIP-Gran cell. The oscillating pistons are colored in light grey. The recorded images of the cell are numerically divided in slices of width d along the y-axis (axis of vibration). Front (b), bottom (c) and side (d) views of the slice are sketched. The front and bottom views are the two accessible shadow profiles while the side view is an arbitrary distribution which could have generated these observations. The link between the measured shadow and the possible number of particles in the slices is explained in the main text. (d) Each slice is divided into rows and columns of dimension d into the x and z directions.

pistons, the amplitude A and frequency f of the forcing. The distance between the walls oscillates as a consequence between $L - 2A$ and $L + 2A$. The packing fraction is then defined as $\Phi = N\mathcal{V}_g/V$, where $\mathcal{V}_g = \pi d^3/6$ is the volume of a single grain, $V = l^2(L + 2A)$ the maximum cell volume, and $l = 30$ mm. We focus here on dilute regimes with $\Phi < 10\%$. All relevant experimental parameters are listed in table 1. The filling parameters were chosen according to numerical simulations predicting the transition from a gaseous state to a clustered state in the VIP-Gran cell [18]. Moreover, since these simulations do not predict a qualitative change with vibration frequency [20], f will not be varied systematically here. To cover the whole ranges of experimental parameters, five ESA Parabolic Flight Campaigns (PFCs #63 to 67) were performed on board of a specially modified Airbus A310 Zero-G aircraft of Novespace through a series of parabolic trajectories which result in low-gravity periods, each of approximatively 22 s. Low-gravity environment is about $\pm 0.05g$. Each PFC lasts 3 days with 31 low-gravity parabolae per day. Among the 465 parabolae performed, 114 were dedicated to the present study.

Results. – The raw data of the experiments consist of two sequences of greyscale pictures of the cell, taken

Table 1: Parameters of each experiment performed during ESA parabolic flight campaigns #63 to 67. Each set of parameters was precisely chosen in order to reach different regimes of the phase diagram displayed in fig. 3.

PFC	#runs	L(mm)	A(mm)	f(Hz)	N	Symbol
63	25	40.0	[1.0; 1.4; 1.8; 2.0; 2.5]	20	[250; 750; 1250; 1750; 2750]	□
64	15	[12.5; 20.0; 27.5]	[0.5; 1.0; 1.5; 2.0; 2.5]	20	[1611; 2578; 3545]	△
65	15	[30.0; 35.0; 40.0]	[2.0; 2.5; 3.0; 3.5; 4.0]	15	[2578; 3008; 3438]	◇
66	12	40.0	[4.0; 5.0]	15	[2578; 3438; 4297; 5157; 6016; 6875]	○
67	30	[20.0; 25.0; 30.0; 35.0; 40.0]	3.0	15	[250; 500; 1000; 1500; 2000; 2500]	⬠

by both high-speed cameras. About 40000 images are recorded for one single parabola, and of the order of 4.5 millions for all parabolae. As displayed in fig. 2, three typical dynamical granular regimes are observed in our experiment depending on the number N of particles in the cell. A granular gas regime is observed for very dilute densities (fig. 2(a)) where particles are homogeneously distributed within the entire cell. When the density is increased, we observe a cluster of particles almost static in the middle of the cell, the cluster being surrounded by lower particle density regions (see fig. 2(b)). In these regions, the particles have fast velocities and transmit the kinetic energy from the pistons to the cluster where it is mainly dissipated. The third observed regime consists in a cluster of all particles that bounces periodically from one piston to the other one (fig. 2(c)), as previously observed [21]. We called this regime afterwards "bouncing aggregate". The period of oscillation of the latter is subharmonics, *i.e.*, twice the piston period. This regime occurs when the vibration amplitude exceeds a critical fraction of the cell size (see below). For the corresponding time evolutions, see supplementary slow-down videos `gas.mp4`, `cluster.mp4` and `bouncing.mp4`. By using image processing tools, we will now infer from these images the spatial density profiles for these three regimes.

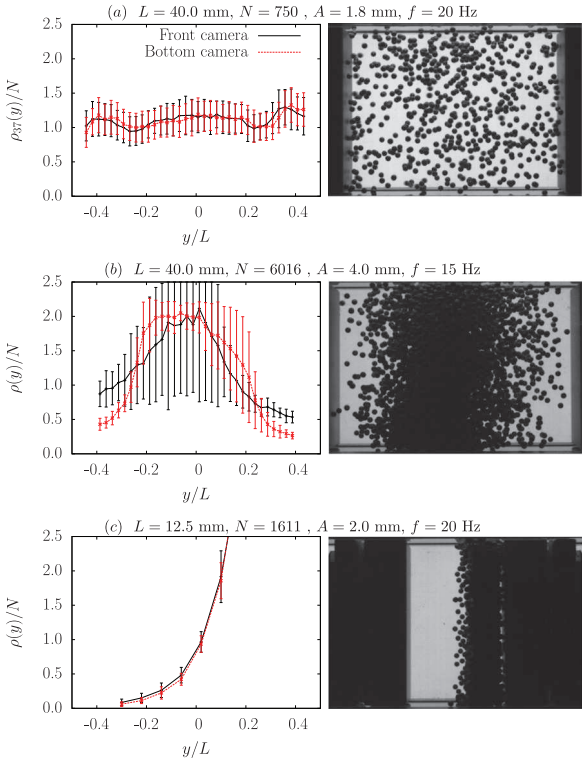

Fig. 2: (Color online) Right: different dynamical regimes for different experimental parameters L, N, A, and f: granular gas (a), cluster (b), and bouncing aggregate (c). The picture come from the front camera. Left: corresponding average density profiles $\rho(y)$ of the system obtained from the image processing (see text). The red (respectively, black) curves are inferred from images from the bottom (respectively, front) camera. For the granular gases and the clusters, the average density profiles are very stable over time. It is not the case for the bouncing aggregate for which the position of the peak in the average density profile varies over time.

Image processing. – For each low-gravity phase, we wait a few seconds ($50T$) before recording data, in order to reach a stationary state within the granular medium. From there on, data is recorded during $100T$ (between 5 and 7 s). This corresponds to the middle of the parabola duration, when the fluctuations of gravity, called g-jitters, are the weakest. In order to obtain some quantitative data from the pictures, we performed image analysis using the open-access software FIJI [22]. First, we applied a threshold on the pictures, coloring each pixel either black (corresponding to the shadow coming from the presence of one or more grains) or white (reporting no particle between the light and the camera), depending on their grey level. The second step consists in dividing the constant free zone of the system into slices along the vibration axis (y-axis) (see fig. 1). Each slice has a width d, the particle diameter, and is located at the dimensionless position $y \in [(-L/2 + A)/Ld; (L/2 - A)/Ld]$.

The aim of the image processing described in this section is to reconstruct the average 3D density profile of the system using the 2D pictures. In the following, the processing will be detailed only for the bottom camera images, *i.e.*, in the (x, y)-direction. The processing in the other direction is exactly the same. First, we divided the considered slice into columns of width d. This implies a division of the (x, y)-plane in squares of area d^2. An example of the division of a slice is given in fig. 1. By assuming a uniform distribution of the grains in the slice, the probability of the presence of one of those grains in a specific

column is $p = d/l$. If the slice contains N_y particles, the probability $P(X = n)$ of finding n grains in the column is given by the binomial distribution

$$P(X = n) = \binom{N_y}{n} p^n (1-p)^{N_y - n}, \tag{1}$$

where X is the random variable representing the number of grains in a column, and $\binom{N_y}{n} = N_y!/[n!(N_y - n)!]$ the binomial coefficient. By equaling $X = 0$ (*i.e.*, by focusing on the light transmitted through the system), the number of particles in the slice can be isolated. One obtains

$$N_y = \frac{\ln(1 - s_x)}{\ln(1 - d/l)}, \tag{2}$$

where s_x, the shadow density measured by the bottom camera, is given by the number of black pixels in the (x, y)-plane divided by the total number of pixels in the surface ld. See the supplementary material `Supplementarymaterial.pdf` for more details.

Note again that the main hypothesis is that the particles are uniformly distributed in each slice. This assumption seems reasonable if there is no external residual acceleration in the system. In addition, note that the number N_y of particles in a slice is undetermined, from eq. (2), for $s_x = 1$. This extreme value is mostly unreached, except for a few pictures given by the bottom camera, for parabolae where the g-jitters were significant. In these cases, the maximal number of grains in the considered slice was fixed at 300. This value corresponds to the detection of a single white pixel in s_x. Finally, the normalized distribution of the number of grains in the slices N_y/N as a function of y can be found for each image provided by the cameras. We have averaged the distributions coming from all the pictures determined by a fixed piston phase in order to obtain f_c/f different distributions.

Statistical analysis. – The average density profiles of the system are shown in fig. 2, for different parabolae (corresponding to different parameters listed in table 1). For the gaseous state, the distribution is approximatively uniform (see fig. 2(a)). By contrast, when a clustered state is reached, the resulting distribution exhibits systematically a peak. If the cluster is stabilized in the middle of the cell, the position of the resulting peak in the distribution is stable over the time, too (see fig. 2(b)). However, in the case of the bouncing aggregate, the bulk moves from one piston to the other one. Consequently, the position of the resulting measured peak varies over the time (see fig. 2(c)). Note that we found nearly always differences between the distributions obtained from the two different cameras. Actually, the g-jitters tend to gather the grains close to the bottom of the cell, making the z-distribution more uniform than the x-distribution over the y-axis. In the cluster regime, the error bars in the distributions are also larger for the z-distribution than for the x one, due to prevailing g-jitters in the z-direction.

In order to extract the state of the system from the averaged distributions coming out of our image processing, we use the one-sample Kolmogorov-Smirnov (KS) test [15,18]. This KS test consists in comparing the measured cumulated distributions with a theoretical one. In analogy with classical gases, we assume that a granular gas is characterized by a uniform distribution of the position of the particles in the cell. In the KS test, the comparison between two distributions is performed by measuring the maximal distance separating the measured cumulated distribution, noted $F(y)$, computed using the corresponding average density profile $\rho(y)/N$, and the theoretical cumulated distribution, noted $U(y)$. This distance is defined as

$$D = \sup_{|y| \leq L/2 - A} |F(y) - U(y)|\cdot \tag{3}$$

Then, we compared D to a given threshold-value K_α coupled to the number of classes characterizing the distributions, noted k. Following our division of the cell into slices, this number of classes is simply given by $k = L/d$. Concerning the threshold K_α, its value depends on the level of significance of the test, α, which has been fixed at 0.01 in order to follow previous works [15,18]. The KS test of eq. (2) allows us to consider that the system has reached a clustered state as soon as the condition $D > K_\alpha/\sqrt{k}$ is fulfilled. On the other hand, as long as the threshold is not crossed, the grains can be considered as uniformly distributed in the cell and the system is considered in a gaseous phase. We applied the KS test on each averaged distribution $F(y)$ (corresponding to each different piston phase) obtained from the image processing. We found two final averaged values of the maximal distances D_x and D_z for all averaged distributions $F(y)$ coming from each camera. These values D_x and D_z are two statistical characterizations of the averaged distribution of the position of the particles along the vibration axis for a given set of parameters. For each parabola of each PFC, we calculated D_x and D_z and compared the obtained values to the related threshold. The state of the system can be deduced from D_x and D_z. We detected a gaseous regime (see the red symbols in the phase diagram of fig. 3) if the conditions $D_x \leq K_\alpha/\sqrt{k}$ and $D_z \leq K_\alpha/\sqrt{k}$ are fulfilled. Otherwise, the system is considered as clustered (see the green symbols in fig. 3). We reported these comparisons in the phase diagram shown in fig. 3.

Phase diagram. – In fig. 3, we plot the typical length scale of the system δ, normalized by the particle radius, R, as a function of the packing fraction ϕ. More precisely, δ is the mean distance that N particles achieve when they pass across a constraint free distance $(L-2A)$. This mean value is numerically calculated and is tabulated as a function of the chosen experimental parameter set (L and A) [18]. The horizontal axis reports the mean packing fraction of the system,

$$\Phi = N \frac{4\pi R^3}{3(L + 2A)l^2}\cdot$$

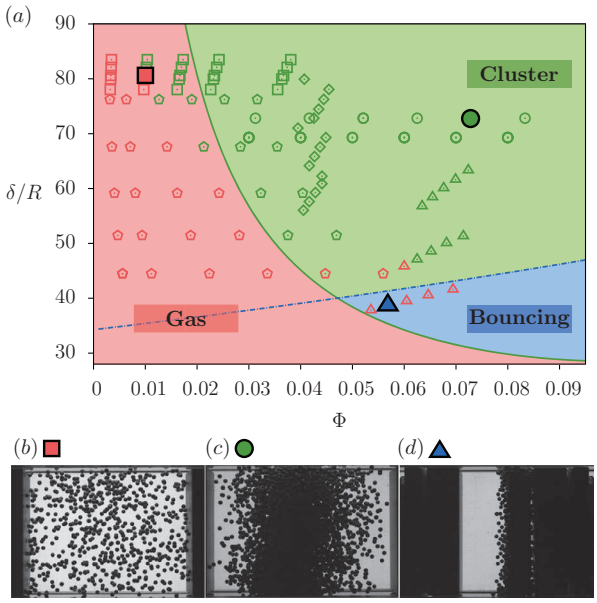

Fig. 3: (Color online) (a) Phase diagram of the dynamical regimes, observed in the PFC experiments, as a function of the dimensionless system size, δ/R, and the packing fraction, ϕ. The experimental parameters and corresponding symbols are listed in table 1. Granular gas (red), cluster (green), and bouncing (blue) regimes are detected with a statistical test (see text). The theoretical solid line is from eq. (4) with $C_0 = 1$, $R_0 = 2$, and $\epsilon = 0.9$. The dashed line corresponds to the right-hand term of eq. (5). Bottom: typical front views of the cell showing gas (b), cluster (c) and bouncing (d) regimes corresponding to the plain symbols in (a).

The instrument geometry limits the accessible region of the phase diagram to $30 < \delta/R < 90$. All experiments performed during PFCs are represented by symbols which correspond to sets of parameters listed in table 1. The solid curve plotted in the phase diagram is the theoretical frontier separating the gaseous regime from the cluster one. This marginal curve comes from a theoretical model comparing the decay time of energy in the system (Haff time [11]) and the time needed for a particle to cross the whole cell in response to an energy impulse coming from the pistons (propagation time), that is [18]

$$\frac{\delta}{R} = \frac{1}{3\Phi} \frac{\ln\left[1 + \frac{C_0}{\varepsilon(1+\varepsilon)(1-3R_0\Phi)}\right]}{\ln\left(1/\varepsilon\right)}, \qquad (4)$$

where ε is the restitution coefficient of the particles and C_0 and R_0 are two adjustable parameters whose values have been evaluated with the help of numerical simulations. The theoretical model of eq. (4) is found to be in good agreement with most experiments (see fig. 3). However, for $\Phi < 3\%$ and $\delta/R \gtrsim 75$, the agreement is not so good (see top left-hand side in fig. 3). This corresponds to experiments performed with a large cell in a diluted regime where the cluster formation is probably induced by g-jitters. Indeed, as soon as a cluster is formed (*e.g.*, by a tiny variation of g), its destruction is very hard to be done since it is located far from the oscillating pistons. The model which considers a uniform distribution of the positions of the particles as initial condition is consequently less adapted in this region of the phase diagram than in others.

The bouncing regime has been only observed for a very narrow cell ($\delta/R \sim 38$, or $L \sim 12.5d$), and has been previously reported numerically for the same configuration as ours [15]. For a configuration where the whole container is vibrated, the condition to observe a bouncing aggregate is predicted theoretically to be $A > (L-e)/\pi$, e being the aggregate thickness [19,21,23]. This means that the cluster center of mass follows the container oscillations when the amplitude of vibration is larger than a fraction of the free space $(L-e)$ between the cluster and the container walls. By adapting this model to our configuration (container walls vibrated in phase opposition), we find that the bouncing regime occurs within a bounded region by the following conditions:

$$\left(\frac{\pi + 2\Phi/\phi_{\mathrm{RLP}}}{1-\Phi/\phi_{\mathrm{RLP}}} - 2\right) < \frac{L}{A} < \left(\frac{2\pi + 2\Phi/\phi_{\mathrm{RLP}}}{1-\Phi/\phi_{\mathrm{RLP}}} - 2\right), \qquad (5)$$

where $\phi_{\mathrm{RLP}} = 0.59$ is the density of a random loose packing pile [24]. Only the upper limit of eq. (5) is visible in fig. 3 (see dashed line separating the cluster region from the bouncing one). Even though the agreement with the single experimental point is good, more experiments are needed to confirm this theory. Finally, note that the analogous of a triple point (δ_t/R, Φ_t) can be defined by the intercept of the two marginal curves within the phase diagram, *i.e.*, by balancing eq. (4) with the right-hand term in eq. (5).

Conclusion. – We have experimentally investigated the gas-like to clustering transition in a driven granular media in 3D low-gravity environment. Experimental parameters have been exhaustively varied (number of particles, cell size, and vibrational parameters). We have observed three dynamical regimes: Granular gas, cluster and bouncing aggregate. These regimes have been characterized by means of two perpendicular cameras leading to the spatial distribution of particles within the cell. We transformed the shadow density measured on each image into profiles of particle density along the vibration axis of the cell. Then, a statistical Kolmogorov-Smirnov test has been performed to compare these experimental distributions with uniform ones in order to deduce the state reached by the system (gas, cluster or bouncing aggregate). The results of these tests were reported in a phase diagram and confronted with theoretical models for the gas-cluster transition and the emergence of the bouncing aggregate. The experimental results are in excellent agreement with the theoretical predictions, except for large and diluted systems where the g-jitters, as small as they can be, have probably a non-negligible impact on the final state of the system. To reach a high level of low-gravity conditions ($\sim 10^{-5}g$) where g-jitters are negligible,

the VIP-Gran instrument is currently in development for the International Space Station. We have thus shown that the gas to clustering transition occurs when the typical propagation time between two collisions is of the order of the relaxation time due to dissipative collisions. This study could lead to applications for space exploration (*e.g.*, handling a granular medium in low gravity by applying vibrations) or to a better understanding of the dynamics of planetary rings in astrophysics.

* * *

We thank M. Braibanti, O. Minster and V. Koehne from ESA for fruitful discussions and for the flight opportunity. VIP-Gran-PF was built by DTM Technologies™ (Modena, Italy). We acknowledge A. Pellegrini, L. Recanatesi, and D. Santachiara from DTM, T. Trittel, University of Madeburg, for technical support, and M. Hou for discussions. We acknowledge the support of Novespace during PFC63 to PFC67, and partial financial support by CNES. This work was funded by ESA Topical Team No. 4000103461.

REFERENCES

[1] de Gennes P. G., *Rev. Mod. Phys.*, **57** (1985) 827.
[2] Liu A. J. and Nagel S. R., *Nature*, **396** (1998) 21.
[3] Corwin E. I., Jaeger H. M. and Nagel S. R., *Nature*, **435** (2005) 1075.
[4] Majmudar T. S. and Behringer R. P., *Nature*, **435** (2005) 1079; Ren J., Dijksman J. A. and Behringer R. P., *Phys. Rev. Lett.*, **110** (2013) 018302.
[5] Jaeger H. M., Liu C. and Nagel S. R., *Phys. Rev. Lett.*, **62** (1988) 1.
[6] Falcon E., Fauve S. and Laroche C., *Eur. Phys. J. B*, **9** (1999) 183.
[7] Falcon E., Aumaître S., Evesque P., Palencia F., Lecoutre-Chabot C., Fauve S., Beysens D. and Garrabos Y., *EPL*, **74** (2006) 830.
[8] Puglisi A., Loreto V., Marconi U. M. B., Petri A. and Vulpiani A., *Phys. Rev. Lett.*, **81** (1998) 3848; Losert W., Cooper D. G. W., Delour J., Kudrolli A. and Gollub J. P., *Chaos*, **9** (1999) 682; Olafsen J. S. and Urbach J. S., *Phys. Rev. E*, **60** (1999) R2468(R); Rouyer F. and Menon N., *Phys. Rev. Lett.*, **85** (2000) 3676; van Zon J. S., Kreft J., Goldman D. I., Miracle D., Swift J. B. and Swinney H. L., *Phys. Rev. E*, **70** (2004) 040301(R); Harth K., Kornek U., Trittel T., Strachauer U., Höme S., Will K. and Stannarius R., *Phys. Rev. Lett.*, **110** (2013) 144102; Scholz C. and Pöschel T., *Phys. Rev. Lett.*, **118** (2017) 198003.
[9] McNamara S., *Phys. Fluids*, **5** (1993) 3056; Goldhirsch I. and Zanetti G., *Phys. Rev. Lett.*, **70** (1993) 1619; Brilliantov N., Salueña C., Schwager T. and Pöschel T., *Phys. Rev. Lett.*, **93** (2004) 134301.
[10] McNamara S. and Young W. R., *Phys. Fluids A*, **4** (1992) 496.
[11] Haff P. K., *J. Fluid Mech.*, **134** (1983) 401.
[12] Maass C. C., Isert N., Maret G. and Aegerter C. M., *Phys. Rev. Lett.*, **100** (2008) 248001; Grasselli Y., Bossis G. and Goutallier G., *EPL*, **86** (2009) 60007; Tatsumi S., Murayama Y., Hayakawa H. and Sano M., *J. Fluid Mech.*, **641** (2009) 521; Harth K., Trittel T., Wegner S. and Stannarius R., *Phys. Rev. Lett.*, **120** (2018) 214301.
[13] Kudrolli A., Wolpert M. and Gollub J. P., *Phys. Rev. Lett.*, **78** (1997) 1383.
[14] Falcon E., Wunenburger R., Évesque P., Fauve S., Chabot C., Garrabos Y. and Beysens D., *Phys. Rev. Lett.*, **83** (1999) 440.
[15] Opsomer E., Ludewig F. and Vandewalle N., *Phys. Rev. E*, **84** (2011) 051306.
[16] See `https://spacegrains.org`.
[17] Aumaître S., Behringer R. P., Cazaubiel A., Clément E., Crassous J., Durian D. J., Falcon E., Fauve S., Fischer D., Garcimartín A., Garrabos Y., Hou M., Jia X., Lecoutre C., Luding S., Mazza D., Noirhomme M., Opsomer E., Palencia F., Pöschel T., Schockmel J., Schröter M., Sperl M., Stannarius R., Vandewalle N. and Yu P., *Rev. Sci. Instrum.*, **89** (2018) 075103.
[18] Opsomer E., Ludewig F. and Vandewalle N., *EPL*, **99** (2012) 40001.
[19] Bannerman M. N., Kollmer J. E., Sack A., Heckel M., Mueller P. and Pöschel T., *Phys. Rev. E*, **84** (2011) 011301; Sack A., Heckel M., Kollmer J. E., Zimber F. and Pöschel T., *Phys. Rev. Lett.*, **111** (2013) 018001; Kollmer J. E., Tupy M., Heckel M., Sack A. and Pöschel T., *Phys. Rev. Appl.*, **3** (2015) 024007.
[20] Opsomer E., PhD Thesis, Univ. Liège (2014).
[21] Kollmer J. E., Sack A., Heckel M. and Pöschel T., *New J. Phys.*, **15** (2013) 093023.
[22] Schindelin J., Arganda-Carreras I., Frise E., Kaynig V., Longair M., Pietzsch T., Preibisch S., Rueden C., Saalfeld S., Schmid B., Tinevez J.-Y., White D. J., Hartenstein V., Eliceiri K., Tomancak P. and Cardona A., *Nat. Methods*, **9** (2012) 676.
[23] Gilet T., Vandewalle N. and Dorbolo S., *Phys. Rev. E*, **79** (2009) 055201(R).
[24] O'Hern C. S., Langer S. A., Liu A. J. and Nagel S. R., *Phys. Rev. Lett.*, **88** (2002) 075507; Onoda G. Y. and Liniger E. G., *Phys. Rev. Lett.*, **64** (1990) 2727; Jerkins M., Schröter M., Swinney H. L., Senden T. J., Saadatfar M. and Aste T., *Phys. Rev. Lett.*, **101** (2008) 018301.

Threshold of gas-like to clustering transition in driven granular media in low-gravity environment

M. Noirhomme, A. Cazaubiel, A. Darras, E. Falcon, D. Fischer, Y. Garrabos, C. Lecoutre-Chabot, S. Merminod, E. Opsomer, F. Palencia, J. Schockmel, R. Stannarius and N. Vandewalle

Supplementary material

The aim of this supplementary material is to derive Eq. (2) from Eq. (1) of the main text.

By assuming a uniform distribution of the grains in the slice, the probability of presence of one grain in a specific column is $p = d/l$. If the slice contains N_y particles, the probability $P(X = n)$ of finding n grains in the column is given by the binomial distribution

$$P(X = n) = \binom{N_y}{n} p^n \, (1-p)^{N_y - n} \,, \tag{1}$$

where X is the random variable representing the number of grains in a column, and $\binom{N_y}{n} = N_y!/[n!(N_y - n)!]$ the binomial coefficient. Remembering that the number of particles n in each column being actually unknown, the number of particles in the slice is a priori unknown too. However, one might observe the realization of the event $X = 0$. Effectively, if there is no grain in a column, the light will go through the system and reach the camera. A white zone is then detected in the corresponding square. Using the previous equation, we deduce the probability to observe a white zone as

$$P(X = 0) = (1-p)^{N_y} \,.$$

In order to deduce the relationship between the observable shadow density s_x and the likely number of particles from which it comes N_y, we introduce the random variable O_x which quantifies the shadow, casted by the particles in the related column. This random variable is defined as

$$O_x = \begin{cases} 0 \text{ if } X = 0 \\ 1 \text{ if } X \geq 1 \end{cases},$$

with the associated probabilities $P(O_x = 0) = P(X = 0)$ and $P(O_x = 1) = 1 - (1-p)^{N_y}$. The expected value of the random variable O_x is given by $E[O_x] = 1 - (1-p)^{N_y}$. To estimate this expected value, we introduce finally the observable o_x as the number of

black pixels in the square divided by the surface of the square expressed in pixels. The average of this observable is not only the estimator of the expected value but also the measured shadow density, $s_x = \langle o_x \rangle = E[O_x]$, and one finds finally

$$s_x = 1 - (1-p)^{N_y} \, .$$

By isolating N_y in this last relation, we found the most probable number of particles in the slice. One obtains

$$N_y = \frac{\ln(1-s_x)}{\ln(1-d/l)} \cdot \tag{2}$$

Chapter 4

Growth of the cluster

4.1 Introduction

The transition from a granular gas to a cluster is now well-defined, modeled and experimentally verified [36, 56]. Indeed, for a given system of fixed dimensions, the exact number of particles to be put in the cell to trigger the transition is known. However, one can wonder what happens once the transition has taken place, i.e. once a cluster emerged in the system. The questions addressed in this chapter are:

- Where is the cluster born? Is it created right in the middle of the cell?
- Once created, what is the growth mechanism and what is its morphology?

Even though the gas-cluster phase transition has been already investigated before this work, the structure and the growth of dynamical clusters in three dimensions were not studied in the literature. Nevertheless, Luu *et al.* were able to make a beautiful analogy between granular and fluid systems in two dimensions [57] by deducing a granular surface tension γ from their experiments. This result is remarkable since no cohesive forces are present in their granular assembly. The experiment consists of horizontally vibrated millimetric spheres confined in a quasi-2D system (of approximative dimensions $L^2(2d)$, where $L = 100$ mm and d is the diameter of the grains). The neighborhood of each particle was studied thanks to image analysis. Based on a local density criterion, Luu *et al.* were able to sort the particles into two categories, one "gas" and the other "liquid". Thanks to this classification, they defined a gas-liquid interface for each image of the experiment (see the solid white line in Fig. 4.1). By averaging these interfaces over time, the average structure of a 2D cluster could be found (see the dashed white curve in Fig. 4.1). Finally, by studying the fluctuations around this average interface, the granular surface tension could be determined. They found $\gamma = 1.5 \pm 0.1$ mN/m, which is about 50 times less than the surface tension of water.

Inspired by the work of Luu [57], we studied the morphology of clusters in three dimensions. Unfortunately, the experimental determination of the positions of all the particles composing a dynamical cluster requires to see inside the system, which is not possible using the VIP-Gran instrument in its current configuration. One possibility would be to mount a camera in the axis of excitation of the instrument (i.e. inside one of the pistons) but it seems that it is a complicated engineering task. Therefore, we numerically studied the clustering in VIP-Gran and in many others geometries. By varying the number of grains in each simulated cell, we were able to identify the places where the clusters were born and their growth mechanism.

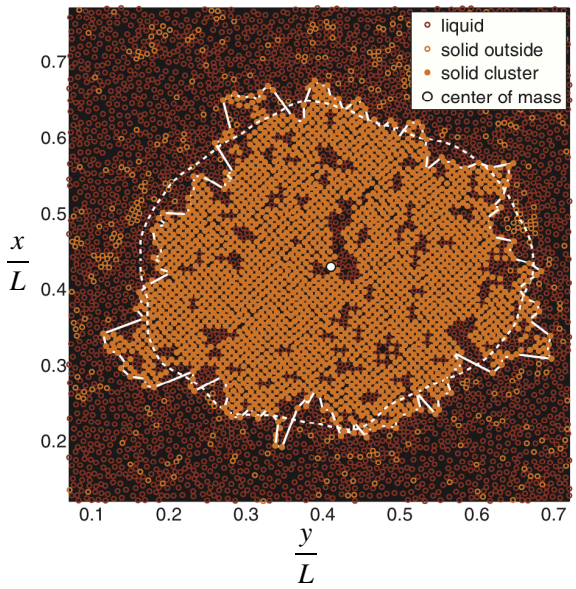

Figure 4.1: Taken from [57]. Millimetric particles are enclosed in a 2D setup and behave as a gas (dark braun) or a liquid (orange). By comparing the fluctuations of the interface (solid white line) around its average position (dashed line), a granular surface tension can be defined.

4.2 Numerical setup

4.2.1 SSDEM model

The simulations were performed using a SSDEM (for Soft Sphere Discrete Element Method) algorithm [58–60]. This model is able to predict the positions of the particles in the system by integrating the forces which act on them. Repulsive normal forces are modeled by a linear spring-dashpot in which the loss of energy due to the inelastic collisions is characterized by the restitution coefficient ε (already defined before). In practice, ε allows to define a viscous coefficient that is purely numeric and that models a viscous dissipation during the contact between particles. Tangential forces are computed by using a regularized form of the Coulomb's law. This model states that a sliding friction force appears at the contact between the particles. This force is proportional to the normal force, except for slow sliding velocities. In that case, the tangential force is proportional to the sliding velocity and to a purely numerical constant, in order to avoid divergence for $v = 0$ in static situations .

4.2.2 Parameters

One advantage of numerical simulations is the freedom concerning the choice of the parameters to investigate. For this study, we changed the following parameters of the VIP-Gran experiment: the length L and the width l of the cell, the frequency

#		L(mm)	l(mm)	f(Hz)	N	ϕ_c (%)
1	□	40	15	20	[500; 6500]	6.08 ± 0.09
2	□	40	15	40	[600; 5000]	6.08 ± 0.09
3	▽	40	25	20	[3000; 15000]	6.24 ± 0.13
4	○	50	15	20	[1000; 6000]	5.44 ± 0.21
5	△	**60**	**30**	**20**	[**1000**; **30000**]	**4.65 ± 0.09**
6	◇	90	15	20	[1000; 10000]	3.57 ± 0.06
7	⬠	150	15	20	[1000; 19000]	3.10 ± 0.19

Table 4.1: Parameters for the 7 different cells. The number of particles has been varied in order to observe the birth and the growth of the dynamical clusters in the different geometries. The constant critical packing fraction of the gaseous phase is denoted in the last column.

f of oscillation of the pistons and the number N of particles in the container. The radius R of the particles and the restitution coefficient ε, as well as the amplitude A of oscillation of the pistons have been kept constant. Table 4.1 gives the parameters investigated for seven different cells. For a given cell, the main measurements were realized as a function of the total packing fraction ϕ of the system. The latter is defined as $\phi = NV_{\text{sph}}/V_{\text{cell}}$, where V_{sph} and $V_{\text{cell}} = Ll^2$ are respectively the volume of a single particle and the mean volume of the cell.

4.3 Main results

In all configurations, we observed either a granular gas or the formation of a cluster. This cluster emerged always in one of the corners of the cell and was systematically surrounded by a less dense gaseous phase. We have followed the structure of the clusters as well as the properties of the two coexisting phases, i.e. the volume fraction and the packing fraction of the gas and the cluster. In order to determine if a particle is included in one phase or in the other, we performed Voronoi tessellations on the system in order to deduce the local density around each particle, noted ϕ_{loc}. According to [36], we have postulated that a grain belongs to the cluster if $\phi_{\text{loc}} \geq 0.285$. This value corresponds to a situation for which a grain is no longer able to escape the cage that its neighbors form around it. Given this sorting, we measured the number of grains N_{Cl} and N_{g} belonging to the cluster and to the gas. Based on the volumes of each Voronoi cell, we measured the volumes of both phases, noted V_{Cl} and of V_{g}. Finally, we defined the mean packing fraction of the cluster and the gas as

$$\Phi_i = \left\langle \frac{N_i V_{\text{sph}}}{V_i} \right\rangle, \tag{4.1}$$

where $i \in \{\text{Cl}, \text{g}\}$ and where the average is made over the entire simulation, once the stationary state is reached. We also followed the volume fraction of the cluster, denoted x and defined as

$$x = \left\langle \frac{V_{\text{Cl}}}{V_{\text{cell}}} \right\rangle. \tag{4.2}$$

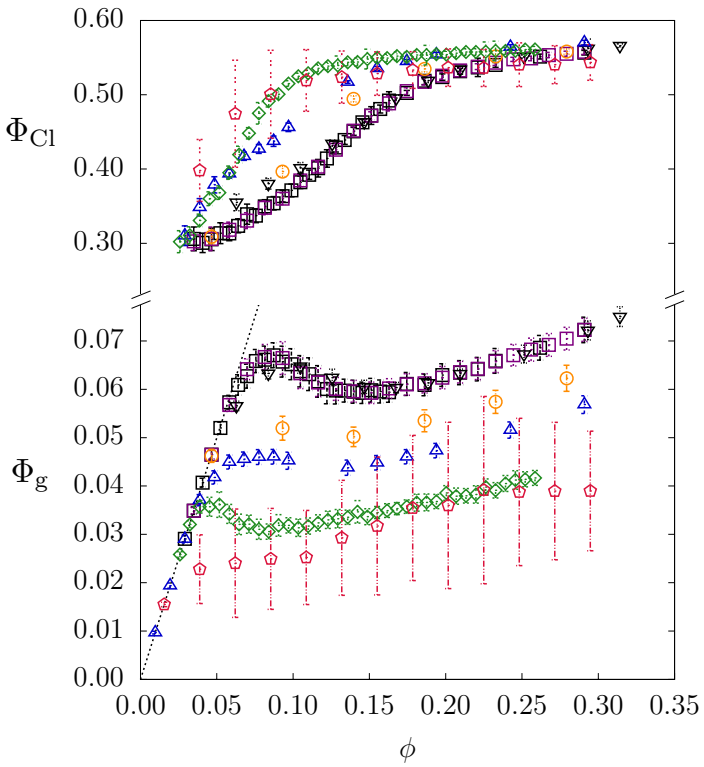

Figure 4.2: Mean packing fraction of the clusters (Φ_{Cl}) and the gases (Φ_g) as a function of the total packing fraction of the system ϕ for the 7 different cells. As long as the critical packing fraction of the gas ϕ_c is not crossed, no cluster is present and $\Phi_g = \phi$. Past this critical value, Φ_g remains approximatively equal to the critical packing fraction ϕ_c while Φ_{Cl} increases until a saturating value which is nothing else than the Random Loose Packing Φ_{RLP}.

The mean packing fractions of the cluster and the gas as well as the volume fraction of the cluster are depicted in Figs. 4.2 and 4.3 as a function of the total packing fraction of the system ϕ.

Two main results have been obtained during this study. First, we have shown that the formation, compaction and growth of the cluster are driven by the fact that the gaseous phase has to keep a constant critical mean packing fraction ϕ_c (see the bottom of Fig. 4.2). This critical packing fraction corresponds to the emergence of condensation. Secondly, we found that the cluster's form depends on the packing fraction of the system and can be either a truncated tori or a filled parallelepiped. These specific morphologies can be found by studying the occupancy of the cell, defined as the regions of the container that are frequently occupied by the clustered particles. In Fig. 4.4, the occupancy of the container has been plotted as a function of the packing fraction ϕ of the system. In this figure, snapshots of the simulations where the gaseous particles have been hidden are also depicted in order to highlight the importance of the occupancy measurements. Clearly, the structure is much

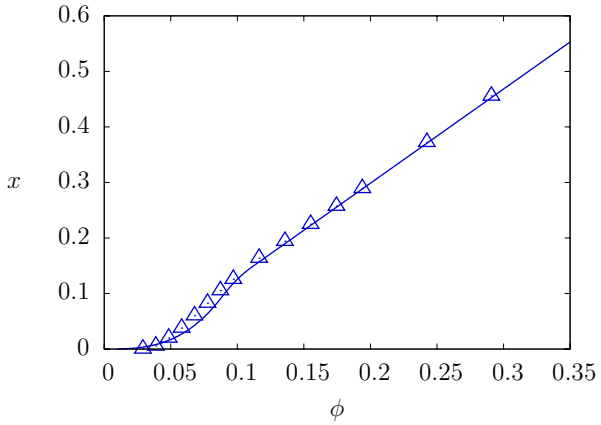

Figure 4.3: Volume fraction of the cluster in the case of the VIP-Gran cell (# 5 in Tab. 4.1). The growth of the cluster is linear for $\phi > 0.1$, when the cluster fills the full width of the cell (see Figure 4.4). The volume fraction increase can be linked to the cluster surface according to Eq. (4.4).

easier to identify by using the occupancy since this measurement is an average. Thanks to the measurements of the occupancy of the container, we have found that the cluster is born in "cold" regions of the system (i.e. in the corners of the box, as far as possible from the pistons). Furthermore, we proposed a model for the growth of the cluster in which the capture of the gaseous grains is a surface phenomenon. Mathematically, we were able to deduce the evolution of the packing fraction Φ_{Cl} and the volume fraction x of the cluster as a function of ϕ. By expressing the conservation of mass in the system, one finds

$$\Phi_{\mathrm{Cl}}(\phi) = \frac{1}{x(\phi)}\,(\phi - \phi_c) + \phi_c. \tag{4.3}$$

The volume fraction x of the cluster is defined as the sum of the volumes of each Voronoi cell corresponding to caged grains, divided by the volume of the container. The variation of this function is given by

$$dx(\phi) = CS(\phi)vd\phi, \tag{4.4}$$

where C is the capture rate of the cluster, $S(\phi)$ is its surface, and $v = V_{\mathrm{sph}}/(0.285V_{\mathrm{cell}})$ is the normalized volume of a newly caged particle. The value and the origin of the capture rates that we observed in our different systems are developed in the next section.

The behaviors highlighted above are not without reminding the condensation mechanism of a molecular gas in which the nucleation of the molecules appears when the pressure of the environment exceeds the saturation vapor pressure.

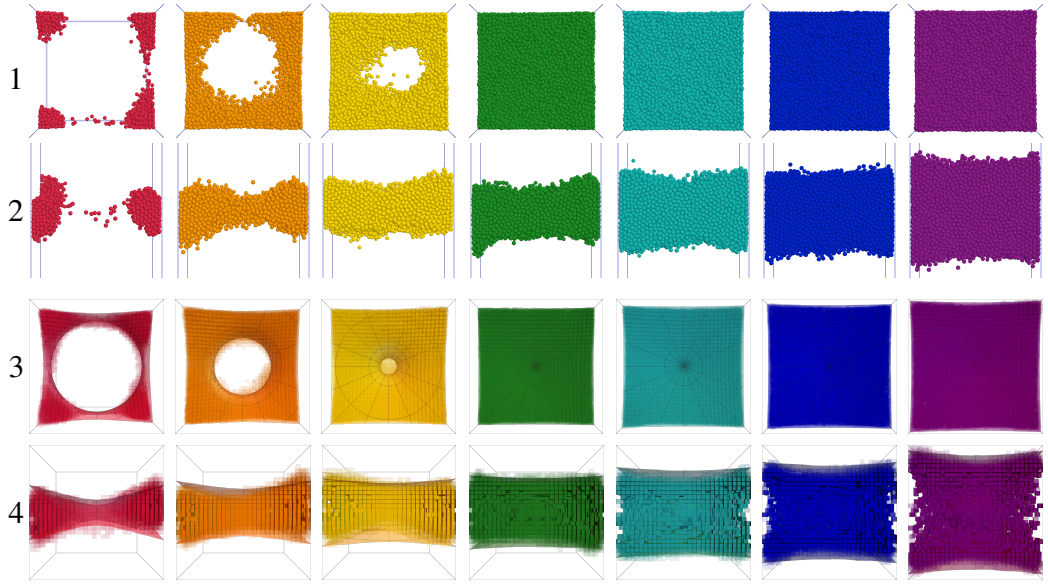

(a) $\phi = 5.8\%$ (b) $\phi = 7.6\%$ (c) $\phi = 9.7\%$ (d) $\phi = 13.6\%$ (e) $\phi = 17.5\%$ (f) $\phi = 19.4\%$ (g) $\phi = 24.2\%$

Figure 4.4: Lines 1 and 2: Bottom and front snapshots of the simulations performed in the case of the fifth cell (see Tab 4.1) for increasing total packing fractions. The gaseous particles (i.e. the one which present a local packing fraction less than 0.285) have been hidden. Lines 3 and 4: Bottom and front views of the occupancy of the cell for increasing total packing fractions. The opacity is high if the regions of the container are frequently occupied by clustered particles. The occupancy allows to see the spatial mean structure of the clusters.

4.4 Complementary measures

4.4.1 Capture rates

As explained in the article, it is the fact that the granular gas has to keep its packing fraction constant ($\Phi_g = \phi_c$) that drives the cluster's growth. The value of this constant ϕ_c, given in Tab. 4.1, varies with the geometry of the system. Let us suppose that the total packing fraction of the system has reached this critical value and that a number dn of particles is added in the container. As a consequence, the grains will separate into two phases. A gaseous phase of packing fraction ϕ_c and a clustered phase with $\Phi_{Cl} > \phi_c$. As long as the cluster has a roughly constant packing fraction, the increase of volume of the clustered phase can be linked to the number of added grains by

$$dV_{Cl} = a\frac{V_{sph}}{0.285}dn. \tag{4.5}$$

The constant a indicates the fact that the gas phase loses particles while the cluster grows in order to maintain ϕ_c constant. As a consequence, the number of grains which will gather in the cluster is higher than only dn and a should be larger than 1, as far as the cluster has a constant packing fraction. Normalizing the last equation by V_{cell} and defining $d\phi = dnV_{sph}/V_{cell}$, the increase of the volume fraction of the cluster can be expressed by

$$dx = \frac{a}{0.285}d\phi. \tag{4.6}$$

As mentioned before, this last equation is valid as soon as the cluster has reached a roughly constant packing fraction, that is, in the linear part of Fig. 4.3 (for $\phi >\sim 0.1$). Finally, assuming that the coefficient a is proportional to the cluster surface and that the cluster had a constant capture rate C [by postulating $a(\phi) = CS(\phi)$], we find Eq. (4.4).

4.4.2 Tri excitation

In this section, we focus on a system with an identical geometry as the cell 5 (see Tab. 4.1). The main difference here is that all the facing walls are oscillating in phase opposition with the same frequency $f = 20$ Hz and the same amplitude $A = 1$ mm. We followed the volume fraction of the cluster x, as well as its density Φ_{Cl} as a function of the total packing fraction in the system. We also studied the morphology of the cluster in this tri-excited system, exactly as what was done for all the other systems. As expected, the cluster arises in the coldest region of the cell, which is located at the geometric center of the container, as far as possible of the 6 pistons. The form taken by the clustered phase is elliptical and the growth of the cluster is linear with the packing fraction of the system, as shown in Fig. 4.5 and 4.6.

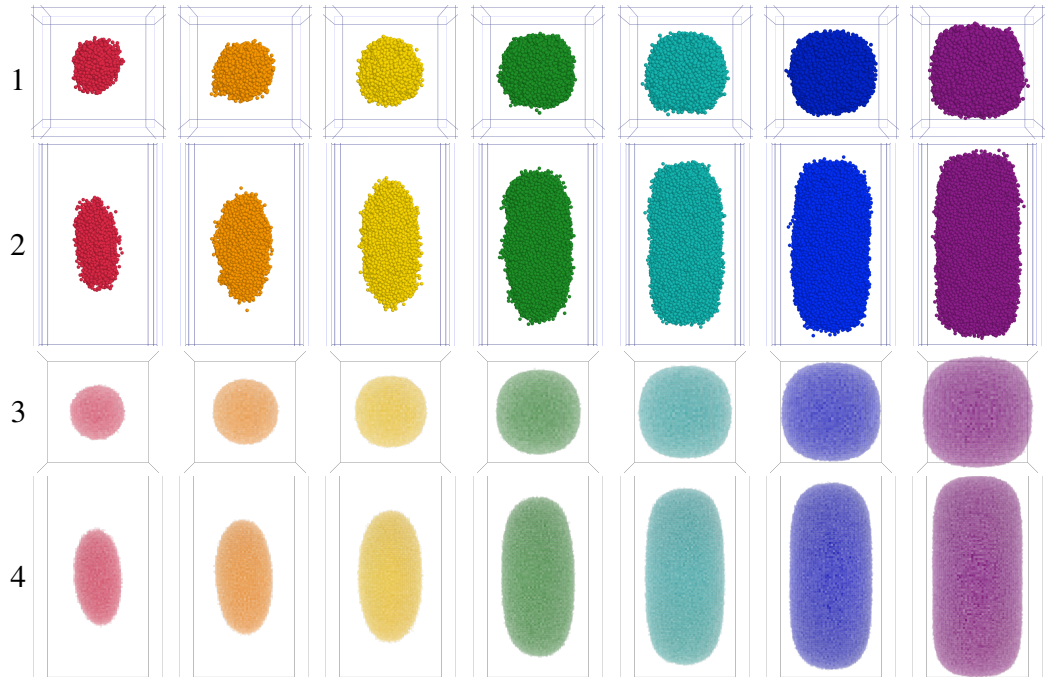

(a) $\phi = 5.8\%$ (b) $\phi = 7.6\%$ (c) $\phi = 9.7\%$ (d) $\phi = 14.5\%$ (e) $\phi = 18.4\%$ (f) $\phi = 20.4\%$ (g) $\phi = 30.1\%$

Figure 4.5: Bottom (line 1) and front (line 2) views of snapshots of the simulation for the tri-excited system, for which all plates of the container are beating in phase opposition, where only the clustered particles are drawn. Lines 3 and 4: Bottom and front view of the occupancy of the container for increasing total packing fraction. In this tri-excited system, the structure of the cluster is elliptical and its birth is done at the center of the container, as far as possible of the hot pistons.

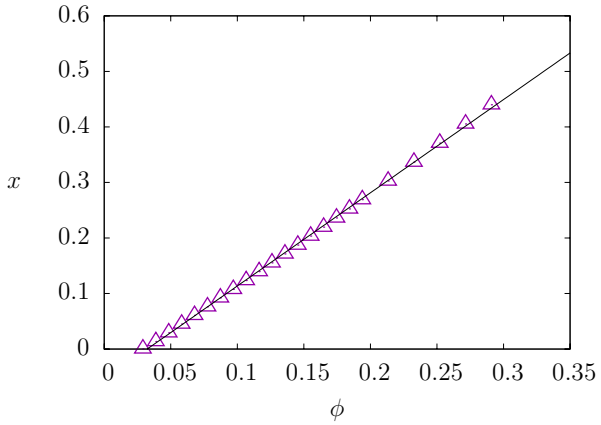

Figure 4.6: Volume fraction of the cluster in the case of the VIP-Gran cell where each plate is oscillating with the same frequency and the same amplitude (see Fig. 4.5 for examples of observed clusters). The cluster growth is in this case entirely linear, reporting the fact that no structural transition takes place. The cluster is indeed always elliptical when the external excitation is given in the three directions x, y and z.

4.5 Summary

This numerical study led to a better understanding of the condensation and growing mechanisms of granular material submitted to an external agitation. Simulations were based on a SSDEM model that does not take the attractive gravitational force that acts between the grains into account. Despite the fact that we have not been able to give a value of the granular surface tension, in the spirit of Luu's experiment, a nice analogy with fluid dynamics was highlighted. Indeed, we have shown that a dynamical cluster is able to cage particles on its own surface by forcing the gaseous particles to condensate.

PHYSICAL REVIEW E **95**, 022905 (2017)

Cluster growth in driven granular gases

Martial Noirhomme,* François Ludewig, Nicolas Vandewalle, and Eric Opsomer
GRASP Laboratory, CESAM Research Unit, Physics Department, B5a, University of Liège, B-4000-Liège, Belgium
(Received 28 September 2016; published 23 February 2017)

We investigate numerically and theoretically the internal structures of a driven granular gas in cuboidal cell geometries. Clustering is reported and particles are classified as gaseous or clustered via a local packing fraction criterion based on a Voronoi tessellation. We observe that small clusters arise in the corners of the box, elucidating early reports of partial clustering. These aggregates have a condensation-like surface growth. When a critical size is reached, a structural transition occurs and all clusters merge together, leaving a hole in the center of the cell. This hole then becomes the new center of particle capture. Taking into account all structural modifications and defining a saturation packing fraction, we propose an empirical model for the cluster growth.

DOI: 10.1103/PhysRevE.95.022905

I. INTRODUCTION

The behavior of granular matter, composed of noncohesive particles, depends on a wide variety of parameters. The balance between the energy injected into the system and the energy lost through the collisions between the grains is certainly the most important parameter controlling the state of the system. According to this energy balance, granular solids, liquids, or gases can be observed [1,2]. For granular gases submitted to a gravitational field, the loss of energy during collisions (inherent to granular matter) can lead to inhomogeneities called clusters in the system [3,4]. Taking advantage of these clusters, Maxwell's demon [5], granular clocks [6–8], and granular fountains [9–11] can be encountered in compartmentalized containers and explained via the particle fluxes between the compartments. Segregation [12] and Brownian motors [13] have also been observed.

Under microgravity conditions, clustering can emerge as well [14]. In these conditions, clusters appear during the cooling of a granular gas, and the kinetic energy of the system decreases according to Haff's law [15,16]. However, if the system is continuously driven, a single cluster, permanently excited by impacting energetic particles, appears. At a stationary state, the system keeps a constant nonzero kinetic energy and the clustering is then said to be "dynamical." This dynamical clustering has been observed in experiments [14] and in simulations [17,18] during the past two decades. Moreover, simulations have predicted collective behavior of granular gas (such as Maxwell's demon [19], segregation [20], and granular transport [21,22]) in microgravity. Finally, segregation has been observed recently during parabolic flight campaigns [23].

Despite the large amount of scientific interest, numerous open questions persist concerning the dynamics of clusters. For instance, the possibility of convection in a low-gravity environment that is submitted to external agitation is still a matter of debate. To tackle the fundamental questions relevant to granular material in space, the European Space Agency (ESA) started the SpaceGrains project [24]. The project consists in the study of granular gases within the VIP-Gran (vibration-induced phenomena in granular materials) instrument.

In previous work [18], based on the balance between the cooling time of a granular system and the time of energy transmission, the transition from a gaseous state to a dynamical cluster was rationalized. Parameters such as the dimensions of the container, the radius of the grains, and the packing fraction of the system play a key role [18]. Moreover, thanks to simulations, a minimal packing fraction leading to the apparition of a cluster could be estimated. Works based on a hydrostatic description of granular materials suggest another model for the gas-cluster transition [25,26]. Although this transition is currently well-understood and rationalized, the cluster as an entity on its own deserves deeper investigations. In this paper, we study numerically the internal structures of dynamical clusters within the framework of the VIP-Gran instrument (described in Sec. II). We focus on their morphology and highlight a complex surface growth mechanism analogous to condensing fluids.

II. SETUP

A. SpaceGrains project: The VIP-Gran cell

Inspired by the SpaceGrains project, we designed several cells of different geometries. All cells have a length denoted by L and a square section of side length denoted by l. The injection of energy is made through two oscillating plates (colored in Fig. 1) which have an amplitude denoted by $A = 1$ mm and a frequency f. The phase shift between the plates is fixed to $\varphi = \pi$. The positions of the pistons at time t are given by

$$z_1(t) = \frac{L}{2} + A\sin(2\pi f t + \varphi),$$
$$z_2(t) = -\frac{L}{2} + A\sin(2\pi f t). \tag{1}$$

Table I summarizes the parameters of the studied containers for seven different series of simulations. A sketch of the cell is given in Fig. 1. The VIP-Gran instrument is equipped with a "bead feeder" that allows us to increase the number of particles in the cell. The bead feeder consists of eight reservoirs that are filled with a chosen number of grains. These grains can be released sequentially into the cell. All cells are filled with different amounts of bronze spheres that have a

*mnoirhomme@ulg.ac.be

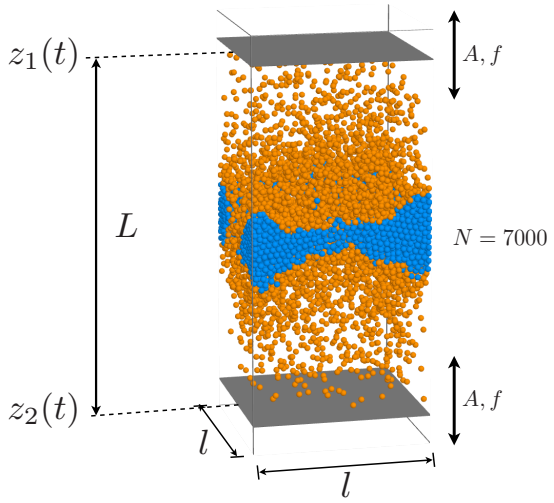

FIG. 1. Sketch of the simulated cell in the case of the VIP-Gran (short for vibration-induced phenomena in granular materials) experiment used in the simulations. The length and the width of the cell are denoted by L and l, respectively. The length is measured for an average position of the plates. The parameters of the oscillation of both pistons are an amplitude $A = 1$ mm and a frequency f. The clustered grains are colored in blue, while the gaseous particles are in orange. The total number of particles in the cell is $N = 7000$.

radius $R = 0.5$ mm and a density $\rho = 9500$ kg/m^3. To take into account the mechanical properties of bronze, a friction coefficient $\mu = 0.7$ and a coefficient of restitution $e = 0.9$ are chosen. Performing numerical simulations grants us a large amount of freedom concerning the choice of the parameters. Our strategy for tuning the parameters was the following: (i) We varied the packing fraction (by tuning the number of particles N) for each given cell in order to examine the morphology and the growth of the cluster in each geometry. (ii) The boundary effects of the side walls have been tested keeping L constant and varying l (lines 1 and 3 in Table I). (iii) The distance between the oscillating plates has been varied by keeping constant all other parameters in order to see if the maximal mean packing fraction reached by the cluster depends on the length of the cell L (lines 1, 4, 6, and 7 in Table I). (iv) We have verified that the frequency of the oscillating plates is a simple rescaling in time that does not affect the clustering mechanism. This work corresponds to lines 1 and 2 in Table I. The run corresponding to line 5 in Table I was performed in order to be implemented experimentally using the VIPGran instrument.

TABLE I. Parameters of the seven sets of simulations, called boxes in the main text. Figures 2, 3, and 4 are issued from the third line in bold. The fifth line corresponds to the VIP-Gran prototype. In all cases, the amplitude of the plate oscillation as well as the phase shift between these latter are fixed to $A = 1$ mm and $\varphi = \pi$, respectively. The ϕ_c value is the critical packing fraction above which a cluster can form in the system. This value can be predicted by the model developed in [18]. Symbols and colors used in the figures are given.

No.		L (mm)	l (mm)	f (Hz)	N	ϕ_c (%)
1	□	40	15	20	[500; 6500]	6.08 ± 0.09
2	□	40	15	40	[600; 5000]	6.08 ± 0.09
3	▽	**40**	**25**	**20**	[**3000**; **15 000**]	$\mathbf{6.24 \pm 0.13}$
4	○	50	15	20	[1000; 6000]	5.44 ± 0.21
5	△	60	30	20	[1000; 30 000]	4.65 ± 0.09
6	◇	90	15	20	[1000; 10 000]	3.57 ± 0.06
7	⬠	150	15	20	[1000; 19 000]	3.10 ± 0.19

B. Numerical approach

Based on the parameters defined above, we are able to predict the dynamics of the system via soft spheres discrete element method (SSDEM) simulations [18,19,27,28]. The SSDEM model computes normal and tangential forces based on the relative positions and velocities of the grains. Normal forces are given by a linear spring-dashpot model that takes into account the energy dissipation between the grains. Tangential forces are proportional to the relative velocities of the particles and bound via Coulomb's criterion. Integrating these forces, both positions and velocities of the particles can be computed. A complete description of the SSDEM algorithm is given in [29].

III. RESULTS

We investigated the internal structures and the packing properties of dynamical clusters as a function of the total packing fraction of the material. The latter is defined by $\phi = N V_{\text{sph}}/V_{\text{cell}}$, where N is the total number of particles, V_{sph} is the volume of a grain, and $V_{\text{cell}} = Ll^2$ is the mean volume of the cell.

To determine if a grain is in the cluster or in the gas phase, we realized Voronoi tessellations. The latter consist in partitioning space into N polyhedral cells, each centered on a grain called a "seed." A cell corresponds to a region in which all points are closer to the seed than to any other grain [30,31]. One obtains a local packing fraction ϕ_{loc} by dividing the volume of a particle by the volume of its Voronoi cell.

The probability density function (PDF) of the local packing fractions for different fillings of the box 3 (see Table I) are plotted in Fig. 2. For each filling, these PDFs are averaged over time once a stationary state is reached. For a low packing fraction of the system, i.e., for $\phi = 0.063$, a single and broad peak is observed about $\phi_{\text{loc}} \sim 0.05$, suggesting a collective gaseous behavior of the grains. For an increasing number of particles, this peak becomes less intense and a second peak appears at high ϕ_{loc} values. The first maximum tends to disappear at high total packing fraction, i.e., for $\phi > 0.189$. We observed, in these cases, an almost uniform distribution for the local packing fraction until $\phi_{\text{loc}} \sim 0.45$, after which the maximum grows in intensity. The apparition of this second peak at high ϕ_{loc} is a clear signature of clustering. It should be noted that ϕ_{loc} remains below 0.7 for all fillings, meaning that only disordered structures exist in the cell. No crystal is observed. These general observations have been made for all the simulations that we performed.

If the properties of cluster and gas phases have to be studied separately, it is essential that the grains belonging to either of

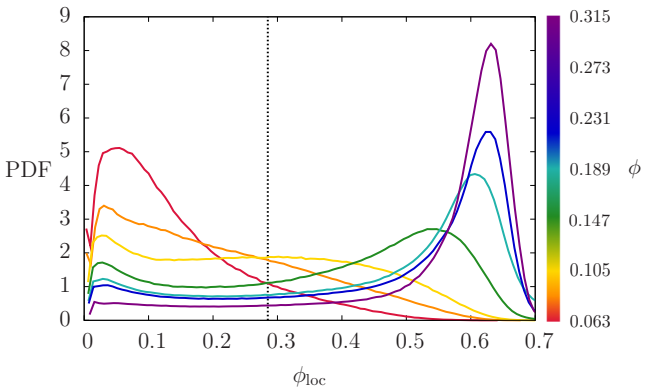

FIG. 2. Probability density function (PDF) of the local packing fraction $\phi_{\rm loc}$ of the grains in the case of cell number 3 (see Table I). Different colors correspond to different numbers of particles in the container, and therefore they correspond to different packing fraction ϕ values as noted in the legend at the right. The vertical dashed line $\phi_{\rm loc} = 0.285$ corresponds to the minimal local packing fraction of a caged grain used as a criterion to distinguish gas particles from cluster ones.

them can de distinguished. For this, we rely on a proximity criterion proposed in previous work [18]. A particle with a local packing fraction $\phi_{\rm loc}$ higher than 0.285 has no possibility to escape the cage formed by its neighbors and is thus considered as clustered. Thanks to this geometrical sorting, we defined the number of grains that form the cluster as $N_{\rm cl}$ and the number of particles in the gas phase as $N_{\rm g}$. In addition, we defined the volume of the cluster $V_{\rm cl}$ ($V_{\rm g}$) as the total volume of the Voronoi cells, which are related to the clustered (gaseous) grains. Finally, the sorting of the particles allows us to observe the cluster without the surrounding gas. Snapshots of these clusters are shown in Fig. 3 (lines 1 and 2) as a function of ϕ in the case of the third set of Table I. As shown in this figure, the clusters encountered in our simulations do not have the same structure for all ϕ. At low densities, four tiny aggregates are observed in the corners of the cell. For an increasing number of particles, the clusters grow and merge together, leaving a hole in the center of the container. The cluster is said to be "partial" as long as it does not spread over the entire horizontal plane. Similar partial clustering was already observed in [14] and numerically reproduced in [18]. For high (enough) ϕ, the hole is finally filled and the cluster is said to be "total." To explain these structural differences, we defined and studied the volume fraction of the cluster x and the related volume fraction of the gas $1 - x$. This quantity is simply given by

$$x = \frac{V_{\rm cl}}{V_{\rm cell}}. \tag{2}$$

Note that we have averaged these volume fractions over time, during the stationary state, for each ϕ. The volume fraction of the cluster x in the case of the third box (see Table I) is plotted as a function of ϕ in Fig. 4. The small fluctuations of x over time are limited, and the error bars have the size of the symbols. The evolution of $x(\phi)$ for low densities is not the same as it is for higher ones. Indeed, for $\phi < 0.15$ the growth of the cluster is accelerating, while for $\phi > 0.15$ the volume of the cluster seems to be a linear function of ϕ.

Knowing the number of particles of each species, we can define the mean packing fractions of the cluster and the gas,

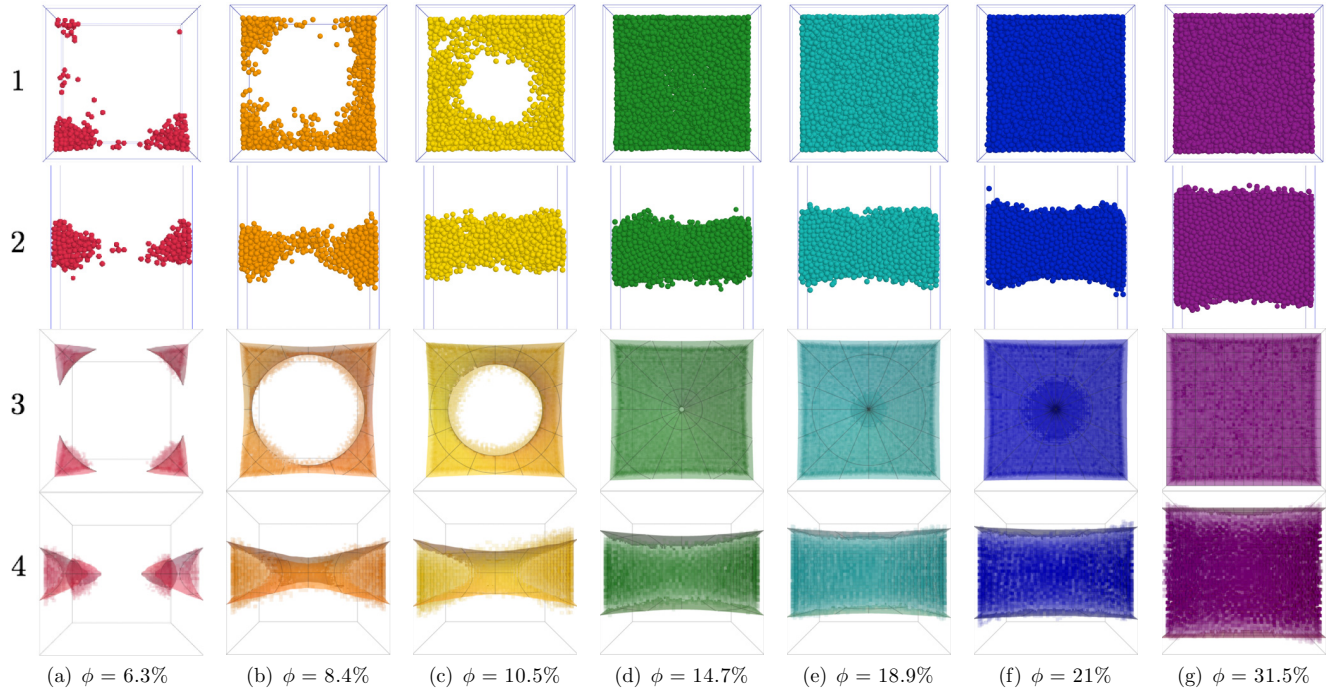

(a) $\phi = 6.3\%$ (b) $\phi = 8.4\%$ (c) $\phi = 10.5\%$ (d) $\phi = 14.7\%$ (e) $\phi = 18.9\%$ (f) $\phi = 21\%$ (g) $\phi = 31.5\%$

FIG. 3. Rows 1 and 2: top and front views of the center of cell number 3 for an increasing packing fraction ϕ. Only grains belonging to the cluster are shown, i.e., only grains with $\phi_{\rm loc} > 0.285$. Rows 3 and 4: top and front views of the occupancy (defined in Sec. IV B) of the same cell and structure of the interface gas-cluster for an increasing packing fraction. The color scale is the same as the one in Fig. 2. At low packing fraction values, the cluster appears in the corners of the box, and then it grows to form a single dense structure.

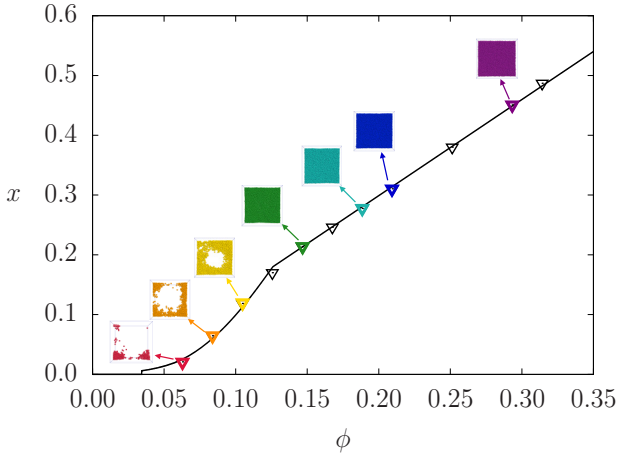

FIG. 4. Volume fraction of the cluster as a function of the total packing fraction of the cell 3. Before the apparition of the cluster, its volume is equal to zero. The curve is provided by Eq. (5) and is adjusted via the capture rate used in the modeling of the cluster's growth.

although averaged over time during the stationary state. These quantities are denoted by $\Phi_{\rm cl}$ and $\Phi_{\rm g}$, respectively, and they are defined by

$$\Phi_{\rm cl} = \frac{N_{\rm cl} V_{\rm sph}}{V_{\rm cl}}, \qquad \Phi_{\rm g} = \frac{N_{\rm g} V_{\rm sph}}{V_{\rm g}}. \tag{3}$$

These averaged mean packing fractions are plotted in Fig. 5 as a function of the total packing fraction of the cells. As shown in the bottom of this figure, at low ϕ, the mean packing fraction of the gas $\Phi_{\rm g}$ is equal to that of the system ϕ. Indeed, the grains exhibit a gaslike behavior with a mean free path of the order of L. There is no clustering. Above a critical value, denoted by $\phi_{\rm c}$, where the packing fraction of the gas reaches a maximum, $\Phi_{\rm g}$ becomes less dependent on ϕ (bottom of Fig. 5). Above $\phi_{\rm c}$, the variation of $\Phi_{\rm g}$ is of the order of 2% in comparison with that of the total packing fraction of the system. This result is remarkable and provides insight into the formation and the evolution of the cluster: the granular gas keeps its packing fraction nearly constant, which forces the additional grains to gather and form the cluster. An analogy with classical thermodynamics can be made here: the granular gas behaves like a real gas that has reached a saturation vapor pressure. Clerc *et al.* highlighted similar results in previous work [32]. Using a van der Waals model in a two-dimensional (2D) granular system, they found a critical density above which a liquid-solid-like transition occurs. Past this critical value, the pressure in the entire system was found to be constant. In the present work, where the van der Waals equation cannot be applied, this is only the packing fraction (linked to the granular pressure) of the gas phase that has been found constant. The error bars in Fig. 5 are small, except for the seventh cell, which has the highest length. The time required for a grain leaving the cluster to reach an oscillating plate is much larger in this geometry. The fluctuations of the mean packing fraction of the gas and the cluster are as a consequence much larger, too.

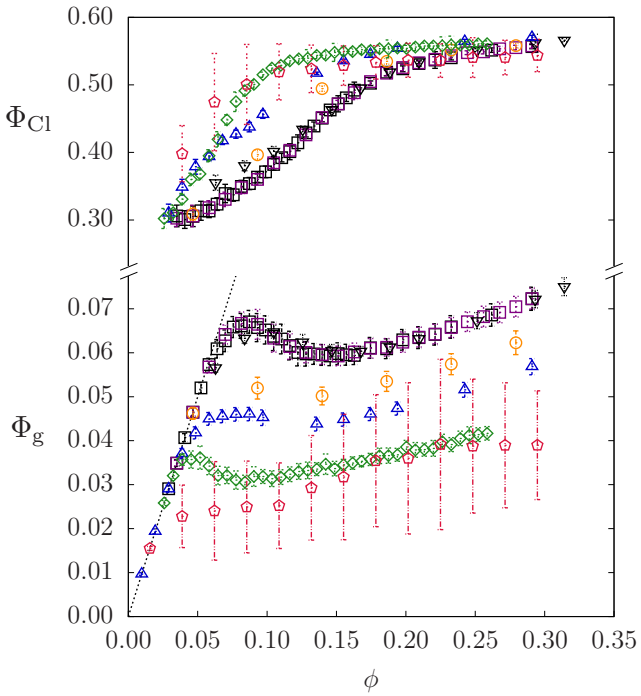

FIG. 5. Mean packing fraction in the gas phase ($\Phi_{\rm g}$) and the dynamical cluster ($\Phi_{\rm cl}$) as a function of the total packing fraction ϕ in each studied cell. The dashed line corresponds to $\Phi_{\rm g} = \phi$. Symbols are chosen according to the conditions listed in Table I.

We observed a compaction of the cluster when the number of particles in the system is increased (see the top of Fig. 5). Indeed, for a given cell (i.e., for a given line in Table I), the mean packing fraction of the cluster increases with ϕ. Past the transitional regime of partial clustering, $\Phi_{\rm cl}$ seems to saturate and to reach an asymptotic value, denoted $\Phi_{\rm cl,max}$. This maximal value is always lower than 0.7, meaning that the cluster is never in a crystalline phase. Depending on the geometry of the cells, some differences in $\Phi_{\rm cl}$ are observed. Varying only the horizontal dimension l of the system (lines 1 and 3 in Table I), we observed that $\Phi_{\rm cl}$ increases with l for fixed $\phi < 0.12$, meaning that partial clusters are denser in broad cells. The black triangles are systematically above the black squares in this region of Fig. 5. When ϕ is higher than 0.12, the mean packing fraction reached by the total cluster $\Phi_{\rm cl}$ seems to be the same for the two cells, and $\Phi_{\rm cl,max}$ is independent of l. On the contrary, by keeping a fixed $l = 15$ mm and varying only the vertical dimension of the cell L (cells 1, 2, 4, 6, and 7 in Table I), one observes that the formation of the total cluster is faster in the longer cell since the saturating regime is reached earlier (compare, for example, the green diamonds with the yellow circles in Fig. 5). In addition, for $\phi > 0.12$, $\Phi_{\rm cl,max}$ seems to be linked to L. Indeed, it appears that the maximal value of $\Phi_{\rm cl}$ (tending toward $\Phi_{\rm cl,max}$) increases with decreasing L. Finally, varying the frequency of the oscillating walls induces no difference in the measurements (see the black and purple squares in Fig. 5). This parameter impacts only the time needed to create the cluster since the loss of energy during the collisions between the grains is proportional to the relative velocity of the impacting particles.

IV. DISCUSSION

To understand the phenomena that we observe in our simulations, we propose a model for (i) the packing fraction of the gas, and (ii) the volume fraction of the cluster as a function of the packing fraction of the system. The packing fraction of the cluster (iii) can be deduced from the two quantities (i) and (ii), as explained in the next subsections.

A. Packing fraction of the gas

The first step of our model is to find the packing fraction of the granular gas. Thanks to our observations, we assumed a constant saturating vapor packing fraction of the gas after the cluster is formed. To support this assumption, we look back to a previous work [18] concerning the gas-cluster transition in similar cell geometries. In their paper, Opsomer *et al.* showed the existence of a critical value ϕ_c above which a cluster can form in the system. This critical value is directly linked to the dimensions of the system and the size of the grains. In our study, the packing fraction of the gas and that of the system are identical before the apparition of the cluster. Let us consider that the packing fraction of the gas Φ_g cannot be higher than the critical packing fraction. If $\Phi_g > \phi_c$, a part of the gaseous particles would aggregate and as a consequence decrease Φ_g. On the contrary, if we suppose that $\Phi_g < \phi_c$, the cluster would evaporate until equilibrium is reached again and $\Phi_g = \phi_c$. As a consequence, the packing fraction of the gas has to be equal to the critical value ϕ_c, even if the latter surrounds a cluster.

Considering that the particles have a classical behavior (i.e., that they adopt quasistraight trajectories) before the transition and that the mean packing fraction of the gas is constant after that, one has

$$\Phi_g = \begin{cases} \phi & \text{if} \quad \phi < \phi_c, \\ \phi_c & \text{if} \quad \phi \geqslant \phi_c. \end{cases} \tag{4}$$

The system is also considered in the gaseous phase as long as the mean packing fraction of the gas is equal to that of the system. The measured values of the critical packing fractions are given in Table I.

B. Volume and growth of the cluster

Our next step is to find a model describing the growth of the cluster as a function of ϕ. In recent works [33] concerning clustering of noncohesive particles in a 2D system, the aggregates were compared to a solid droplet in equilibrium with a surrounding liquid. Moreover, the authors were able to define a granular surface tension despite the absence of attractive forces between the particles. In analogy, we consider that our dynamical cluster is able to exchange particles with the surrounding gas at the interface between the gas and the cluster, like a liquid vapor that is condensing on a cold surface.

We consider that the system has a total packing fraction ϕ and has reached an equilibrium state where the packing fraction of the gas has the constant critical value ϕ_c. Given these hypotheses, if some particles are added in the system, they will automatically gather in the cluster. The volume fraction variation of the cluster can be expressed by

$$dx = C S(\phi) v \, d\phi, \tag{5}$$

where C is the capture rate of the cluster expressed in the number of particles per unit of surface, $S(\phi)$ is the surface of the gas-cluster interface, and $v = V_{\text{sph}}/(0.285 V_{\text{cell}})$ is the volume fraction of a newly caged particle. Note that C is *a priori* unknown.

The last (but not least) task is to define analytically the morphology of the cluster in order to have access to its surface. To find the shape of the cluster, we analyzed the regions of the containers that occupied the clusters during the entire simulations. We divided the cells into little cubes of size R^3 and defined their occupancy as follows: for each data record, if a cube contains the center of a clustered grain, its occupancy is incremented (starting from 0). At the end of the simulation, the occupancy of each cube is divided by the total number of records to obtain a value between 0 and 1. A region of the cell that has not contained any clustered particle has an occupancy equal to zero. Plotting the occupancy of the cell instead of the clustered grains permit us to smooth the structure of the cluster in addition to eliminating the gaseous grains. These plots are shown in the bottom of Fig. 3 (lines 3 and 4), where the opacity of each box was chosen as a function of the value of its occupancy. This first analysis provides a good idea of the shape adopted by a cluster. Actually, the best empirical structure we found to model the form of the cluster is a truncated elliptical torus, centered in the middle of the cell. This region is completely defined by the value of its radius, its semimajor axis, and its semiminor axis, denoted, respectively, by R_T, a, and b. The semiminor axis is always in the vertical direction, and the numerical analysis of the structure of the cluster allows us to assume a constant value. Indeed, we observed that the mean thickness of the cluster, measured at the vertical walls, remains roughly constant as long as the cluster is partial. The parameters R_T and a are related to the curvature of the gas-cluster interface. For convenience and in order to lighten the model, we decided to consider R_T as a constant and a as the variable that controls the morphology of the cluster.

The parameters a, b, and R_T allow us to compute the surface and the volume of the modeled cluster. Since the clustering takes place systematically and simultaneously in the four corners of the box, we assume that the volume fraction of the cluster at nucleation (when $\phi = \phi_c$) is equal to $4v$. Based on this volume, we are able to calculate the surface of the correspondent torus and thus the increase of the volume by using Eq. (5). By iterating on the volume and the surface of the cluster, the evolution of $x(\phi)$ can be deduced and adjusted on our measured volume fraction of the cluster via the capture rate C (in the case of the third cell of Table I). The result of this fit, plotted in Fig. 4, agrees remarkably well with our simulations. Finally, the geometrical shapes given by our iterative model are compared to the measures of the occupancies of the third cell for different packing fractions in the bottom (lines 3 and 4) of Fig. 3.

C. Packing fraction of the cluster

The mean packing fraction of the cluster can be linked to that of the gas and to the volume of the cluster by following equations expressing the conservation of mass and volume.

One has

$$N_g + N_{cl} = N_{tot},$$
$$V_g + V_{cl} = V_{tot}. \quad (6)$$

Using the definition of Φ_{cl} and Φ_g given by Eq. (3), we can express the mean packing fraction of the cluster as a function of the total packing fraction of the system ϕ:

$$\Phi_{cl}(\phi) = \frac{1}{x(\phi)}(\phi - \phi_c) + \phi_c. \quad (7)$$

Note that ϕ has to be higher than ϕ_c in order to observe a cluster in the system.

The asymptotic value of Φ_{cl} as a function of the total packing fraction of the system is also found. According to Eq. (5) and assuming $x(\Phi_{cl,max}) = 1$, we find the mean packing fraction of the cluster for a fully filled cell. We observe that the width of the boxes has no influence on the packing fraction of the cluster, while the distance L between the pistons has a notable impact. Assuming that $\Phi_{cl,max}$ is linear with $1/L$, we found the mean packing fraction of a granular material that would be free in terms of volume (i.e., in an infinite system) even though it was externally excited. This result provides an original value of the random loose packing of granular clustered media in a low-gravity environment, $\Phi_{RLP} = 0.55 \pm 0.02$. This value agrees with previous results from other authors [34–36], although the process is very different in our study. Moreover, the result is universal since the width of the system impacts only the structure of partial clusters.

V. CONCLUSION AND PERSPECTIVES

In this work, we investigated numerically the structures of dynamical clusters in several cuboidal geometries. Using a geometrical criterion that enables us to sort the particles of the system as gaseous or clustered, we were able to identify how the cluster captures surrounding gaseous grains. Based on previous work [18], we defined a saturating vapor packing fraction and obtained an empirical model for the cluster's growth. This model suggests that the granular gas behaves like a molecular gas in terms of nucleation and condensation on cold regions of the system.

In future works, we will study the possible dissolution of the cluster when the energy injection is increased. Moreover, we will focus on potential hysteretic effects when a granular system is alternatively frozen (cluster formation) and then melted (cluster dissolution). We will also investigate the similarities between a granular medium and hydrodynamical systems in order to determine the shape of the gas-cluster interface. Finally, we will try to adopt the works of Mujica [33] to our system and define an effective granular surface tension for 3D systems.

ACKNOWLEDGMENTS

This work was supported by Belspo-PRODEX and the European Space Agency through the SpaceGrains project.

[1] I. S. Aranson and L. Stimring, *Granular Patterns* (Oxford University Press, Oxford, 2009).
[2] M. H. Jaeger, S. R. Nagel, and R. P. Behringer, Rev. Mod. Phys. **68**, 1259 (1996).
[3] I. Goldhirsch and G. Zanetti, Phys. Rev. Lett. **70**, 1619 (1993).
[4] A. Kudrolli, M. Wolpert, and J. P. Gollub, Phys. Rev. Lett. **78**, 1383 (1997).
[5] J. Eggers, Phys. Rev. Lett. **83**, 5322 (1999).
[6] M. Hou, H. Tu, R. Liu, Y. Li, K. Lu, P. Y. Lai, and C. K. Chan, Phys. Rev. Lett. **100**, 068001 (2008).
[7] R. Liu, Y. Li, and M. Hou, Phys. Rev. E **79**, 052301 (2009).
[8] M. Hou, Y. Li, R. Liu, Y. Zhang, and K. Lu, Phys. Status Solidi A **207**, 2739 (2010).
[9] D. van der Meer, K. van der Weele, M. Versluis, and D. Lohse, Europhys. Lett. **53**, 328 (2001).
[10] D. van der Meer, P. Reimann, K. van der Weele, and D. Lohse, Phys. Rev. Lett. **92**, 184301 (2004).
[11] D. van der Meer, K. van der Weele, and P. Reimann, Phys. Rev. E **73**, 061304 (2006).
[12] R. Mikkelsen, D. van der Meer, K. van der Weele, and D. Lohse, Phys. Rev. Lett. **89**, 214301 (2002).
[13] P. Eshuis, K. van der Weele, D. Lohse, and D. van der Meer, Phys. Rev. Lett. **104**, 248001 (2010).
[14] E. Falcon, R. Wunenburger, P. Évesque, S. Fauve, C. Chabot, Y. Garrabos, and D. Beysens, Phys. Rev. Lett. **83**, 440 (1999).
[15] P. K. Haff, J. Fluid Mech. **134**, 401 (1983).
[16] C. C. Maaß, N. Isert, G. Maret, and C. M. Aegerter, Phys. Rev. Lett. **100**, 248001 (2008).
[17] E. Opsomer, F. Ludewig, and N. Vandewalle, Phys. Rev. E **84**, 051306 (2011).
[18] E. Opsomer, F. Ludewig, and N. Vandewalle, Europhys. Lett. **99**, 40001 (2012).
[19] E. Opsomer, M. Noirhomme, N. Vandewalle, and F. Ludewig, Phys. Rev. E **88**, 012202 (2013).
[20] E. Opsomer, N. Vandewalle, M. Noirhomme, and F. Ludewig, Eur. Phys. J. E **37**, 115 (2014).
[21] Y. Li, M. Hou, and P. Evesque, J. Phys. Conf. Ser. **327**, 012034 (2011).
[22] M. Noirhomme, E. Opsomer, N. Vandewalle, and F. Ludewig, Eur. Phys. J. E **38**, 9 (2015).
[23] E. Opsomer, M. Noirhomme, N. Vandewalle, S. Merminod, and E. Falcon, Microgravity **3**, 1 (2017).
[24] European Space Agency's SpaceGrains project, http://www.spacegrains.org/.
[25] M. Argentina, M. G. Clerc, and R. Soto, Phys. Rev. Lett. **89**, 044301 (2002).
[26] R. Liu, Y. Li, M. Hou, and B. Meerson, Phys. Rev. E **75**, 061304 (2007).
[27] F. Ludewig and N. Vandewalle, Phys. Rev. E **85**, 051307 (2012).

[28] F. Ludewig, S. Dorbolo, T. Gilet, and N. Vandewalle, Europhys. Lett. **84**, 44001 (2008).
[29] P. A. Cundall and O. D. L. Strack, Géotechnique **29**, 47 (1979).
[30] F. W. Starr, S. Sastry, J. F. Douglas, and S. C. Glotzer, Phys. Rev. Lett. **89**, 125501 (2002).
[31] F. M. Schaller, S. C. Kapfer, J. E. Hilton, P. W. Cleary, K. Mecke, C. De Michele, T. Schilling, M. Saadatfar, M. Schröter, G. W. Delaney, and G. E. Schröder-Turk, Europhys. Lett. **111**, 24002 (2015).
[32] M. G. Clerc, P. Cordero, J. Dunstan, K. Huff, N. Mujica, D. Risso, and G. Varas, Nat. Phys. **4**, 249 (2008).
[33] L. H. Luu, G. Castillo, N. Mujica, and R. Soto, Phys. Rev. E **87**, 040202(R) (2013).
[34] M. Jerkins, M. Schröter, H. L. Swinney, T. J. Senden, M. Saadatfar, and T. Aste, Phys. Rev. Lett. **101**, 018301 (2008).
[35] C. S. O'Hern, S. A. Langer, A. J. Liu, and S. R. Nagel, Phys. Rev. Lett. **88**, 075507 (2002).
[36] G. Y. Onoda and E. G. Liniger, Phys. Rev. Lett. **64**, 2727 (1990).

Chapter 5

Dynamics of the cluster

5.1 Introduction

Now that the birth and the growth of the cluster have been discussed [61], our final goal is to identify and rationalize the dynamics of the cluster. We show in this chapter that a cluster can be considered as an independent entity which can be of two different forms. The cluster can consist of either all the particles (a "bouncing aggregate"), or a part of them surrounded by a granular gas (a "granular oscillator"). In fact, in one case or the other, the cluster presents different dynamics consisting in both cases of a collective motion of the grains. Three points will be discussed here. In Sec. 5.1, we theoretically describe the emergence of the bouncing aggregate, mentioned in Sec. 5.1, that have been observed during the PFC 64. Then, in Sec. 5.3, we numerically study the dynamics of a big cluster which is submitted to an asymmetrical excitation. Finally, in Sec. 5.4, we numerically and experimentally discuss the dynamics of a cluster formed by two different kinds of particles and show that these two different species can segregate in microgravity.

5.2 Bouncing aggregate

During PFC 64, which was conducted in 2016, we observed a dynamical regime that was unexpected in the VIP-Gran geometry. In this regime, the grains were all gathered in a single dense cluster which periodically bounced from one plate to another. In addition, the period of oscillation of the cluster was twice that of the pistons. Moreover, the phenomenon seemed very stable over time (we recorded about 150 round trip). This state has been named "bouncing aggregate" with reference to the collective motion of all the particles in the cell. Fig. 5.1 shows pictures of the bouncing aggregate during one period of oscillation.

5.2.1 Emergence of the bouncing aggregate

The bouncing aggregate had previously been observed in microgravity in granular systems similar to VIP-Gran [62–64]. However, in their experiments, Sack *et al.* [63] designed a solid cell of length L that is vibrated entirely from left to right with an amplitude A and a frequency f. This corresponds to an in phase motion of the walls. In this configuration, they were able to deduce a mathematical condition, linking the excitation parameters with the dimensions of the system and allowing

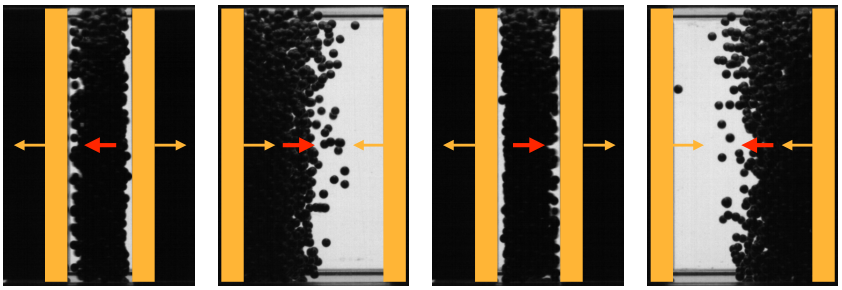

(a) (b) (c) (d)

Figure 5.1: Four consecutive images showing a bouncing aggregate oscillating from one piston to another. The motion of the pistons (resp. the cluster) is depicted by the orange (resp. red) arrows. The period of oscillation of the cluster is twice that of the pistons.

to predict the granular regime of collective motion. This condition is given by

$$\frac{L-e}{\pi} < A_0, \tag{5.1}$$

e being the cluster thickness and A_0 the minimum amplitude necessary for the emergence of their "collect-and-collide" regime. The main difference between both regimes observed in the experiment of Sack *etal.* [63] and in ours lies in the fact that the pistons oscillate in phase in the first case and in phase opposition in the second. Nevertheless, the condition developed in [63] can be adapted to our system. In order to express the motion of the pistons and the bouncing aggregate along the excitation axis (denoted y), we define the position of the pistons y_1 and y_2 and the position of the aggregate y_b as

$$\begin{aligned} y_1(t) &= A\sin(\omega t) \\ y_2(t) &= L + A\sin(\omega t + \pi) = L - A\sin(\omega t) \\ y_b(t) &= v_{y,b}\ t\ . \end{aligned} \tag{5.2}$$

In these equations, L is the length of the cell, A is the amplitude of oscillation of the pistons, $\omega = 2\pi f$ is the pulsation of the pistons and $v_{y,b}$ is the velocity of the bouncing aggregate (see Fig. 5.2). Let us consider that the bouncing aggregate is a solid bulk that has an effective coefficient of restitution equal to 0 and is stuck to the first piston at the beginning of its motion. Since the system is in microgravity, the velocity of the aggregate is $A\omega$ when it leaves the piston. The position of the cluster (measured from its left side) is then $y_b = 0$. We assume now that the collision with the second piston occurs at an instant t_c. The right side of the cluster then coincides with the position of the second piston and one finds

$$\begin{aligned} & y_b(t_c) = y_2(t_c) - e \\ \Leftrightarrow\ & A\omega t_c = L - A\sin(\omega t_c) - e \end{aligned} \tag{5.3}$$

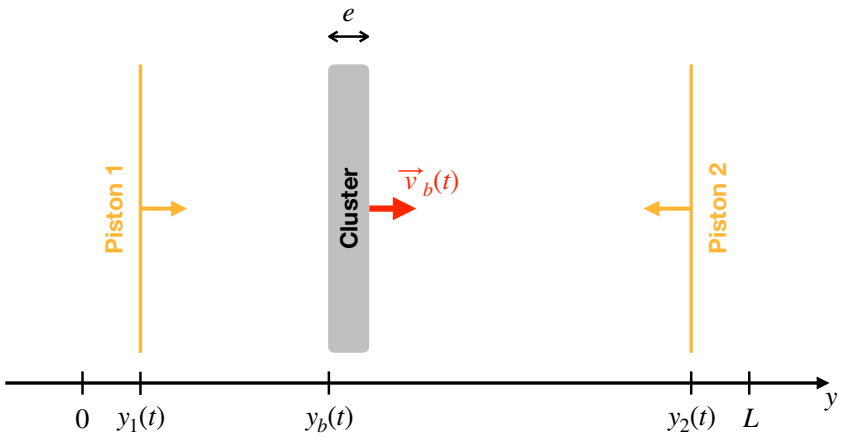

Figure 5.2: Sketch of an observation of the bouncing aggregate. The position of the pistons is denoted $y_1(t)$ and $y_2(t)$. The position of the aggregate is measured from its left side and is denoted $y_b(t)$. The bouncing aggregate can be seen as a solid of thickness e that inelastically bounces from one piston to the other.

where e is the thickness of the cluster. Defining the phase of the bouncing aggregate as $\varphi = \omega t_c$, one finds

$$P(\varphi) := \varphi - \frac{L-e}{A} + \sin(\varphi) = 0. \tag{5.4}$$

This last equation cannot be resolved analytically. However, the bouncing state can be stable only if the direction of the acceleration of the second piston is opposed to the velocity of the bulk at the time of the collision [62, 63]. Mathematically, this condition results in

$$\frac{d^2 y_2(t)}{dt^2} = A\omega^2 \sin(\varphi) < 0, \tag{5.5}$$

which is satisfied for

$$\pi + 2k\pi < \varphi < 2\pi + 2k\pi, \tag{5.6}$$

with $k \in \mathbb{N}$. Since the function $P(\varphi)$ is monotonously increasing ($dP/d\varphi \geq 0 \ \forall \ \varphi$), the interval where the bouncing can emerge is given by

$$P(\pi + 2k\pi) < P(\varphi) < P(2\pi + 2k\pi). \tag{5.7}$$

The condition that links together L, e and A can be derived from these last inequations. Considering that L and e are fixed, the minimal and maximal amplitudes in between the bouncing aggregate is observable are given by

$$\begin{aligned} P(\pi + 2k\pi) &= \pi(2k+1) - \frac{L-e}{A_{max}} = 0 \\ P(2\pi + 2k\pi) &= 2\pi(k+1) - \frac{L-e}{A_{min}} = 0. \end{aligned} \tag{5.8}$$

The conditions on the amplitude are finally given by

$$\frac{L-e}{2\pi(k+1)} < A < \frac{L-e}{\pi(2k+1)}. \tag{5.9}$$

From eq. (5.9), we see that a large number of intervals are allowed for the value of A, depending on the subharmonic k. In fact, the only observable harmonic is the first one (i.e. $k = 0$), as demonstrated in [64]. The bouncing aggregate is actually not an inelastic solid and, the longer it will fly between both pistons, the more it will deform and expand in the system to finally completely disaggregate. Finally, the conditions that have to be fulfilled in order to observe a bouncing aggregate in the VIP-Gran cell are given by

$$\frac{L-e}{2\pi} < A < \frac{L-e}{\pi}. \tag{5.10}$$

Concerning the only observation of the bouncing aggregate we made during the PFC 64 (see Fig. 3.6), the parameters were $L = 12.5$ mm, $A = 2.0$ mm and $N = 1611$ (see Tab. 3.1). The thickness of the cluster can be estimated by hypothesizing that the aggregate has the packing fraction of a Random Loose Packing $\phi_{RLP} = 0.55$. One has

$$e = \frac{\frac{4}{3}\pi R^3 N l^2}{\phi_{RLP}} \approx 1.7 \text{ mm}, \tag{5.11}$$

where R and l are the radius of the particles and the width of the VIP-Gran cell. Eq. (5.10) becomes

$$\frac{12.5-1.7}{2\pi} = 1.72 \text{ mm} < 2.0 \text{ mm} < \frac{12.5-1.7}{\pi} = 3.44 \text{ mm}, \tag{5.12}$$

which is obviously verified.

5.3 Granular oscillator

If the transition between the gas and the cluster is gradual, we can still differentiate these two phases. As explained in our article entitled "Cluster growth in driven granular gases", we observed a clear transition in the measurement of local particle density when the statistical threshold from the KS test is crossed. In addition, we have observed that the transition from a granular gas to a clustered state is continuous (see Sec. 3). Nevertheless, we know, from simulations, that a cluster state in the system has its own dynamics that are totally different from the gas regime. Indeed, we will show in this section that a dynamical cluster can oscillate in the box (the particles in clusters adopt a collective motion), with a frequency whose value depends on the number of particles enclosed in the cluster [65].

5.3.1 Numerical setup

The numerical setup has been designed to comply with the geometry of the VIP-Gran experiment. We enclosed $N = 2000$ 1 mm spheres in a cell of dimensions Ll^2. The only difference with the 3D cell of The VIP-Gran instrument lies in the dimension l. We decided to reduce this width to $l = 15$ mm in order to accelerate the simulations (which are exactly the same as the one described in Sec. 4.2.1). The

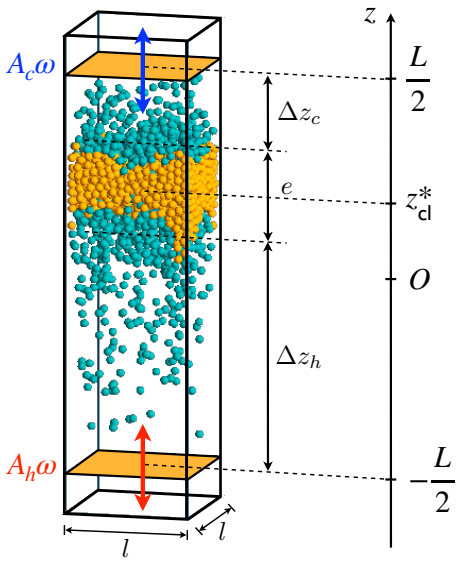

Figure 5.3: Adapted from [65]. Sketch of the numerical setup. $N = 2000$ spherical particles are enclosed in a container of dimensions Ll^2 and excited by two oscillating pistons (see the orange plates) whose pulsation is the same $\omega = 2\pi f$. The amplitude of oscillation of the bottom piston is $A_h = 5$ mm and the amplitude of oscillation of the top piston A_c is the tunable parameter of the system. The gathered grains are colored in orange and the thickness of the cluster, measured between the extreme positions of the clustered grains, is denoted e.

length L of the cell was fixed at 50 mm. Just like the VIP-Gran configuration, the excitation of the system is mechanical and provided by two pistons oscillating with a phase shift φ which can also be tuned. The oscillations of the pistons are sinusoidal and characterized by a fixed amplitude $A_h = 5$ mm and a tunable amplitude $A_c < A_h$xz, and the same frequency $f = 5$ Hz. The position of the oscillating pistons are given by $z_h(t)$ and $z_c(t)$. The mean distance between the hot (resp. cold) plate is Δz_h (resp. Δz_c). These latter are useful in order to find the equilibrium position of the cluster z^*_{cl}, which is defined as the averaged position of the center of mass of the system. Fig. 5.3 gives a sketch of the numerical setup.

5.3.2 Main results

Varying the amplitude of the (so called) cold plate A_c, we were able to express the equilibrium position z^*_{cl} and the natural pulsation ω_{cl} of the oscillation of the cluster as a function of the amplitude ratio $a = A_c/A_h$ (z^*_{cl} and ω_{cl} are effectively directly linked to the excitation parameters in terms of momentums received by the cluster). Indeed, in order to remain indefinitely in an equilibrium position, the cluster must receive not only the same momentum from the hot plate as from the cold plate but in addition, it must receive these two pulses at the same time. By expressing the time needed for two grains coming from each piston with their typical velocities $A_i\omega$

($i \in \{c, h\}$), we were able to define an equilibrium criterion. Starting from

$$\Delta t_c = \frac{\Delta z_c}{A_c \omega} = \frac{\Delta z_h}{A_h \omega} = \Delta t_h, \tag{5.13}$$

we found

$$z^*_{\mathrm{cl}} = \frac{L-e}{2}\frac{1-a}{1+a}. \tag{5.14}$$

That being, we observed that the cluster did not remain at its equilibrium position but performed periodic oscillations. In order to determine the natural pulsation of the cluster, we expressed the momentum rates given by the pistons when the position of the cluster is changed by a small distance δ from the equilibrium position. The total force acting on the cluster when it leaves its equilibrium position can be found in that way. One has

$$\begin{aligned} F(z^*_{\mathrm{cl}} + \delta) &= \left(\frac{N_h A_h^3}{\left(\frac{L-e}{1+a} + \delta\right)^2} - \frac{N_c A_c^3}{\left(\frac{(L-e)a}{1+a} - \delta\right)^2} \right) m\omega^2 \\ &\approx -\frac{2(A_c + A_h)^3 (N - N_{\mathrm{cl}})}{(L-e)^3} m\omega^2 \delta, \end{aligned} \tag{5.15}$$

where N_h, N_c and m denote respectively the number of particles in the hot and the cold gases and the mass of a single grain. The first order expansion, around δ, of this force gives the last expression, which is similar to an equation of motion of a harmonic oscillator, $F(z^*_{\mathrm{cl}} + \delta) = -k_{\mathrm{cl}}\delta$. We derived finally the pulsation of the cluster, $\omega_{\mathrm{cl}} = \sqrt{k_{\mathrm{cl}}/M_{\mathrm{cl}}}$ and found

$$\omega_{\mathrm{cl}} = \left(\frac{A_c + A_h}{L-e}\right)^{3/2} \left(2\frac{N - N_{\mathrm{cl}}}{N_{\mathrm{cl}}}\right)^{1/2} \omega, \tag{5.16}$$

where $N_{\mathrm{cl}} = N - N_c - N_h$ is the number of particles composing the cluster.

5.3.3 Summary

We have shown through this study that the position of a dynamical cluster can be tuned, and even chosen, simply by adjusting the oscillation amplitudes of the pistons that inject the energy into the system. We have also shown that the fact that the gases do not transmit energy in a continuous way leads to an oscillation of the cluster. Moreover, we found that the pulsation of the cluster can also be tuned by adjusting the controllable excitation parameters of the system. Finally, this work has shown that the cluster, which is composed of gathered grains forming a dense and dissipative phase, can be seen as a unique entity in itself, with a mass and proper dynamics. All this while not forgetting that the cluster and the gases are constantly exchanging particles.

5.3.4 Complementary measures

In the previous sections, we deduced from numerical simulations that both the equilibrium position z^*_{cl} and the pulsation ω_{cl} adopted by the cluster were related to the momentum rates received from the pistons. We therefore wondered whether varying the surfaces of the pistons could influence both measurements. The results were surprising, as explained in what follows.

5.3.4.1 Setup

The numerical setup consists of a cone-shaped cell whose volume is set at Ll^2, exactly as for the cell described in section 5.3.1. The length L of this cell and the number N of grains it contains were kept equal to 50 mm and 2000, respectively, in order to be able to compare the results with the previous simulations. The new tunable parameter is the surface ratio, defined as $s = S_c/S_h$, where $S_c = \pi R_c^2$ and $S_h = \pi R_h^2$ are the surfaces of the cold and hot oscillating plates (see Fig. 5.4).

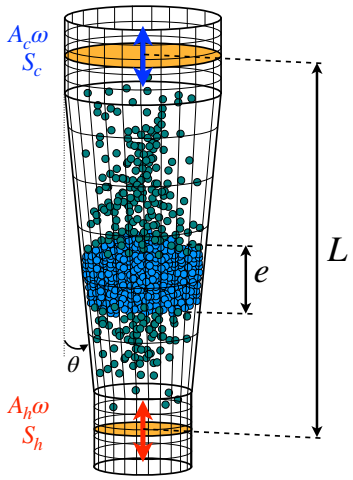

Figure 5.4: Sketch of one of the cells designed, for a surface ratio $s = S_c/S_h = 2.5$ and an amplitude ratio $a = A_c/A_h = 1$. The volume of each cell as well as the distance between the hot and the cold plates were kept constant at $V = L * 15^2$ mm^3 and $L = 50$ mm in order to be able to compare the results with the initial cell (see Sec. 5.3.1). The oscillating pistons are colored in orange and their related maximal velocities $A_i\omega_i$ and surfaces S_i (with $i = \{c, h\}$) are respectively written in blue for the cold plate and in red for the hot one. The thickness of the cluster and the opening angle are noted e and θ.

Note that a new cell has been designed for each surface ratio and that the hot plate has always been kept at the bottom of the cell. Since we decided to keep the volume of the truncated cone constantly equal to Ll^2, we can easily derive the values

Symbol	♦	▼	▲	●	■	□	○	△	▽	⊞	×	⬠	+	◇
$s = S_c/S_h$	0.2	0.4	0.5	0.6	0.8	5/4	5/3	2.0	2.5	3.0	3.5	4.0	4.5	5.0
R_c (mm)	5.1	6.5	7.0	7.4	8.0	8.9	7.6	9.9	10.3	10.6	10.9	11.1	11.3	11.4
R_h (mm)	11.4	10.3	9.9	9.5	8.9	8.0	9.3	7.0	6.5	6.1	5.8	5.5	5.3	5.1
θ (°)	-7.2	-4.3	-3.3	-2.5	-1.1	1.1	-2.0	3.3	4.3	5.1	5.8	6.3	6.8	7.2

Table 5.1: Parameters and associated symbols of the 14 cells numerically designed. Each conical cell was filled with $N = 2000$ millimeter beads. For each set, the amplitude ratio a was varied from 0.2 to 1.0. The parameter θ is the opening angle of the cone measured from the vertical as shown in Fig. 5.4.

of S_c and S_h as a function of the surface ratio s. One finds

$$\begin{cases} S_c = \dfrac{3l^2 s}{s + \sqrt{s} + 1} \\ S_h = \dfrac{3l^2}{s + \sqrt{s} + 1}. \end{cases} \tag{5.17}$$

For each cell of fixed surface ratio s, the amplitude ratio a was varied in the interval $\{0.2, 0.4, 0.6, 0.8, 1.0\}$. The parameters given the geometry of the cells for each surface ratio are listed in Tab. 5.1.

5.3.4.2 Results

Three snapshots of the simulations are shown in Fig. 5.5 for three different surface ratios, $s = 0.4$, $s = 2.0$ and $s = 4.0$, and for the same amplitude ratio $a = 1.0$. It is clear from this figure that the position of the cluster depends directly on the surface ratio.

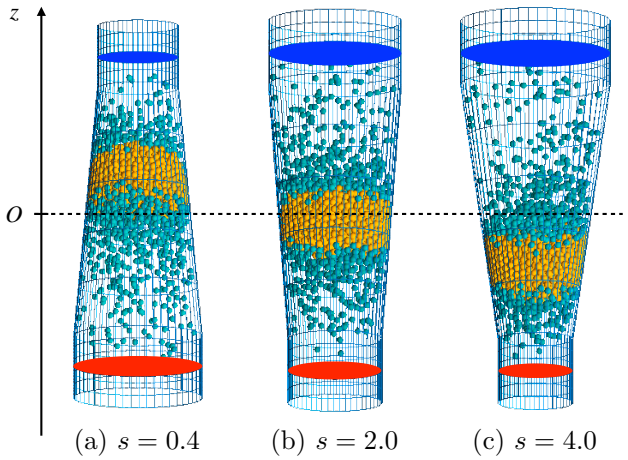

(a) $s = 0.4$ (b) $s = 2.0$ (c) $s = 4.0$

Figure 5.5: Snapshots of the different numerical cells corresponding to three different surface ratios (a) $s = 0.4$, (b) $s = 2.0$ and (c) $s = 4.0$ and an amplitude ratio fixed at $a = 1.0$. The cluster is always closer to the smaller piston.

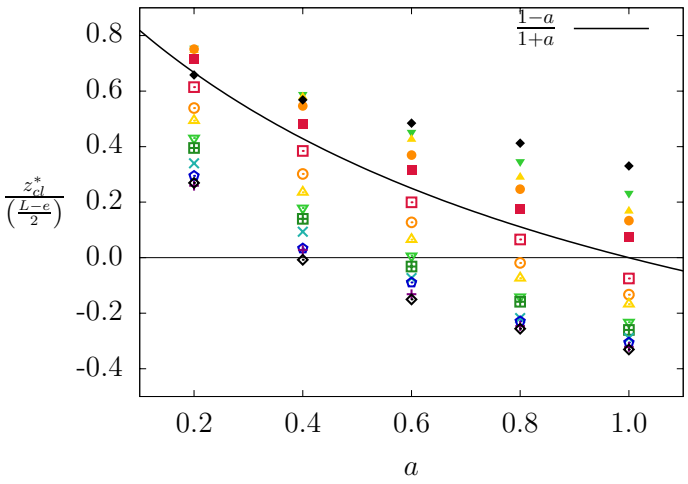

Figure 5.6: Normalized position of the cluster as a function of the amplitude ratio for the 14 different cells listed in Tab. 5.1. The black curve gives the equilibrium position of the cluster in the case of the parallelepiped box previously studied.

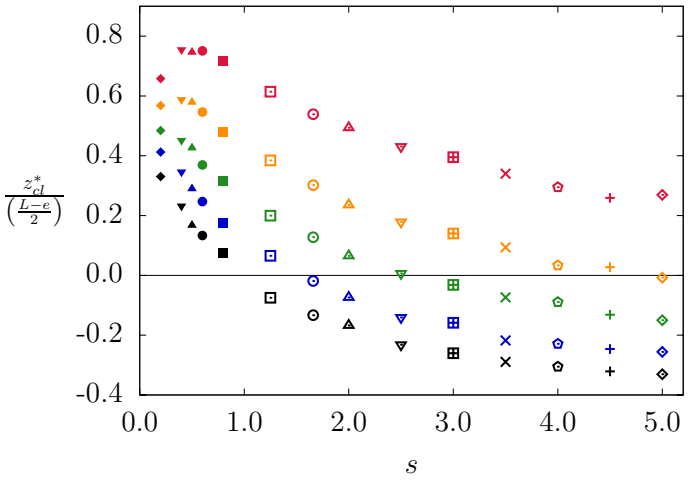

Figure 5.7: Normalized position of the cluster as a function of the surface ratio for the 14 different cells listed in Tab. 5.1. The black curve gives the equilibrium position of the cluster in the case of the parallelepiped box previously studied and each color corresponds to a fixed amplitude ratio, from $a = 0.2$ (red points) to $a = 1.0$ (black points).

Similar to what was done in the previous study, we measured the equilibrium position of the cluster z^*_{cl} which we plotted against the amplitude ratio a, for each fixed s. The normalized position of the cluster is reported as a function of the amplitude ratio a in Fig. 5.6 and as a function of the surface ratio s in Fig. 5.7. Actually, the smaller (resp. the larger) the surface ratio [for $s < 1$ (resp. $s > 1$)],

the closer the cluster is to the cold (resp. hot) plate. This indicates the influence of the number of particles sent by the plates. From this measurement, we clearly see that the simple condition (5.13), which was valid for the parallelepiped box, is no more sufficient. Another fact to note is that the position of the cluster can also be tuned by regulating the amplitude ratio, even for these conical systems.

Finding a theoretical expression of the cluster's position as a function of the surface and the amplitude ratios is not trivial in the case of conical cells. Currently, we are still working on a model based on the pressure balance exerted on the cluster.

Eur. Phys. J. E (2015) **38**: 9
DOI 10.1140/epje/i2015-15009-4

THE EUROPEAN PHYSICAL JOURNAL E

Regular Article

Granular transport in driven granular gas

M. Noirhomme[a], E. Opsomer, N. Vandewalle, and F. Ludewig

GRASP, Physics Department B5a, University of Liège, B-4000 Liège, Belgium

Received 16 July 2014 and Received in final form 23 November 2014
Published online: 25 February 2015 –

Abstract. We numerically and theoretically investigate the behavior of a granular gas driven by asymmetric plates. The injection of energy in the dissipative system differs from one side to the opposite one. We prove that the dynamical clustering which is expected for such a system is affected by the asymmetry. As a consequence, the cluster position can be fully controlled. This property could lead to various applications in the handling of granular materials in low-gravity environment. Moreover, the dynamical cluster is characterized by natural oscillations which are also captured by a model. These oscillations are mainly related to the cluster size, thus providing an original way to probe the clustering behavior.

1 Introduction

For high enough filling fraction, driven granular materials can exhibit a collective behavior known as dynamical clustering. Given the dissipative character of the collisions, kinematic energy is lost at each particle interaction. This loss leads to the formation of slow and dense regions within the granular medium [1, 2]. However, energy is also continuously injected into the system and rapidly a steady state is reached. The latter phenomenon was studied experimentally in microgravity [3–7] and rationalized theoretically and numerically [8–14].

The dynamical clustering can be explained considering the competition between a characteristic dissipation time, called Haff time, and a characteristic time of energy propagation through the system [14–16]. Since, gravity would induce another characteristic time in the system and affect dynamical clustering [17], low-gravity condition is needed for the study of this phenomenon. This motivates the European Space Agency's (ESA) VIPGRAN project [18] in which granular gas will be experimentally investigated under various conditions on the International Space Station (ISS). Numerical work is essential to prepare the VIPGRAN project and to fix the experimental parameters.

The behavior and the stability of a granular cluster is poorly understood when the excitation parameters are changed. The main motivation of this article is to address the question of variable injection of energy in the system. The first step is to study the case of an asymmetric driving and to study the position of the cluster in the system. In the second step, the possible motion of the cluster will be analyzed. We will see in this paper that it is possible to control both position and motion of dynamical cluster, opening ways to achieved a granular transport in microgravity.

[a] e-mail: mnoirhomme@ulg.ac.be

2 Numerical approach

Our numerical study relies on intensive Molecular Dynamic (MD) simulations, using a linear spring-dashpot model [14, 20, 21]. At each collision, normal and tangent forces are evaluated, respectively, through particle deformations and tangential velocities. The value of the coefficient of restitution ε and the spring stiffness k_n are both constant and fixed at 0.9 (corresponding to bronze beads) and $5 \cdot 10^5$ N/m, respectively. A complete description of MD simulation is given by Taberlet in [22] Moreover, the algorithm was already used by the authors in [13,14,20,21,23]. Based on the VIPGRAN concept [18], we designed a box with fixed lateral walls and moving top and bottom boundaries, modeling the pistons. The width and depth of the container are equal to $l = 15$ mm. The length $L(t) = z_h(t) - z_c(t)$ is variable and depends on the positions of the oscillating plates according to following equations of motion:

$$\begin{cases} z_h(t) = z_h^* + A_h \sin(2\pi f t), \\ z_c(t) = z_c^* + A_c \sin(2\pi f t + \varphi). \end{cases} \quad (1)$$

The pistons are oscillating with a fixed frequency $f = 5$ Hz and a phase shift φ as proposed in the VIPGRAN project. The average distance between the plates is $L = 50$ mm. To ensure clustering in the system [14], the cell is filled with $N = 2000$ grains of radius fixed at $r = 0.5$ mm. The amplitudes A_h and A_c, defining the amplitude ratio $a = A_c/A_h$, and the phase shift φ have been modified. We choose to keep the frequencies fixed at 5 Hz for both plates in order to change the intensity of the injected energies while keeping a constant time scale in the system from one simulation to another. In addition, the residual vibration of the instrument is minimized if the frequencies are the same for both walls. This fact is important in order to reproduce the

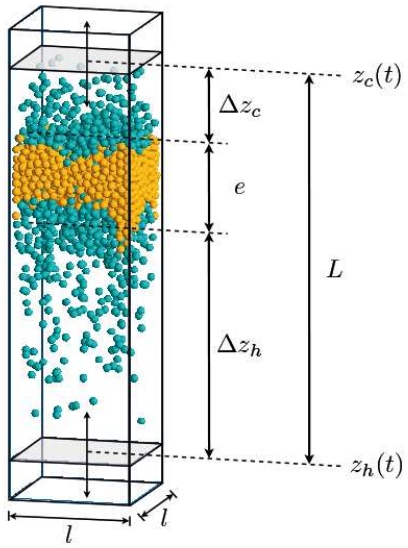

Fig. 1. Sketch of the VIPGRAN cell used in simulations. Its dimensions are $L = 50\,\text{mm}$ and $l = 15\,\text{mm}$. The oscillating plates have the following parameters: a common frequency fixed at $f = 5\,\text{Hz}$ and tunable amplitudes, A_c and A_h. The length L is measured between plate equilibrium positions. The relevant parameter is the amplitude ratio $a = A_c/A_h$.

Table 1. View of the variable parameters of the four runs of simulations. (Symbols correspond to those of figs. 5 and 4.)

Run	A_h (mm)	a	φ	Symbol
1	5	$[0;1]$	π	●
2	7.5	$[0.2;0.8]$	π	■
3	10	$[0.2;0.8]$	π	▲
4	5	1	$[0;2\pi]$	▼

simulated experiment in the VIPGRAN project. A sketch of the described cell is shown on fig. 1. Four campaigns of simulations have been realized. In the first three, we investigated the impact of the amplitude ratio while the fourth was devoted to the influence of the phase shift. We choose to fix the amplitude of the hot plate (the bottom ones on fig. 1) at $A_h = 5\,\text{mm}$, $7.5\,\text{mm}$ and $10\,\text{mm}$ in the first, second and third campaign, respectively. The tunable parameter of the experiment was the amplitude ratio a and was varied in the interval $\{0; \frac{1}{10}; \frac{1}{9}; \ldots; 1\}$ and in the interval $\{0.2; \ldots; 0.8\}$ in second and third runs. In the last ones, the amplitudes of both vibrating plates were set to $A_h = A_c = 5\,\text{mm}$ while the phase shift φ was varied in the interval $\{0; \frac{\pi}{4}; \ldots; \frac{7\pi}{4}\}$. Table 1 gives a simplified view of the parameters used in the four campaigns. Each run corresponds to 300 periods of plates oscillation, requiring about 10^8 iterations of the algorithm.

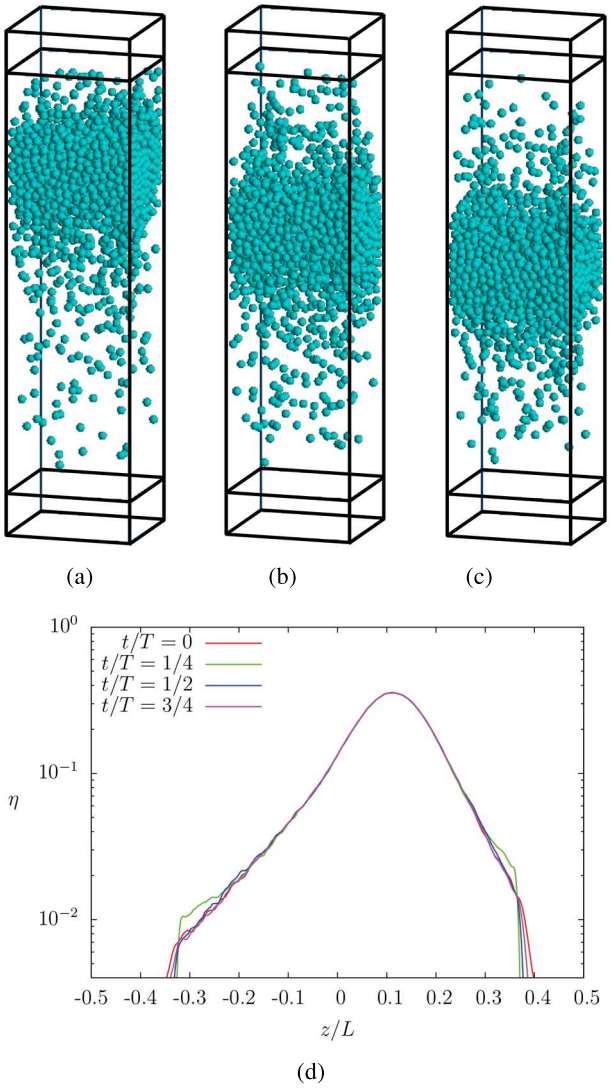

Fig. 2. Three snapshots of the simulated experience for amplitude ratios $a = 0.25$ (a), $a = 0.5$ (b) and $a = 1$ (c). The cluster's position is directed by the value of a. The "hot" plate is always the bottom one and has an oscillation amplitude $A_h = 5\,\text{mm}$ corresponding to the first campaign. (d) Semi-log plot of the packing fraction of the grains contained in the cell along the z-axis for $a = 0.5$. The energy injection is made from $t/T = 0$ to $t/T = 1/4$. In this phase, both hot and cold gases are compressed by the pistons. The packing fraction for $0 < z/L < 0.2$ (corresponding approximatively to the localization of the cluster) remains very stable over the whole period T.

3 Results

Figures 2(a), (b) and (c) present the granular system in the cell for different amplitude ratios a. As remarked previously [13,24,25], we observe the formation of a dense region gathering together approximatively 95% of the grains in the box. This low energetic region is separated from the pistons by two dilute gases of particles which transmit energy from the oscillating plates toward the cluster. One observes that the position of the cluster is a function of the amplitude ratio. Indeed, the smaller the amplitude ra-

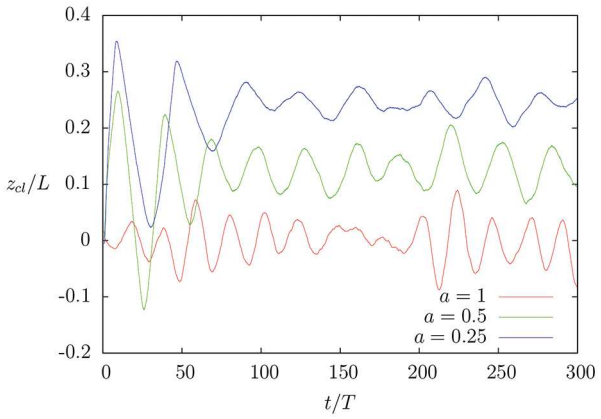

Fig. 3. Dimensionless time evolution of the center of mass of the system for amplitude ratios $a = 1$ (red), $a = 0.5$ (green) and $a = 0.25$ (blue). The center of mass represents the cluster's position and is noted $z_{\rm cl}$. The cluster is oscillating around an equilibrium position $z^*_{\rm cl}$ with a pulsation $\omega_{\rm cl}$. Both $z^*_{\rm cl}$ and $\omega_{\rm cl}$ depend on the amplitude ratio a.

tion is, the closer the cluster is to the "cold" plate (*i.e.* the one with the smallest oscillation amplitude). In addition, the packing fraction η of the system for $a = 0.5$ is shown in semi-log scale on fig. 2(d) along the z-axis. One can note that the cluster remains very stable over a whole period $T = 1/f$. However, the packing fraction of both hot and cold gases are fluctuating with the position of the oscillating pistons taken at different times between $t = 0$ and $t = T$. A second observation we made is the long-time oscillation of the cluster in the box. The position of the agglomerated grains is indeed not stable over multiple periods but makes a periodic motion with a pulsation very different from the plate's ones. These oscillations are shown on fig. 3 for three different amplitude ratios, corresponding to the cases (a), (b) and (c) of fig. 2.

The condensation behavior of the grains was already studied and theoretically characterized [14]. The new feature of driven that is investigated in this paper is the control of the cluster's position by amplitude tuning. This position, denoted by $z_{\rm cl}$, corresponds to the center of mass of the system. We observed that this quantity corresponds in good approximation to the densest region encountered in the cluster. For convenience, the z-axis is calculated from the center of the cell ($z = 0$) toward the cold plate.

Our simulations give evidence for an original behavior of driven granular media submitted to asymmetrically constraints in microgravity: a cluster is formed and is able to move in the cell and oscillates about its equilibrium position. Although the cluster is oscillating during long simulations, an average position, noted $z^*_{\rm cl}$, can be calculated and linked to the amplitude ratio. Figure 4 gives this normalized average position for the first three campaigns. Note that the phase shift between both plates has no influence on the equilibrium position of the cluster.

4 Cluster equilibrium position

To model the equilibrium position process in a simple way, we consider the cluster like a dense and stable pile of condensed grains receiving two momentums coming from both hot and cold plates. The model is based on two fundamental hypotheses: i) the cluster has reached equilibrium and does not move anymore and ii) the momentums coming from both hot and cold plates are sent after each period to the cluster, with the help of gaseous grains. Two conditions coming out of these hypotheses are also found. The momentums sent by the vibrating walls have to be equal and the time needed for each momentums to cross the cell has to be the same. Assuming that the number of particles contained in the cluster is constant, *i.e.* that the cluster captures as many grains as it loses through evaporation, we can model the cluster's equilibrium position. As stated in previous works [8,24,26,27], the distribution of the velocities in both hot and cold gases can be normalized by the maximal velocities of their respective pistons. This scaling leads to identical distributions for both hot and cold gases and supports our hypothesis that a grain coming from the plate $i = \{h, c\}$ has a typical velocity

$$v_i = A_i\omega. \tag{2}$$

Moreover, we consider that the grains coming from the plates impact the cluster with unchanged velocities. This hypothesis has been confirmed by measuring gas densities. The mean free path we calculated was indeed roughly $l \approx 80\,\text{mm}$. In comparison with the length of the cell L, this value implies that a grain coming from a vibrating plate will probably not collide with another grain before it attains the cluster. As discussed above, the equilibrium is reached when the time needed to reach the cluster is equal for both plates. Considering a straight and uniform movement of the grains, this time is directly linked to the plate-cluster distance by $\Delta t_i = \Delta z_i/v_i$. Equaling Δt_h and Δt_c, we find the following equilibrium condition:

$$\frac{\Delta z_c}{\Delta z_h} = \frac{A_c}{A_h}\,. \tag{3}$$

Taking into account the cluster's thickness e along the z-axis, we can develop Δz_i in (3) in order to link it to the cluster's position $z_{\rm cl}$. These distances are illustrated on the sketch of fig. 1. Using eq. (3) we find the cluster's equilibrium position

$$z^*_{\rm cl} = \frac{L-e}{2}\left(\frac{1-a}{1+a}\right), \tag{4}$$

where the dependence of the amplitude ratio a is obtained. The next step consists in finding the cluster's thickness e. For this purpose, we used an algorithm that measures the local density η around each sphere in the cell. Previous work [14] has shown that the clusters have an approximative local density larger than 0.285. Using this criterion, we defined the cluster's thickness by the maximal vertical distance that separates two particles with a local density

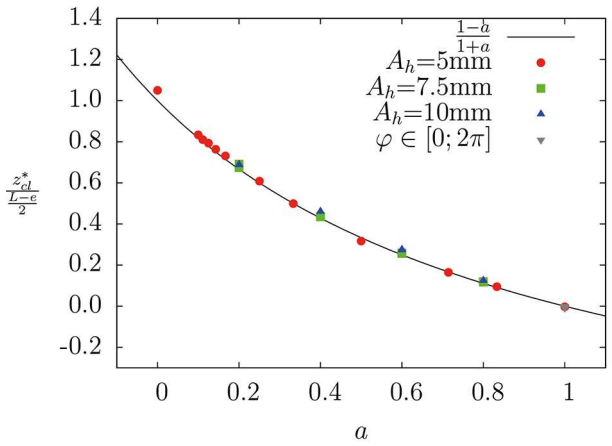

Fig. 4. Averaged and normalized equilibrium position $z^*_{\rm cl}$ of the cluster as a function of the amplitude ratio a. The equilibrium position is always measured from the center of the box towards the coldest plate and the cluster's thickness used for the normalization is fixed at $e = 10\,\text{mm}$. Different symbols correspond to the four simulation runs. The model developed in the main text is plotted using eq. (4) and is in excellent agreement with numerical results.

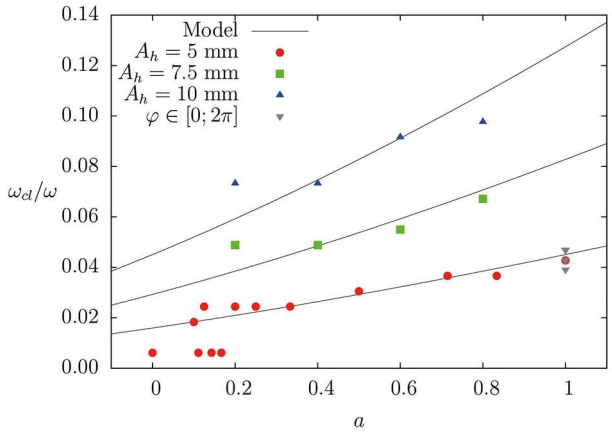

Fig. 5. Normalized pulsation $\omega_{\rm cl}$ of the cluster's oscillation as a function of the amplitude ratio a. The measures were performed with a Fast Fourier Transform (FFT) algorithm. The model described in the main text given by eq. (10) is in good agreement with the simulations. For small amplitude ratios, the algorithm was not always able to give relevant results because the oscillations of the cluster were too weak.

$\eta \geq 0.285$. Measurements were made on the entire simulation and averaged to finally find $e \approx 10\,\text{mm}$, whatever the value of a. This result is not surprising since the excitation given by the oscillating plates is so intense that the cluster cannot be more compressed, even for the first campaign, making its density fairly constant. As a consequence, the cluster's thickness is stable since its definition is directly linked to the local density of the grains. In fig. 4, we have plotted eq. (4) with a fixed value of $e = 10\,\text{mm}$. The model is in excellent agreement with the results found in our numerical campaigns.

5 Cluster oscillations

As discussed before and illustrated in fig. 3(b), clusters are able to oscillate in the box around their equilibrium position $z^*_{\rm cl}$. The oscillations originate from a Hopf bifurcation as proposed previously in [25,28]. Note that the amplitude of these oscillations is significative in regards to the value of the cluster thickness e. The cluster's inertia is given by the total mass $M_{\rm cl} = N_{\rm cl}m$, where $N_{\rm cl}$ is the number of grains of mass m contained in the cluster. According to our observations, this number of particles is roughly constant. In addition, we consider that the cluster interacts with the moving planes via both hot and cold gases that contain, respectively, N_h and N_c particles with N_h not necessarily equal to N_c. These numbers of particles are linked together by the total number of grains injected in the box $N = N_{\rm cl} + N_c + N_h$. However, within our strongly dilute granular gases (see fig. 3), only a part $n_h < N_h$ and $n_c < N_c$ of the particles are close enough to the vibrating walls to collide with them. These grains carry momentum towards the cluster. One has

$$\begin{cases} \Delta p_h = n_h m A_h \omega, \\ \Delta p_c = n_c m A_c \omega. \end{cases} \tag{5}$$

Considering that the cluster's position is perturbed by δ, we can find an equation giving the momentum rate received by the cluster as a function of δ. Momentum rates out of equilibrium can be decomposed into two parts corresponding to the oscillating plates:

$$\begin{cases} \dfrac{\Delta p_h}{\Delta t_h} = \dfrac{n_h(z^*_{\rm cl}+\delta)m(A_h\omega)^2}{(L-e)/(1+a)+\delta}, \\ \dfrac{\Delta p_c}{\Delta t_c} = -\dfrac{n_c(z^*_{\rm cl}+\delta)m(A_c\omega)^2}{(L-e)a/(1+a)-\delta}. \end{cases} \tag{6}$$

In order to solve eq. (6), one has to evaluate the number of grains carrying momentums from the hot and the cold plates. Assuming that both hot and cold gases are uniformly distributed along the z-axis, $n_h(z^*_{\rm cl}+\delta)$ and $n_c(z^*_{\rm cl}+\delta)$ are given by

$$\begin{cases} n_h(z^*_{\rm cl}+\delta) = \dfrac{N_h A_h}{(L-e)/(1+a)+\delta}, \\ n_c(z^*_{\rm cl}+\delta) = \dfrac{N_c a A_h}{(L-e)a/(1+a)-\delta}. \end{cases} \tag{7}$$

From eqs. (6) and (7), the total force that acts on the cluster as a function of the perturbation δ is defined as

$$\begin{aligned} F(z^*_{\rm cl}+\delta) = & \frac{N_h A_h^3 m\omega^2}{\left((L-e)/(1+a)+\delta\right)^2} \\ & - \frac{N_c A_c^3 m\omega^2}{\left((L-e)a/(1+a)-\delta\right)^2}. \end{aligned} \tag{8}$$

In order to find a theoretical value for the cluster's oscillation frequency, we linearized the force $F(z^*_{\rm cl}+\delta)$ around the point $z^*_{\rm cl}$. This linearization leads finally to

$$F(z^*_{\rm cl}+\delta) \approx -\frac{2(1+a)^3 A_h^3 m(N_h+N_c)\omega^2}{(L-e)^3}\delta. \qquad (9)$$

The equation giving the evolution of the perturbation δ is then reduced to a harmonic oscillator with a typical pulsation

$$\omega_{\rm cl} = \left(\frac{A_c+A_h}{L-e}\right)^{3/2}\left(2\frac{N-N_{\rm cl}}{N_{\rm cl}}\right)^{1/2}\omega. \qquad (10)$$

This pulsation is only function of a single free parameter which is the number of grains contained in the cluster. As a consequence, eq. (10) gives the natural frequency of the cluster even for symmetric energy injection. Moreover, the mass of the cluster could be evaluated by measuring this pulsation. Measures of $\omega_{\rm cl}$ for different amplitude ratios were performed with a Fast Fourier Transform (FFT) algorithm and plotted on fig. 5. The data are fitted with the free fitting parameter $N_{\rm cl}$ using eq. (10) and are in good agreement with the model except for small values of a for which the oscillations of the cluster are too weak to be detected by the algorithm. A remarkable feature is that the fitting number of particles in the cluster was found to be equal to $N_{\rm cl} \approx 1860$ for all campaigns. This result means that the dilute gases are composed of approximatively 140 grains, as observed in many simulations.

As seen from eqs. (4) and (10), the phase shift between the hot and cold plates should have neither influence on the equilibrium position nor on the pulsation of the cluster. These results are expected because the models are both based on a momentum balance over one period of oscillation. If the driving amplitudes and frequencies are fixed, the average momentums transmitted to the system remain the same regardless of the phase shift. The fourth campaign that was devoted to the phase shift influence has confirmed this fact.

Finally, notice that such oscillations of granular materials have been recently reproduced numerically under gravity by Rivas *et al.* [28]. The authors have performed simulations of a vibrated granular medium composed of particles confined in a quasi–one-dimensional system. In this case, low-frequency oscillations of the media have been observed. If the behaviors are similar, some differences have to be highlighted. First, Rivas *et al.* have been able to describe theoretically their observations with a continuum model. In our work, the granular gases observed are so dilute that this way is not relevant. Secondly, the authors have seen that when more energy is injected, the frequency of cluster oscillations becomes smaller. We observed exactly the inverse. The simplest explication is found in the nature of the movements observed. In the gravitational open environment of the authors, the energy given to the cluster determines its parabolic flight, which increases with the initial energy of the body. The time of flight of the cluster increases also with the initial energy injected. It is not the case in our closed system under microgravity where the cluster adopts a straight and uniform motion. The time to cross a determined distance is then so small that the kinetic energy of the moving cluster is intense. Surprisingly, the existence of a periodic collective motion is not only observed under gravity field but also in microgravity environment, although the nature of these motions are different.

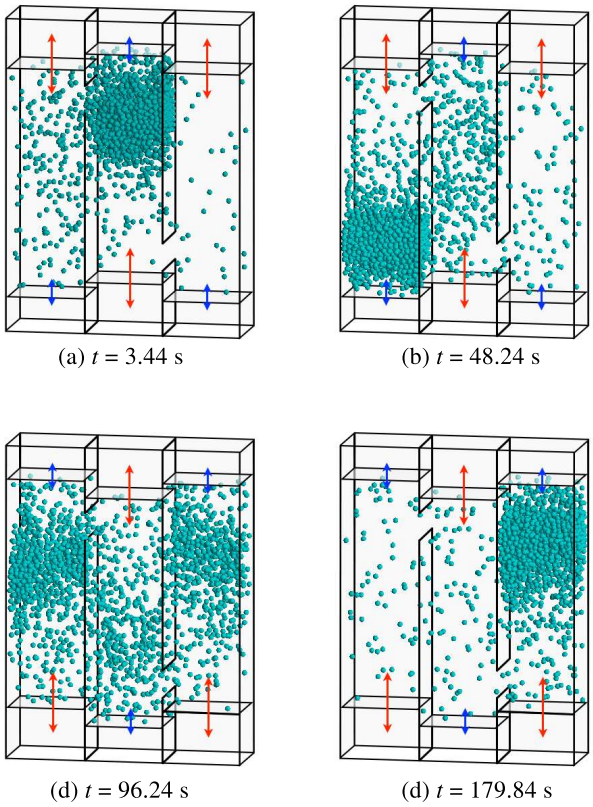

Fig. 6. Snapshots of a directed-grains simulation. The simulation starts with all the grains in the central cell (a). The amplitude condition in this one drives the cluster in front of the first slit, while in the first cell the amplitude ratio is inverted in order to drive the incoming cluster at the bottom of the cell. After a while, most of the grains are trapped at the bottom of the first cell (b). Then, after 60 s of simulation, the amplitude ratios are inverted in all cells in order to drive the cluster from the left to the right box. No intermediate cluster is observed in the central cell (c) but the grains directly gather in the right one (d).

6 Application to granular transport

The above results suggest that it is possible to create and control grain displacements in microgravity. In order to prove this concept, we propose a system inspired by Maxwell's demon [23,29] and granular ratchets [30–33] for generating granular transport in low-gravity environment. Several cells with independent pistons are placed in a row. Specific apertures at different heights allow a granular exchange between neighboring cells. By controlling the amplitude ratio of the independent pistons it is possible to drive the cluster in a selected cell. Figure 6

shows a simulation of a directed-grains experiment. Three boxes are placed together and connected with two slits placed at different heights. The simulation starts with all the grains in the central cell (fig. 6a). The amplitude condition in the central cell drives the cluster in front of the first slit, while in the first cell the amplitude ratio is inverted in order to drive the incoming cluster at the bottom of the cell. After a while, most of the grains are trapped at the bottom of the first cell (fig. 6b). Then, the amplitude ratios are inverted in all cells in order to drive the cluster from the left to the right cell. Note that no intermediate cluster is observed in the central cell (fig. 6c) but that the grains directly gather in the right cell (fig. 6d). We performed different simulations with different numbers of cells and similar behaviors have been found. By inverting the amplitude ratios, the granular transport is reversible.

7 Conclusion

In this paper, a study of the behavior of a dynamical cluster of grains excited by an asymmetric constraint was performed with the help of Molecular Dynamics. A model was developed in order to link both cluster's position and cluster's oscillations to both hot and cold amplitudes. The natural frequency of a dynamical cluster has been emphasized and could be used to estimate the mass of the cluster. The model provides a way to produce granular transport as checked in our simulations.

This work has been supported by Prodex (Belspo, Brussels) and the European Space Agency program TT VIPGRAN SpaceGrains. The authors thank the T-REX Morecar project (Feder, Wallonia) for supporting the development of the numerical model.

References

1. I. Goldhirsch, G. Zanetti, Phys. Rev. Lett. **70**, 1619 (1993).
2. A. Kudrolli, M. Wolpert, J.P. Gollub, Phys. Rev. Lett. **78**, 1383 (1997).
3. C.C. Maaß, N. Isert, G. Maret, C.M. Aegerter, Phys. Rev. Lett. **100**, 248001 (2008).
4. M. Hou, R. Liu, G. Zhai, Z. Sun, K. Lu, Y. Garrabos, P. Evesque, Microgravity Sci. Technol. **20**, 73 (2008).
5. E. Falcon, R. Wunenburger, P. Evesque, S. Fauve, C. Chabot, Y. Garrabos, D. Beysens, Phys. Rev. Lett. **83**, 440 (1999).
6. E. Falcon, S. Aumaître, P. Evesque, F. Palencia, C. Lecoutre-Chabot, S. Fauve, D. Beysens, Y. Garrabos, Europhys. Lett. **74**, 830 (2006).
7. E. Falcon, J.-C. Bacri, C. Laroche, EPL **103**, 64004 (2013).
8. J.S. Olafsen, J.S. Urbach, Phys. Rev. E **60**, R2468 (1999).
9. N.V. Brilliantov, T. Poschel, Europhys. Lett. **74**, 424 (2006).
10. J. Javier Brey, F. Moreno, R. Garcia-Rojo, M.J. Ruiz-Montero, Phys. Rev. E **65**, 011305 (2001).
11. T. Zhou, Phys. Rev. Lett. **80**, 3755 (1998).
12. Y. Li, M. Hou, P. Evesque, J. Phys. Conf. Ser. **327**, 012034 (2011).
13. E. Opsomer, F. Ludewig, N. Vandewalle, Phys. Rev. E **84**, 051306 (2011).
14. E. Opsomer, F. Ludewig, N. Vandewalle, EPL **99**, 40001 (2012).
15. Y. Grasselli, G. Bossis, G. Goutallier, EPL **86**, 60007 (2009).
16. S. Aumaître, J. Farago, S. Fauve, S. Mc Namara, Eur. Phys. J. B **42**, 255 (2004).
17. S. Mc Namara, E. Falcon, in *Lectures Notes in Physics*, Vol. **624**, edited by T. Pöschel, N.V. Brilliantov (Springer, Berlin, 2003) pp. 347–366.
18. European Space Agency's VIPGRAN project, URL: `http://www.spacegrains.org/`.
19. P.A. Cundall, O.D.L. Strack, Geotechnique **29**, 47 (1979).
20. F. Ludewig, N. Vandewalle, Phys. Rev. E **85**, 051307 (2012).
21. F. Ludewig, S. Dorbolo, T. Gilet, N. Vandewalle, EPL **84**, 44001 (2008).
22. N. Taberlet, PhD Thesis, University of Rennes (2005).
23. E. Opsomer, M. Noirhomme, N. Vandewalle, F. Ludewig, Phys. Rev. E **88**, 012202 (2013).
24. E.L. Grossman, Tong Zhou, E. Ben-Naim, Phys. Rev. E **55**, 4200 (1997).
25. E. Khain, B. Meerson, Europhys. Lett. **65**, 193 (2004).
26. A. Kudrolli, J. Henry, Phys. Rev. E **62**, R1489 (1999).
27. F. Rouiller, N. Menon, Phys. Rev. Lett. **85**, 3676 (2000).
28. N. Rivas, S. Luding, A.R. Thornton, New J. Phys. **15**, 113043 (2013).
29. J. Eggers, Phys. Rev. Lett. **83**, 5322 (1999).
30. D. van der Meer, K. van der Weele, P. Reimann, Phys. Rev. E **73**, 061304 (2006).
31. R. Liu, Y. Li, M. Hou, Phys. Rev. E **79**, 052301 (2009).
32. M. Hou, Y. Li, R. Liu, Y. Zhang, K. Lu, Phys. Status Solidi A **207**, 2739 (2010).
33. D. van der Meer, P. Reimann, K. van der Weele, D. Lohse, Phys. Rev. Lett. **92**, 184301 (2004).

5.4 Segregation

We showed in the section 3.2.1 that clustering could appear as long as the particles are quite small compared to the size of the system (see Eq. (3.6)). The natural question that arises from this observation is what happens when two species of grain are mixed? On Earth, a mixture of particles of different sizes that is undergoing a vertical vibration can present the separation of both species [66]. This effect is called Brazil Nut Effect (BNE) and depends directly on the value of the gravitational acceleration [67], which tends to bring the whole pile back to the ground. If there are two different species in terms of size or density (i.e. of the same size but of different composition), spectacular effects such as the granular clock can appear [68–71]. In this experiment, the mixture of both species is placed in a compartmentalized box which is vibrated vertically. Depending on the intensity of the vibration, Mikkelsen *et al.* found that all grains could gather in one compartment, one species after another, before leaving this compartment to join the other, always one after the other. The phenomenon is repeated periodically in time.

In this last part, we tried to find out more about the gas-cluster transition in the VIP-Gran experiment when two species of particles are mixed. We also tried to define the structure of a possible cluster that would appear in the system and tried to see if the mixture influences this structure. The numerical results of the simulations as well as the experimental results obtained during the PFC 64 are presented in the last two articles of this work.

5.4.1 Numerical simulations

The setup we chose for this study is the 3D cell of the VIP-Gran experiment. We decided to set the length L and to vary only the number of particles of both species, denoted N_s and N_l. Before actually simulating the experience that would be achieved in the VIP-Gran instrument, where bronze particles of different diameters were mixed, we first wanted to decouple the effects of mass and size. In fact, a bronze grain that has a doubled diameter compared to another sees not only its volume but also its mass multiplied by 8. So we studied three different types of mixtures: a mixture of particles (A) of the same size but of different masses, (B) of different sizes but of the same mass and (C) different sizes and masses. A sketch of the setup is given in Fig. 5.8, where two species of same density are colored in blue (large) and green (small).

5.4.1.1 Main results

In the first series of simulations (A), we showed that increasing the number of particles in the system had two simultaneous effects. First, at small filling of the cell, a gas composed of two perfectly mixed species was observed. Then, by increasing the filling, we observed the appearance of a cluster, but not a cluster formed by the mixture of both species. Indeed, only the heavier grains gathered in the center of the system, surrounded by a gas formed by light particles. Clustering took place at

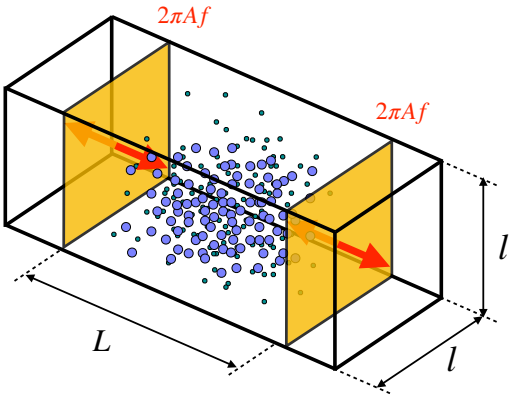

Figure 5.8: Sketch of the 3D cell of the VIP-Gran instrument. The width and depth are always equal to $l = 30$ mm and the length L is kept constant at 40 mm. Two species of particles consisting of N_s small (in green) and N_l large (in blue) grains are enclosed in the cell. The pistons have a constant amplitude and frequency $A = 5$ mm and $f = 10$ Hz.

the same time as a clear segregation between the different species. In the second series (B), where the particles had the same mass, we also observed at low filling a gas formed of both mixed species. On the other hand, by increasing the number of grains in the system, we have this time highlighted that the emerging cluster consisted of small particles, surrounded by larger ones. In both series (A) and (B), the phenomenon of segregation can be explained by a minimization of the total kinetic energy of the system. It is clear that the system will have the least energy when collisions are favored (large balls in the gas) and when the heavier particles are slowed down (they therefore condense in the cluster).

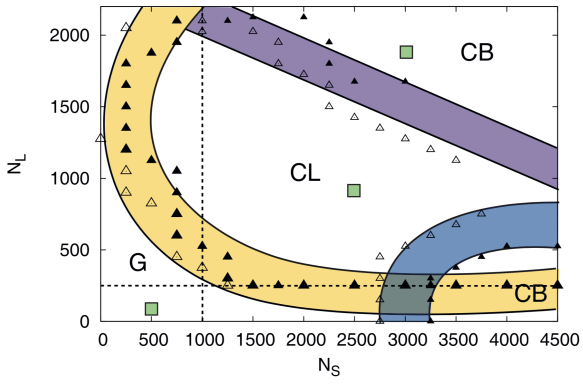

Figure 5.9: (Taken from [52]) Phase diagram (Ns, Nl) obtained through a statistical test performed on the distributions of the positions of both species of particles in the case of the simulation series (C). The different gaseous (G) and cluster (CL and CB) states are observed.

Finally, when the effects of mass and size are mixed (C), a competition between both phenomena starts. If the filling of the cell is rather low, a gas formed of both species is always present in the system. On the other hand, the cluster which appears when the number of grains increases does not have the same structure according to the filling in the different types of grains. We observed as well a cluster of heavy particles surrounded by a gas of light grains (the effects of mass take the upper hand), than a cluster of small grains trapped between two stripes of large particles, all again surrounded by a gas of small grains. The state of the system (gaseous or cluster) could be determined by the same statistical test as that used in the section 3.3.1, from the distributions of the positions of the grains along the axis of excitation. These different observed dynamics have been reported in a phase diagram which is presented in Fig. 5.9 (taken from [52]).

5.4.2 Experimental evidence of the segregation

In order to clearly see the segregation that may appear, we decided to work with the quasi-two dimensional cell. The sketch of the experiment is given in Fig. 5.10. The cell was filled with N_s grains of diameter $R_s = 0.5$ mm and N_l grains of diameter $R_l = 1$ mm, all of bronze. With the data of the numerical simulations previously carried out, we varied the numbers of particles in the different species in the intervals $N_s \in \{0; 500; 1000\}$ and $N_l \in \{80; 230\}$. The experiment was conducted during PFC 64 in April 2016.

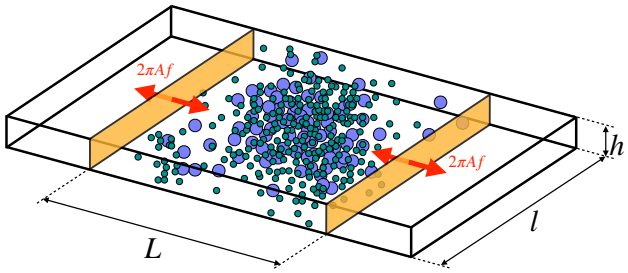

Figure 5.10: Sketch of the 2D cell of the VIP-Gran instrument. The width, the depth and the length are equal to $l = 30$ mm, $h = 5$ mm and $L = 45$ mm. Two species of particles consisting of N_s small (in green) and N_l large (in blue) grains are enclosed in the cell. The pistons have a constant amplitude and frequency $A = 3$ mm and $f = 20$ Hz.

5.4.2.1 Main results

As predicted by our simulations, the different granular gas regimes, cluster of large particles, and cluster composed of both species were observed during the PFC. Images of these different states are shown in Fig. 5.11, where the corresponding simulations are also confronted with the experimental results. Everything fits perfectly.

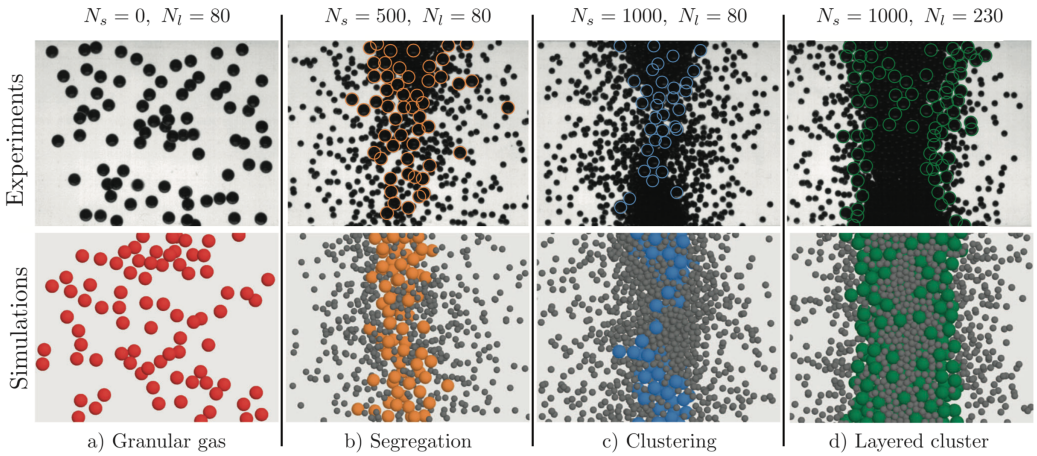

Figure 5.11: (Taken from [53]) Top: Pictures of the segregation experiment taken during the PFC 64. Bottom: corresponding numerical simulations. The different granular regimes predicted by the simulations are observed, i.e., a granular gas (a), a cluster made of large particles (b), a cluster made of both species (c) and a layered cluster (d).

5.4.3 Summary

Depending on the size and the nature of the particles interacting with each other, we have shown through these numerical and experimental studies that the observed cluster could adopt different structures. Indeed, the cluster is composed of the heaviest particles if the mixture is made of different species of equal sizes or it is composed of the smaller particles if the mixture is made of different species of equal masses. When the effects of size and mass are entangled, a competition begins and a "sandwich" structure can appear. The cluster's structure is therefore directly influenced by the composition of the mixture and a segregation between the different species is always observed once the cluster has emerged. The emerging clustering criterion developed in Sec. 3.2 could be modified taking into account the mixture of two species and we could deduce the phase diagram giving the state of the system. All the numerical results were finally verified experimentally during the parabolic flight campaign 64.

Eur. Phys. J. E (2014) **37**: 115
DOI 10.1140/epje/i2014-14115-1

THE EUROPEAN PHYSICAL JOURNAL E

Regular Article

Clustering and segregation in driven granular fluids

E. Opsomer[a], N. Vandewalle, M. Noirhomme, and F. Ludewig

GRASP, Physics Department B5a, University of Liège, B-4000-Liège, Belgium

Received 24 June 2014 and Received in final form 29 September 2014
Published online: 24 November 2014 –

Abstract. In microgravity, the successive inelastic collisions in a granular gas can lead to a dynamical clustering of the particles. This transition depends on the filling fraction of the system, the restitution of the used materials and on the size of the particles. We report simulations of driven bi-disperse gas made of small and large spheres. The size as well as the mass difference imply a strong modification in the kinematic chain of collisions and therefore alter significantly the formation of a cluster. Moreover, the different dynamical behaviors can also lead to a demixing of the system, adding a few small particles in a gas of large ones can lead to a partial clustering of the taller type. We realized a detailed phase diagram recovering the encountered regimes and developed a theoretical model predicting the possibility of dynamical clustering in binary systems.

1 Introduction

Granular materials present a large diversity of spectacular phenomena [1,2]. Compaction [3–5], arch formation [6–8] and non-Newtonian behaviors [9, 10] are only a few examples. When energy is continuously injected into a system containing granular material, the latter is fluidized and presents a gas-like behavior that has been studied intensively during the last decades [11–13] as well as in two- [14–17] and in three-dimensional systems [18–20]. However, the granular gas is different from a classical gas: velocities do not follow a Maxwell-Boltzmann distribution [21–25] and the usual thermodynamical gas models cannot be applied directly [26, 27]. Being a paradigm of dissipative systems, driven granular media tend to dissipate the mechanically injected energy through multiple inelastic collisions. Eventually, the system "cools down" locally and dense regions of low mobility appear. These regions are the result of the energetic equilibrium in the system and are the signature of a stationary regime known as dynamical clustering [28,29]. The formation of such dynamical clusters can be linked to three essential factors: the restitution coefficient ε, the packing fraction ϕ and the particle radius R in regards to the typical length scale δ of the system. Our previous work [30] presented a theoretical model, based on these parameters, that gives an accurate criterion for the upcoming of the phenomenon.

Since the size of the driven particles has a fundamental impact on the dynamics of the system, it is of wide interest to study the behavior of driven polydisperse granular materials. Indeed, the chains of collisions that typically occur when the pistons inject energy into the system are dramatically modified. A large grain could collide simultaneously several smaller ones and so be slowed down considerably. Moreover, the difference of mass between particles leads to a more complex transfer of momentum than in the monodisperse case. The geometric characteristics of the particles could also lead to segregation phenomena. For instance, shaking vertically a container filled with grains of different sizes generates an uprise of the large bodies. This demixing, commonly called the Brazil Nut Effect, has been studied intensively [31–33] and recent research [34] has investigated the impact of gravity on the phenomenon. Note that mass differences can also create similar effects [35]. In order to study this wide field of behaviors presented by driven granular materials, the European Space Agency (ESA) has programmed a series of experiments in complete weightlessness, called SpaceGrains [36] that will take place in a near future.

Given the fundamental interest and the need of predictive results, we decided to explore numerically the complex dynamics of driven bidisperse granular media in the frame of a particular experimental cell. We analyze the impact of size and mass variations between particles on the dynamics of the system. Dynamical clustering is observed and the theoretical gas-cluster transition curve for monodisperse media [30] could be adapted. Finally, complex segregation phenomena appear for diverse sets of parameters. Our results are promising and contribute to a deeper comprehension of the clustering. Moreover they provide ways to manipulate the granular media and to sort out particles within the frame of SpaceGrains or other later space missions.

2 Numerical approach

We choose to simulate an experimental setup of ESA's future SpaceGrains experiment that is dedicated to the

[a] e-mail: eric.opsomer@ulg.ac.be

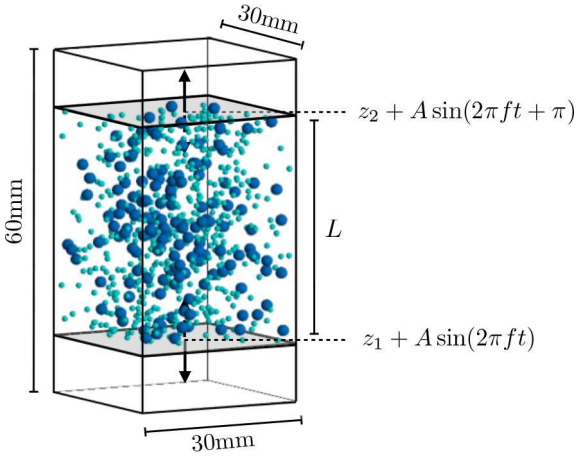

Fig. 1. (Color online) Sketch of ESA's SpaceGrains cell. Particles are enclosed in a $60 \times 30 \times 30\,\mathrm{mm}^3$ box. Two pistons are oscillating in phase opposition with an amplitude $A = 5\,\mathrm{mm}$ and a frequency $f = 10\,\mathrm{Hz}$ around their respective positions z_1 and z_2. The average distance between the pistons $L = |z_2 - z_1|$ is fixed to 40 mm.

study of convection and segregation. For this purpose, a binary mixture of spherical particles is enclosed in a cell of dimensions $60 \times 30 \times 30\,\mathrm{mm}^3$, as represented in fig. 1. To ensure the driving of the granular material, two pistons are oscillating in phase opposition with an amplitude A and a frequency f around their positions of equilibrium z_1 and z_2. We define the origin of the z-axis at the center of the cell, in the middel of $|z_1 z_2|$. The distance L between z_1 and z_2 can be tuned in order to modify the accessible volume of the system but will be fixed to 40 mm in our case. The width of the cell is noted l and is 30 mm.

Our simulations rely on a Molecular Dynamics (MD) algorithm. This numerical model is broadly used in the simulation of granular materials [37,38] and has been validated through the two last decades. The normal forces are evaluated via a linear spring-dashpot model. Dissipation is taken into account by viscous forces that are function of the normal velocity of the contact point and the restitution coefficient ε. It is to note that we use the same value of ε for both, grain-grain and grain-wall collisions. The tangent forces are bounded according to Coulomb's law and depend on the relative tangent velocities as well as the coefficient of friction μ between the colliding solids. Further details are given in previous works [19, 30] and a complete description of this MD approach is given by Taberlet [39].

3 Mass and size effects

In the SpaceGrains experiment, the granular media is composed by two types of bronze spheres with respective radii of 0.5 and 1 mm. It is important to note that this difference in size between the particles also induces a difference in mass. Accordingly, the observed effects while driving the mixture cannot be linked properly to either one of those parameters. In order to study their individual influence we work with three particular setups (A, B, C) involving four different types of grains. Each type is described in table 1 and will be referred to in the latter by its corresponding symbol or number. In order to observe and to detail first phenomena, we investigated the system for fillings N ranging between 500 and 4000 grains. In each simulation, the granular material is composed by two particle types of equal concentration and is driven during 10 seconds. Note that for all runs, we fixed the values of $\varepsilon = 0.9$ and $\mu = 0.7$.

Table 1. Parameters for the different simulated particle types. Symbols are given according to the results presented in following figures. The forth column describes in which study the concerned species is implied.

Type	r (mm)	ρ (kg/dm^3)	Setup	Symbol
1	0.5	2.5	A	∘
2	0.5	8	A,B,C	•
3	1.0	1	B	○
4	1.0	8	C	●

The presence of dynamical clustering and segregation in the system can be highlighted by the Probability Density Function (PDF) of the positions of the grains. On the one hand, gas-like systems present distributions close to uniform laws since the granular material is spread evenly through the entire cell. On the other hand, the distributions of each particle type can be compared one to another in order to detect a demixing of the system. A summary of the encountered behaviors is given in fig. 2 that presents the results for the setups A, B and C for $N \in [1000, 4000]$ according to the symbols in table 1. Depending on the components of the granular mixture and the number of particles, different dynamical behaviors are reported:

3.1 Setup A: Grains of same sizes but different masses

When a mixture of granular types 1 and 2 is driven, several dynamics can be encountered depending on the filling of the system. Indeed, by analyzing the distributions of both species, severe differences appear as one can note in the top row of fig. 2. For a diluted case, both distributions are typical for a system in a gas regime since particles can be found everywhere in the system with roughly the same probability. In denser cases, one can assist to a migration of the heavy grains towards the center of the cell. Accordingly, their distribution is much more peaked about 0 than for the light particles. A similar phenomenon is encountered in rotating drums where the denser particles travel to the core of the system [35]. This behavior simply corresponds to a minimization of the kinematic energy in the systems. Please note that the segregation goes hand in hand with the formation of a dynamical cluster of heavy particles that coexists with a granular gas of light ones.

3.2 Setup B: Grains of same masses but different sizes

By considering the difference of density between the particles of type 2 and 3, mass will play no more role in the

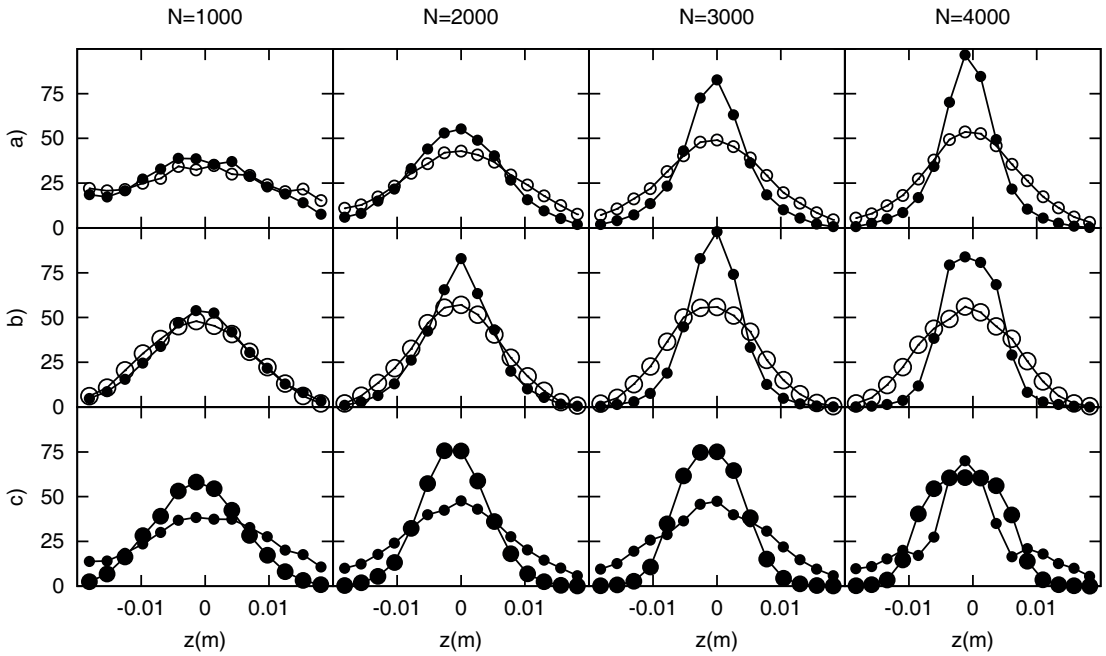

Fig. 2. Particle Density Function for the three presented driven mixtures of granular material. Large dots stand for large particles and filled dots for heavy ones. a) For grains of identical size, heavy particles gather in the central part of the cell and form a cluster once the filling is high enough. b) If both particle types are of identical mass, increasing N leads to a cluster of small grains. c) If mass and size are different, one can observe the gathering of the large particles as well as a particular clustering of both species for large N.

grain-grain interactions and only geometric parameters as cross section and volume will influence the dynamics of the system. Like in case A, the distribution of both particle types depend on N as presented in the central row of fig. 2. For low fillings, both curves are close one to another. However, they are not as horizontal as expected for a gas. This tendency to concentrate in the center of the system is the signature of the dynamical clustering effect. Indeed, since the granular type 3 has a radius that is twice as large as the radius of type 2, the global packing fraction of the system increases dramatically. Accordingly, for the same total number of grains this setup corresponds to a denser system than the first one. For larger fillings, the distribution of the small grains presents a wide peak in the central region while the large grains spread like in the gaseous case. Both particle types have segregated and one observes a dynamical cluster of small grains surrounded by a gas of large one. Once again, this is the most favorable configuration in terms of kinematic energy. Indeed, given their important cross section, the large particles are slowed down more efficiently than small ones.

3.3 Setup C: Grains of different sizes and masses

Since the particles are made of the same material, both the mass and size effects can lead to segregation. It is interesting to note that the effects presented in the setups A and B will counteract in this third version since the largest spheres are also the heaviest. We realized simulations with a mixture of particles of type 2 and 4 and the corresponding distributions are represented in the bottom row of fig. 2. Opposite to both previous cases, the dilute system presents already a slight difference in the distributions of the small and the large grains. At this state one cannot speak properly of segregation. Nevertheless, it seems that the heavy particles are more likely to be found in the central region of the cell. This behavior can be explained with regards to the setup A. Indeed, in a dilute system, the interaction between particles is low and thus the mass effects overtake the size effects. Increasing the number of particles leads to a more stressed difference between both distributions. Segregation and clustering are observed simultaneously. However, above some critical packing fraction, small particles are also likely to be found in the center of the system. Indeed, in this region, the local density is high and accordingly the size effects become important compared to the mass effects. As in setup B, this configuration leads to a gathering of the small grains in a central region. The system is finally composed of a dense cluster of small and large grains surrounded by a gas of small particles. Consequently, the system is no longer segregated.

4 Phase diagram

From now on, we will focus on the setup designed for the SpaceGrains project. The parameters of the system correspond to what has been presented in the subsection C. However, the number of small and large spheres, noted respectively N_S and N_L can be tuned independently. We

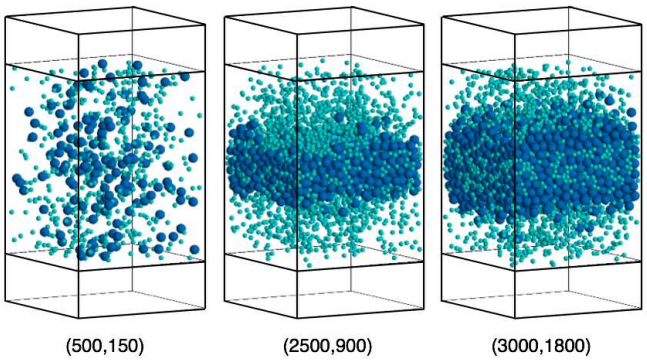

Fig. 3. (Color online) Overview of three typical regimes that are observed. From left to right on can see a gas phase (G), a cluster of only large particles (CL) and a cluster composed by both particle types (CB). Couples of numbers correspond, respectively, to N_S and N_L.

Table 2. Possible outcomes of the Kolmogorv-Smirnov test comparing the particle distributions against a uniform law. H_0: the null hypothesis cannot be refuted, the corresponding distribution is accepted as uniform. H_1: the null hypothesis is not valid, the concerned granular type presents a spatial inhomogeneity (*i.e.* clustering).

Dynamical regime	Small	Large
(G) gas phase	H_0	H_0
(CL) cluster of only large particles	H_0	H_1
(CS) cluster of only small particles	H_1	H_0
(CB) cluster of both particle types	H_1	H_1

realized 150 predictive simulations for couples (N_S, N_L) ranging in the interval $[0, 4500] \times [0, 2100]$ in order to establish a phase diagram recovering the encountered dynamics. Each simulation starts with independent initial conditions. Figure 3 gives an overview of the three typical regimes that are observed. From left to right, one can see a gas phase (G), a cluster of only large particles (CL) and a cluster composed by both particle types (CB).

The detection of each regime can be realized via two Kolmogorov-Smirnov (KS) tests [19], evaluating the uniformity of the distributions of small and large grains along the z-axis of the system. Both granular types are tested separately starting with a null hypothesis H_0 of uniformity that correspond to the gas regime. If H_0 is rejected, what we note H_1, the system can no longer be considered to be homogeneously distributed and is qualified as clustered. In addition to this statistical criterion, we also impose a minimum size of one granular layer to a cluster. This last condition verified, table 2 summarizes any possible outcome of the tests.

Applying the above detection method to all our simulations allows us to define the frontiers between the encountered dynamical regimes and to place them on a (N_S, N_L) phase diagram. Figure 4 describes with small (respectively, large) triangles the detected transition points relative to

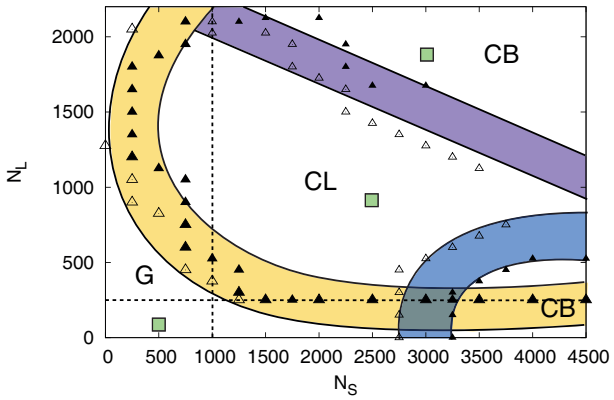

Fig. 4. (Color online) Phase diagram describing the different dynamical regimes of the system. Shaded frontier zones recover the transition points that are detected according to our statistical and geometrical criteria. Dashed lines give the minimum cluster sizes. Simulations corresponding to fig. 3 are represented by grey (green) squares.

the clustering of the small (respectively, large) particles. Dashed lines give the minimum cluster sizes, hollow triangles correspond to a KS test with a level of significance $\alpha = 0.05$ and filled to $\alpha = 0.01$. Taking account of the dispersion of these points, three transition zones can be obtained. Consequently, the diagram is divided into four subsections corresponding to the different regimes of the system. G is found in the lower left corner of the diagram. CL is present for wide ranges in the centre of the diagram. However, in our configuration, it cannot exist in a pure system so that the presence of small particles is necessary. On the contrary, CS is only present in a pure small grains system for $N_S > 3250$. Finally, CB comes up even twice. The upper part corresponds to a cluster of large particles surrounding a cluster of small ones whereas the lower part consists in a cluster of mainly small grains containing locally some large ones. The grey (green) squares correspond to the simulations presented in fig. 3. A closer look at this diagram highlights two intriguing transitions. Starting with a small number of large particles and adding more and more small ones into the cell will lead to a dynamical clustering of the large grains. Accordingly, injecting gaseous, hot, granular material into the system will cool it down. Starting with a pure cluster of small particles and adding large ones has the opposite effect. First, both granular types contribute to the cluster but, once enough large grains are present, most of the small ones are forced into the surrounding gas phase. In this configuration, adding cold granular material in the system will warm it up.

As mentioned in the previous section, the formation of CL leads to a demixing of the system. In order to validate this assumption, we measured the segregation intensity I_s proposed by Windows-Yule *et al.* [40] in the constraint-free zone of our system. As expected, the highest values are obtained in the region corresponding to a cluster of large particles. Considering the latest interest of international space agencies and private companies in a possible

mining of asteroid and other near-Earth objects [41][1], the understanding as well as the control of segregation in microgravity is of broad interest. Note that, opposite to traditional methods as sieving or sedimentation, we achieve to separate different grain species without the help of gravity or buoyancy.

All the transition lines presented in fig. 4 are guidelines for the eyes. Nevertheless, in the following section we develop an integrative model allowing us to describe the gas-cluster transition.

5 Modeling the transition

According to our previous work [30], the formation of a dynamical cluster is strongly linked to the balance between the energy propagation and the energy dissipation during a period of excitation. The energy injected by the pistons, stirs up the granular material and therefore fluidizes the system. On the contrary, the successive collisions between particles lead to a loss of energy and a collapse of the granular gas. Depending on which behavior is dominant, the system is rather in a gas or a cluster regime. In order to determine the impact of these different mechanics, we compared the two typical timescales of the system *i.e.* the Haff time τ_H, which characterizes the cooling of the system [42] and the energy propagation time τ_P. Given the poly-dispersity of the granular media, it was not possible for us to obtain an analytical expression for τ_P. Nevertheless, we could evaluate the edge between the gas and the cluster regime by numerical integration.

A grain that travels from one side of the cell to the other realizes on average a displacement δ. The number of collisions n that this grain will encounter can be derived from the filling of the system

$$n = \frac{N_S}{N}\left(\gamma_{SS}\eta_S + \gamma_{SL}\eta_L\right) + \frac{N_L}{N}\left(\gamma_{LS}\eta_S + \gamma_{LL}\eta_L\right), \quad (1)$$

where η_S (respectively, η_L) is the number density of the small (respectively, large) particles and $\gamma_{ij} = \pi\delta(R_i+R_j)^2$ is the effective collisional volume for a grain i colliding with a grain j. The energetic transfer through the system can then be seen as a dissipative chain reaction between $n+1$ grains and the Haff time can be defined by

$$\tau_H = \frac{2\delta}{v_0(1-\varepsilon^2)n}, \quad (2)$$

where $v_0 = 2\pi Af$ is the typical velocity of the grains. Mechanical energy coming from the pistons is also injected into the granular material via those collisions. If the energetic impulses have enough time to travel across the granular whole media and to fluidize it, the system remains in a gas-like state. In order to estimate this propagation time, we generate a random chain of $n+1$ particles in which the proportion N_S/N_L is roughly the same as in the entire system. The first particle of the chain takes off with a starting velocity v_0. Then, each collision will modify the velocity of the carried impulse by taking into account the coefficient of dissipation ε and the masses m_i and m_{i-1} of the two successive impacting grains. The following relation is obtained:

$$\tau_P = \sum_{i=0}^{n} \frac{\ell_i - cr_i}{v_i}, \quad (3)$$

where

$$v_i = v_0 \frac{m_0}{m_i}\varepsilon^i. \quad (4)$$

The corrective term cr_i, with $c = 1.654$, takes account of the finite size of the system in regards to the radius r_i of the particles [30]. The distance ℓ_i is the mean free path between the i-th and the $(i+1)$-th collisions and can be defined as follows:

$$\ell_i = r_i\delta\left(\sum_{j=0}^{n} r_j\right)^{-1}. \quad (5)$$

Note that for a mono-disperse case $\ell_i = \delta/n$ for all i.

Using the latter method a thousand times for each couple (N_S, N_L), the average timescales $\bar{\tau}_P$ and $\bar{\tau}_H$ are obtained and the transition is possible once their ratio $\tau = \bar{\tau}_P/\bar{\tau}_H > 1$. Indeed, in this configuration the system cools down faster than the granular media is fluidized and consequently a cluster is formed. The transition curve can be visualized in fig. 5 by plotting iso-τ curves on the (N_S, N_L) phase diagram. The red region corresponding to $\tau \in [1, 3]$ is in good agreement with our previous measures concerning the gas-cluster transition. Indeed, the transition points between the G regime and any cluster state, which is represented by square symbols, lay all in the predicted region. Once again hollow symbols (□) correspond to a KS test with a level of significance $\alpha = 0.05$ and filled ones (■) to $\alpha = 0.01$. The small differences and the width of the transition zone can be explained by the fact

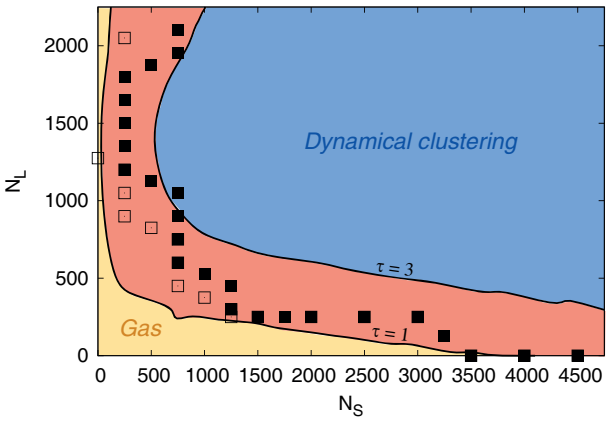

Fig. 5. (Color online) Theoretical phase diagram describing the evolution of the ratio τ using a linear color scale. The curve corresponding to $\tau =$ 1-3 is in good agreement with our measures concerning the G-CL transition.

[1] National Aeronautics and Space Administration (NASA) mission OSIRIS-REx could help to prepare mining of asteroids, `http://www.nasa.gov/content/goddard/new-nasa-mission-to-help-us-learn-how-to-mine-asteroids`.

that $\tau = 1$ is a minimum criterion based on a mean field theory meanwhile only one MD simulation was realized per (N_S, N_L) couple. Nevertheless, one can note that the model recovers the fact that CL cannot be observed in a pure system of large particles.

6 Conclusion

We investigated numerically the dynamics of a driven binary granular gas within the frame of ESA's SpaceGrains experiment. The respective effects of mass and size differences between both granular species have been highlighted through molecular dynamics simulations and could be explained by simple energetic arguments. In the case of a mixture of bronze particles, for which both effects are present, a gaseous regime as well as two different clustered states can be encountered. We realized a complex phase diagram as a function of the filling numbers N_S and N_L in which the transitions are detected via statistical uniformity tests of the particle distributions along the vertical axis. For filling parameters corresponding to the central zone, a clustering of mainly large particles can be triggered. This phenomenon leads to a demixing of the granular media and could be used in order to sort out particles in microgravity. Finally, an iterative model based on the balance between the typical times of energy propagation τ_P and energy dissipation τ_H provides a theoretical frontier between gaseous and clustered systems of any kind.

This work has been supported by Prodex (Belspo, Brussels) and the European Space Agency program TT SpaceGrains. We also thank the T-REX Morecar project (Feder, Wallonia) for supporting the development of our numerical model.

References

1. P.G. de Gennes, Rev. Mod. Phys. **71**, 374 (1999).
2. I.S. Aranson, L.S. Tsmiring, Rev. Mod. Phys. **78**, 641 (2006).
3. J.B. Knight, C.G. Fandrich, Chun Ning Lau, H.M. Jaeger, S.R. Nagel, Phys. Rev. E **51**, 3957 (1995).
4. G. Lumay, N. Vandewalle, Phys. Rev. Lett. **95**, 028002 (2005).
5. F. Ludewig, N. Vandewalle, S. Dorbolo, Granular Matter **8**, 87 (2006).
6. F. Vivanco, S. Rica, F. Melo, Granular Matter **14**, 563 (2012).
7. A. Garcimartín, I. Zuriguel, L.A. Pugnaloni, A. Janda, Phys. Rev. E **82**, 031306 (2010).
8. C. Lozano, G. Lumay, I. Zuriguel, R.C. Hidalgo, A. Garcimartín, Phys. Rev. Lett. **109**, 68001 (2012).
9. K. Hutter, K.R. Rajagopal, Continuum Mech. Thermodyn. **6**, 81 (1994).
10. F. Boyer, E. Guazzelli, O. Pouliquen, Phys. Rev. Lett. **107**, 188301 (2011).
11. I. Goldhirsch, Annu. Rev. Fluid Mech. **35**, 267 (2003).
12. T. Pöschel, N.V. Brilliantov, *Granular Gas Dynamics*, Vol. **624** (Springer, 2003).
13. F. Spahn, J. Schmidt, M. Sremcevic, Lect. Notes Phys. **557**, 507 (2000).
14. I. Goldhirsch, G. Zanetti, Phys. Rev. Lett. **70**, 1619 (1993).
15. J.S. Olafsen, J.S. Urbach, Phys. Rev. Lett. **81**, 4369 (1998).
16. J. Schockmal, E. Mersch, N. Vandewalle, G. Lumay, Phys. Rev. E **87**, 062201 (2013).
17. S. Merminod, M. Berhanu, E. Falcon, EPL **106**, 44005 (2014).
18. E. Falcon, S. Fauve, C. Laroche, Eur. Phys. J. B **9**, 183 (1999).
19. E. Opsomer, F. Ludewig, N. Vandewalle, Phys. Rev. E **84**, 051306 (2011).
20. K. Harth, U. Kornek, T. Trittel, U. Strachauer, S. Höme, K. Will, R. Stannarius, Phys. Rev. Lett. **110**, 144102 (2013).
21. S.E. Episov, T. Pöschel, J. Stat. Phys. **86**, 1385 (1997).
22. T.P.C. Van Noije, M.H. Ernst, Granular Matter **1**, 2 (1998).
23. E.L. Grossman, T. Zhou, E. BenNaim, Phys. Rev. Lett. **55**, 4200 (1997).
24. J.S. Olafsen, J.S. Urbach, Phys. Rev. E **60**, R2468 (1999).
25. A. Kudrolli, J. Henry, Phys. Rev. E **62**, R1489 (2000).
26. P. Jop, Y. Forterre, O. Pouliquen, Nature **441**, 04801 (1999).
27. J. Eggers, Phys. Rev. Lett. **83**, 5322 (1999).
28. E. Falcon, R. Wunenburger, P. Evesque, S. Fauve, C. Chabot, Y. Garrabos, D. Beysens, Phys. Rev. Lett. **83**, 2, 440 (1999).
29. S. Aumaître, J. Farago, S. Fauve, S. Mc Namara, Eur. Phys. J. B **42**, 255 (2004).
30. E. Opsomer, F. Ludewig, N. Vandewalle, EPL **99**, 40001 (2012).
31. M. E. Möbius, B.E. Lauderdale, S.R. Nagel, H.M. Jaeger, Nature **414**, 6861 (2001).
32. F. Ludewig, N. Vandewalle, Eur. Phys. J. E **18**, 4 (2005).
33. A. Kudrolli, Rep. Prog. Phys. **67**, 209 (2004).
34. C. Güttler, I. von Borstel, R. Schräpler, J. Blum Phys. Rev. E **87**, 044201 (2013).
35. J.M. Ottino, D.V. Khakhar, Annu. Rev. Fluid Mech. **32**, 55 (2000).
36. European Space Agency's SpaceGrains project, URL: `http://www.spacegrains.org/`.
37. T. Pöschel, T. Schwager, *Computational Granular Dynamics* (Springer-Verlag, Berlin, Heidelberg, 2005).
38. S. Luding, Granular Matter **10**, 235 (2008).
39. N. Taberlet, PhD Thesis, Université de Rennes I (2005).
40. C.R.K. Windows-Yule, T. Weinhart, D.J. Parker, A.R. Thornton, Phys. Rev. Lett. **112**, 098001 (2014).
41. `http://www.planetaryresources.com`.
42. C.C. Maaß, N. Insert, G. Maret, C.M. Aegerter, Phys. Rev. Lett. **100**, 248001 (2008).

npj | Microgravity

www.nature.com/npjmgrav

BRIEF COMMUNICATION OPEN

Segregation and pattern formation in dilute granular media under microgravity conditions

Eric Opsomer[1], Martial Noirhomme[1], Nicolas Vandewalle[1], Eric Falcon[2] and Simon Merminod[2]

Space exploration and exploitation face a major challenge: the handling of granular materials in low-gravity environments. Indeed, grains behave quite differently in space than on Earth, and the dissipative nature of the collisions between solid particles leads to clustering. Within poly-disperse materials, the question of segregation is highly relevant but has not been addressed so far in microgravity. From parabolic flight experiments on dilute binary granular media, we show that clustering can trigger a segregation mechanism, and we observe, for the first time, the formation of layered structures in the bulk.

npj Microgravity (2017)3:1 ; doi:10.1038/s41526-016-0009-1

During the past decades space exploration and exploitation has remained in the spotlight of the scientific community and industry. Indeed, landing probes on distant planetoids, extracting rare earth elements on asteroids and 3D printing infrastructures on the Moon is as exciting as it could be lucrative.[1] However, difficulties arise when it comes to the handling of regolith, the granular materials present on the surface of dusty celestial bodies.[2] The physical ingredients of granular physics in space are straightforward: dissipative collisions, cohesion and electrostatic interactions for fine grains. For inelastic particles, i.e. with only dissipative collisions, a clustering of the granular material can occur. The latter phenomenon has been studied in microgravity since the nineties and was observed experimentally for the first time during a sounding rocket mission.[3] Since then, many numerical and experimental studies in low gravity[4–7] were realised mainly with mono-disperse systems. However, recent numerical studies[8] indicate that the poly-dispersity of the granular media impacts strongly on its behaviour and may lead to segregation in zero g even though the usual mechanisms responsible for this phenomenon rely on the presence of gravity.

Here, we present novel experimental results from the European Space Agency's parabolic flight campaign PFC64 exhibiting spectacular pattern formation within a binary granular system under microgravity conditions. Our experiments were performed within the framework of the VIP-Gran instrument, whose setup consists in a $45 \times 30 \times 5\,\mathrm{mm}^3$ rectangular box in which two opposing walls ($30 \times 5\,\mathrm{mm}^2$) act as pistons. They oscillate sinusoidally in anti phase along the longitudinal axis (45 mm) of the box with a typical amplitude of 3 mm and a typical frequency of 20 Hz. We studied four different granular loadings composed of N_s small and N_l large bronze beads with respective diameters $d_s = 1$ mm and $d_l = 2$ mm. Both species have respective masses $m_s = 4.8$ mg and $m_l = 38.4$ mg. The restitution coefficient for the different types of collisions were not measured experimentally. However, given the low grain velocities encountered in our experiment, a value of $\varepsilon = 0.9$ can be assumed for bronze-bronze interaction[9].

The initial loading of the cell is 80 large beads; we then inject sequentially two slots of 500 small particles and a slot of 150 large ones. This leads to volume fractions ϕ between 3% and 17% corresponding to low-density regimes. The parameter ϕ is defined as follows:

$$\phi = \phi_s + \phi_l = \pi \frac{N_s d_s^3}{6V} + \pi \frac{N_l d_l^3}{6V}, \quad (1)$$

where V is the volume of the cell. While shaking the system in microgravity, four different dynamics are observed: First, the mono-disperse system exhibits typical dilute granular gas dynamics. Particles move erratically and are equally distributed everywhere in the container (Fig. 1a). After the injection of 500 small particles, clustering occurs. However, given the dissipative nature of the collisions, the large beads cool down more rapidly than the small ones and migrate toward the centre of the bulk (Fig. 1b). An analogous segregation phenomenon, relying on the gradient of granular fluctuation energy, has been observed in the case of a collisional granular shear flow.[10] If one continues to increase N_s, small particles also contribute to the cluster, but the kernel of the bulk remains mainly composed of large grains (Fig. 1c). Once the additional 150 large beads are added into the system, the structure of the bulk changes dramatically. More and more small beads contribute to the cluster and force the large ones towards the interface with the surrounding gas (Fig. 1d). Finally, the system exhibits a complex pattern constituted of successive layers with alternatively high concentrations of small and large particles. Although this particular behaviour was theoretically predicted,[11] it is the first time that such pattern is experimentally observed in microgravity.

In addition to our experiments, we realised Soft Sphere Discrete Element Method simulations of our setup and established a (ϕ_s, ϕ_l) phase diagram presented in Fig. 2. Normal contact forces are modelled via a linear spring-dashpot. Tangential friction forces are proportional to the sliding velocity and are bounded via Coulomb's criterion. For all types of contacts, the restitution coefficient is fixed to $\varepsilon = 0.9$ and the friction coefficient to $\mu = 0.4$. As described in Opsomer et al.[8] the clustering of the individual granular species can be detected via a statistical uniformity test and the frontiers between the different dynamical regimes can be drawn accordingly. Granular gas is found in the lower left corner

[1]Université de Liège, GRASP, Unité de Recherche CESAM, Liège B-4000, Belgium and [2]Université Paris Diderot, Sorbonne Paris Cité, MSC, UMR 7057 CNRS, Paris F-75013, France
Correspondence: Eric Opsomer (eric.opsomer@ulg.ac.be)

Received: 22 August 2016 Revised: 7 November 2016 Accepted: 10 November 2016
Published online: 05 January 2017

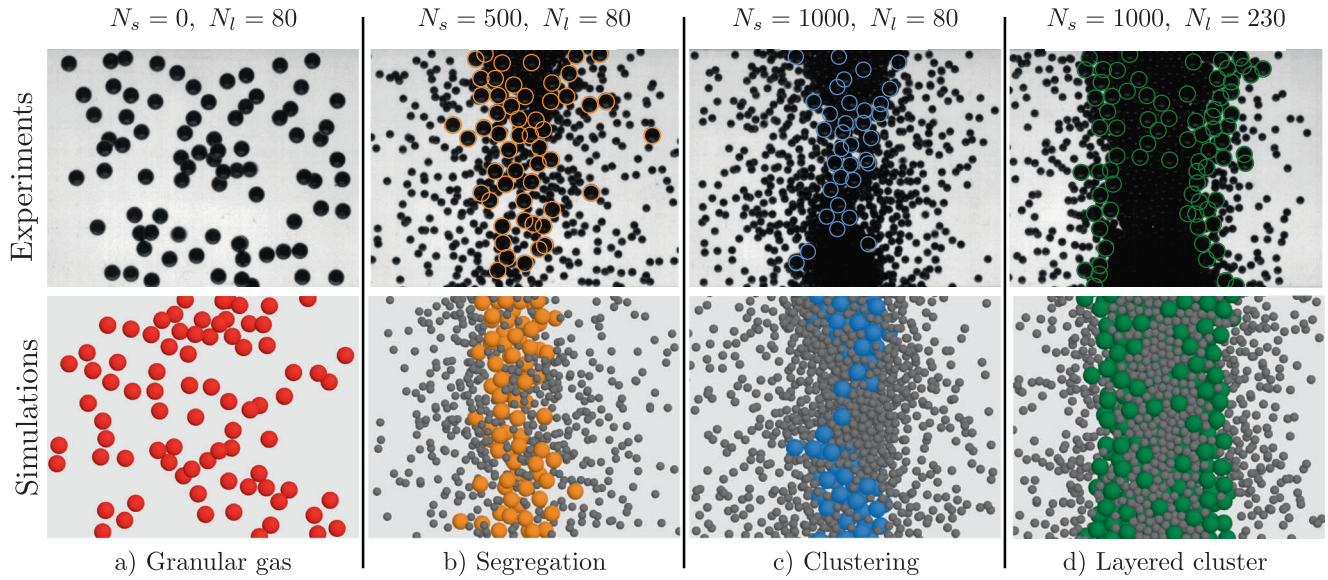

Fig. 1 Snapshots (*bottom view*) during experiments (*top*) and simulations (*bottom*). Large beads are highlighted with coloured circles. In the system with 80 (**a**) large beads, granular gas is observed. After the addition of 500 (**b**) and 1000 (**c**) small particles, segregation occurs and the large beads gather in the central bulk. Then 150 additional large grains (**d**) are injected and a complex pattern arises. The sinusoidal forcing is along the horizontal axis

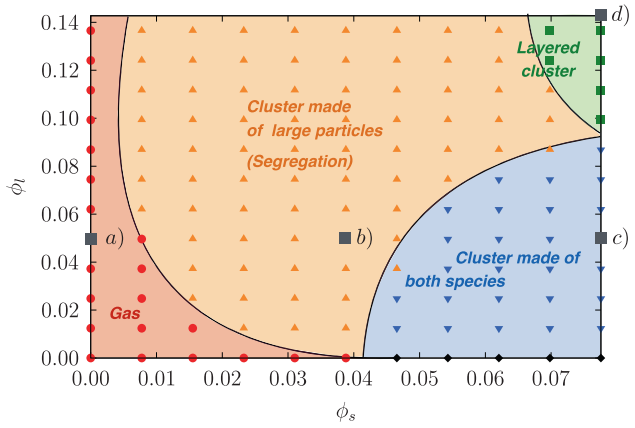

Fig. 2 Phase diagram obtained via numerical simulations by varying filling concentrations of ϕ_s and ϕ_l. Clustering of the individual species is detected using a statistical test of uniformity of the particle's positions in the cell. Different colours and symbols are used depending on the detected regime. *Solid curves* serve solely as guides. Large *square* symbols correspond to experimental conditions Fig. 1

of the diagram (red). Segregation is observed for a wide range of fillings in the central region of the diagram (orange). Clustering of both particle species is encountered for high numbers of small grains, in the lower right corner (blue). Stripy patterns can only be found for the highest filling values, in the upper right corner (green). Snapshots of all presented experiments as well as corresponding simulations are compared in Fig. 1. Large beads are highlighted with coloured circles. Filling increases from left to right and the sinusoidal driving is along the horizontal direction.

We observed, for the first time, segregation coupled to complex pattern formation in a driven binary mixture of grains under microgravity conditions. Our results are intriguing since the usual mechanisms responsible for segregation, such as convection and percolation, all rely on the presence of gravity. Our work could lead to a better understanding of the surface properties of dusty planetoids and enhance the handling and transport procedures of granular materials in space.

ACKNOWLEDGEMENTS

The authors thank L. Recanatesi, A. Pellegrini, D. Santachiara and V. Köhne for experimental support during PFC64, and O. Minster as well as D. Fischer for fruitful discussions. This work has been funded by Prodex (Belspo, Brussels) and the European Space Agency through Topical Team SpaceGrains.

COMPETING INTERESTS

The authors declare no competing interests.

REFERENCES

1 Hartmann, W. K. The shape of Kleopatra. *Science* **288**, 820–821 (2000).
2 Murdoch, N., Sanchez, P., Schwartz, S. R., & Miyamoto, H. in Asteroid Surface Geophysics (eds. Michel, P., DeMeo, F. E., & Bottke, W. F.) Asteroids IV (University of Arizona Press, 2015).
3 Falcon, E. *et al.* Cluster formation in a granular medium fluidized by vibrations in low gravity. *Phys. Rev. Lett.* **83**, 440 (1999).
4 Noirhomme, M., Opsomer, E., Vandewalle, N., & Ludewig, F. Granular transport in driven granular gas. *Eur. Phys. J. E.* **38**, 1–6 (2015).
5 Harth, K. *et al.* Granular gases of rod-shaped grains in microgravity. *Phys. Rev. Lett.* **110**, 144102 (2013).
6 Falcon, E. *et al.* Collision statistics in a dilute granular gas fluidized by vibrations in low gravity. *Europhys. Let.* **74**, 830 (2006).
7 Tatsumi, S., Murayama, Y., Hayakawa, H., & Sano, M. Experimental study on the kinetics of granular gases under microgravity. *J Fluid Mech.* **641**, 521–539 (2009).
8 Opsomer, E., Vandewalle, N., Noirhomme, M., & Ludewig, F. Clustering and segregation in driven granular fluids. *Eur. Phys. J. E.* 2014; **37**, 1–6 (2014).
9 Johnson K. L. *Contact Mechanics* (Cambridge University Press, 1987).
10 Louge, M. Y., Jenkins, J. T., Xu, H., & Arnarson, B. O. in Granular segregation in collisional shearing flows. (eds. Aref, H., & Phillips, J. W.) Mechanics for a New Millennium (Springer Netherlands, 2001).
11 Serero, D., Noskowicz, S. H., Tan, M. L., & Goldhirsch, I. Binary granular gas mixtures: theory, layering effects and some open questions. *Eur. Phys. J. Special Topics* **179**, 221–247 (2009).

Conclusion and perspectives

In this work, we have studied numerically and experimentally the clustering that can occur in excited granular systems. The numerical study was realized using a homemade SSDEM software developed in order to prepare the experiments. The latter, commissioned by the European Space Agency (ESA) under the SpaceGrains project, were carried out using the VIP-Gran-PF instrument during Parabolic Flight Campaigns (PFCs).

Our first goal, which was realized over five years, was to experimentally verify the gas-cluster frontier theoretically and numerically obtained [36] at the very beginning of the project. Five PFCs were necessary in order to reach our objective. During this study, three different dynamical regimes were observed, i.e. granular gases, clusters, and bouncing aggregates, in the images provided by the instrument. We have developed an original image processing method that allows, from the two-dimensional images, to reconstruct the three-dimensional density distributions in the system. Comparing these distributions with uniform distributions using a statistical test gave the state of the system for a wide variety of parameters. We were able to validate the phase diagram that had been previously constructed using numerical simulations [36]. Concerning the bouncing aggregate regime, which was unexpected in the VIP-Gran geometry, we modified an existing model [63] thanks to which the emergence of this regime can be predicted.

In parallel to our experimental work, we realized numerical simulations in order to study the growth of clusters. Actually, the granular gas is a relatively well known state but the dynamical cluster, as an entity, still had to be investigated. By varying the number of particles in an excited granular system, we observed different clusters of different structures. We identified these structures first by sorting the grains using a local criterion and then by studying the occupancy of the cell by the clustered particles. We defined this occupancy as the regions of the cell that are often visited by the particles belonging to the cluster. Then, the structures being identified, we turned our attention to the mean packing fraction of the gas and the cluster and showed that the mechanism behind the growth is that the gas has to maintain a constant packing fraction, similar to a kind of saturating vapor pressure in the system. We finally showed that the growth of the cluster was made on its surface by capturing gaseous grains. Unfortunately, this numerical research can not be tested experimentally since the VIP-Gran-PF instrument does not allow to take the appropriate measurements.

Another numerical study concerning the structure of clusters has been performed by mixing two different types of particles, i.e. small and large particles, within the VIP-Gran 3D cell. In this study, the impact of mass and size have been investigated and we found that a segregation between both species can occur, in one case as well

as in the other. We were able to explain the observed segregation patterns by using physical arguments, that is, minimization of the energy of the system. For a system composed of two species of the same mass but of different sizes, the loss of energy is equal for all types of collision. As a consequence, this is the collision rate that has to be the highest as possible. The collisions are promoted if the largest particles remain in the gas, leaving the small ones to agglomerate in the center of the cell. For a system composed of two species of the same size but of different masses, the loss of energy is promoted for collisions between heavy particles. As a consequence, the energetic most stable configuration is the one where the heavy particles collide frequently. The cluster is thus made of heavy particles and surrounded by a gas of light grains. If both masses and sizes are different, both configurations can be observed as a function of the fraction of each species. Finally, by modifying the model for the gas-cluster transition, we have derived a phase diagram showing all different observed regimes.

During PFC 65, we dedicated parabolas to the observation of the segregation. In order to differentiate two different species of different masses and sizes, we performed the experiment within the quasi-2D cell. All the predicted regimes were observed.

In our last numerical study, we studied the dynamics of a cluster, surrounded by an excited granular gas, all of it submitted to an asymmetrical excitation in a parallelepiped or conical cell. We investigated the position of the center of mass of the system (defined as the equilibrium position of the cluster) as well as the natural oscillations of the cluster around its equilibrium position. We developed a mathematical model, based on a momentum balance, that link together the asymmetry of the system to the equilibrium position and to the pulsation of oscillation of the cluster. The latter was found to also depend on the mass of the cluster (i.e. the number of particles it contains) and the frequency of the driving. This momentum based model is only valid for the parallelepiped box. The modeling for the cones is still under development.

We performed a lot of experiments, recording about 16 Terabytes of images, which attempt to be treated. These experiments concern the behavior of intruders in a granular gas, the behavior of a mobile wall placed in between two granular gas of different densities, the possibility of creating granular osmosis and the gas cluster transition in the case of elongated particles. Moreover, our experimental work has shown that the level of microgravity achieved in parabolic flights is not sufficient if the cooling or the convection had to be study within the VIP-Gran-PF instrument. Furthermore, we show that the initial conditions of filling could displace the gas-cluster transition. For these reasons, ESA decided to develop another version of the VIP-Gran instrument which is adapted to the International Space Station. This instrument is currently in development and will be launched in orbit in the very near future.

Bibliography

[1] H. A. Janssen, Zeitschr. d. Vereines deutscher Ingenieure **39**, 1045 (1895). (Cited on pages 3, 5 and 6.)

[2] M. Balme and R. Greeley, Rev. Geophys. **44**, RG3003 (2006). (Cited on page 3.)

[3] http://deepspaceindustries.com, 2018. (Cited on page 3.)

[4] http://planetaryresources.com, 2018. (Cited on page 3.)

[5] B. Andreotti, Y. Forterre, and O. Pouliquen, *Granular Media: Between Fluid and Solid* (Cambridge University Press, 2013). (Cited on page 4.)

[6] F. Pacheco-Vázquez, G. A. Caballero-Robledo, and J. C. Ruiz-Suárez, Phys. Rev. Lett. **102**, 170601 (2009). (Cited on pages 4 and 5.)

[7] O. Reynolds, Philos. Mag. Ser. 5 **20**, 127 (1885). (Cited on page 4.)

[8] Y. Bertho, F. Giorgiutti-Dauphiné, and J.-P. Hulin, Physics of Fluids **15**, 3358 (2003). (Cited on page 6.)

[9] K. Y. Shen and B. L. Scott, American Journal of Physics **53**, 787 (1985). (Cited on page 6.)

[10] A. Sack and T. Pöschel, American Journal of Physics **85**, 98 (2017). (Cited on page 6.)

[11] GDR MiDi, Eur. Phys. J. E **14**, 341 (2004). (Cited on page 6.)

[12] K. Kawamura, J. S. Laberg, and T. Kanamatsu, Mar. Geol. **356**, 44 (2014). (Cited on page 7.)

[13] R. Delannay, A. Valance, A. Mangeney, O. Roche, and P. Richard, J. Phys. D: Appl. Phys. **50**, 053001 (2017). (Cited on page 7.)

[14] F. Melo, P. B. Umbanhowar, and H. L. Swinney, Phys. Rev. Lett. **75**, 3838 (1995). (Cited on page 7.)

[15] H. M. Jaeger, S. R. Nagel, and R. P. Behringer, Rev. Mod. Phys. **68**, 1259 (1996). (Cited on pages 7 and 8.)

[16] L. Butzhammer, S. Völkel, I. Rehberg, and K. Huang, Phys. Rev. E **92**, 012202 (2015). (Cited on page 7.)

[17] A. Puglisi, V. Loreto, U. M. B. Marconi, A. Petri, and A. Vulpiani, Phys. Rev. Lett. **81**, 3848 (1998). (Cited on page 8.)

[18] J. J. Brey, D. Cubero, and M. J. Ruiz-Montero, Phys. Rev. E **59**, 1256 (1998). (Cited on page 8.)

[19] T. P. C. van Noije and M. H. Ernst, Gran. Mat. **1**, 57 (1998). (Cited on page 8.)

[20] J. S. Olafsen and J. S. Urbach, Phys. Rev. E **60**, R2468 (1999). (Cited on page 8.)

[21] A. Kudrolli and J. Henry, Phys. Rev. E **62**, R1489 (2000). (Cited on page 8.)

[22] F. Rouyer and N. Menon, Phys. Rev. Lett. **85**, 3676 (2000). (Cited on page 8.)

[23] S. J. Moon, J. B. Swift, and H. L. Swinney, Phys. Rev. E **69**, 011301 (2004). (Cited on page 8.)

[24] O. Herbst, P. Müller, M. Otto, and A. Zippelius, Phys. Rev. E **70**, 051313 (2004). (Cited on page 8.)

[25] G. Marty and O. Dauchot, Phys. Rev. Lett. **94**, 015701 (2005). (Cited on page 8.)

[26] P. M. Reis, R. A. Ingale, and M. D. Shattuck, Phys. Rev. E **75**, 051311 (2007). (Cited on page 8.)

[27] M. Hou *et al.*, Microgravity Sci. Technol **20**, 73 (2008). (Cited on page 8.)

[28] S. Merminod, M. Bernahu, and E. Falcon, EPL **106**, 44005 (2014). (Cited on page 8.)

[29] C. Scholz and T. Pöschel, Phys. Rev. Lett. **118**, 198003 (2017). (Cited on page 8.)

[30] K. Harth *et al.*, Phys. Rev. Lett. **110**, 144102 (2013). (Cited on page 8.)

[31] K. Harth, T. Trittel, S. Wegner, and R. Stannarius, Phys. Rev. Lett. **120**, 214301 (2018). (Cited on page 8.)

[32] P. K. Haff, J. Fluid. Mech. **134**, 401 (1983). (Cited on pages 8, 9, 13 and 36.)

[33] S. McNamara and W. R. Young, Phys. Rev. E **53**, 5089 (1996). (Cited on pages 9 and 13.)

[34] S. E. Esipov and T. Pöschel, J. Stat. Phys. **86**, 1385 (1997). (Cited on page 9.)

[35] S. Aumaître, A. Alastuey, and S. Fauve, Eur. Phys. J. B **54**, 263 (2006). (Cited on pages 9 and 17.)

[36] E. Opsomer, F. Ludewig, and N. Vandewalle, EPL **99**, 40001 (2012). (Cited on pages 10, 22, 35, 55, 57 and 99.)

[37] A. Kudrolli, M. Wolpert, and J. P. Gollub, Phys. Rev. Lett. **78**, 1383 (1997). (Cited on pages 11, 12 and 18.)

[38] E. Falcon, S. Fauve, and C. Laroche, Eur. Phys. J. B **9**, 183 (1999). (Cited on page 11.)

[39] P. Eshuis, K. van der Weele, D. van der Meer, R. Bos, and D. Lohse, Physics of Fluids **19**, 123301 (2007). (Cited on pages 11 and 12.)

[40] N. Rivas, S. Luding, and A. R. Thornton, New J. Phys. **15**, 113043 (2013). (Cited on page 12.)

[41] I. Goldhirsch and G. Zanetti, Phys. Rev. Lett. **70**, 1619 (1993). (Cited on page 13.)

[42] S. McNamara and W. R. Young, Phys. Fluids A **5**, 34 (1993). (Cited on page 13.)

[43] S. McNamara and W. R. Young, Phys. Rev. Lett. **50**, R28 (1994). (Cited on page 13.)

[44] C. C. Maaß, N. Isert, G. Maret, and C. M. Aegerter, Phys. Rev. Lett. **100**, 248001 (2008). (Cited on pages 13 and 14.)

[45] E. Falcon *et al.*, Phys. Rev. Lett. **83**, 440 (1999). (Cited on pages 14 and 35.)

[46] J. B. Knight, H. M. Jaeger, and S. R. Nagel, Phys. Rev. Lett. **70**, 3728 (1993). (Cited on page 18.)

[47] J. Earman and J. D. Norton, Stud. Hist. Philos. M. P. (2007). (Cited on page 18.)

[48] L. Brillouin, J. Appl. Phys. **22**, 334 (1951). (Cited on page 18.)

[49] J. Eggers., Phys. Rev. Lett. **83**, 25 (1999). (Cited on page 18.)

[50] E. Opsomer, M. Noirhomme, N. Vandewalle, and F. Ludewig, Phys. Rev. E **88**, 012202 (2013). (Cited on page 18.)

[51] A. Rosato, K. J. Strandburg, F. Prinz, and R. H. Swendsen, Phys. Rev. Lett. **58**, 1038 (1987). (Cited on page 19.)

[52] E.Opsomer, N.Vandewalle, M.Noirhomme, and F.Ludewig, Eur. Phys. J. E **37**, 115 (2014). (Cited on pages 19, 88 and 89.)

[53] E. Opsomer, M. Noirhomme, N. Vandewalle, S. Merminod, and E. Falcon, npj Microgravity **3**, 1 (2017). (Cited on pages 19 and 90.)

[54] D. Hestroffer *et al.*, EPJ Web of Conferences **140**, 14011 (2017). (Cited on page 19.)

[55] http://www.novespace.fr. (Cited on page 21.)

[56] M. Noirhomme *et al.*, EPL **123**, 14003 (2018). (Cited on pages 40, 41 and 55.)

[57] L.-H. Luu, G. Castillo, N. Mujica, and R. Soto, Phys. Rev. E **87**, 040202(R) (2013). (Cited on pages 55 and 56.)

[58] N. Taberlet, *Écoulements gravitaires de matériaux granulaires*, PhD thesis, Université de Rennes 1, 2005. (Cited on page 56.)

[59] F. Ludewig, *Contribution aux approches numériques de la densification d'assemblées granulaires*, PhD thesis, University of Liège, 2007. (Cited on page 56.)

[60] E. Opsomer, *Gathering and Handling of Granular Materials under Microgravity Conditions*, PhD thesis, University of Liège, 2015. (Cited on page 56.)

[61] M. Noirhomme, F. Ludewig, N. Vandewalle, and E. Opsomer, Phys. Rev. E **95**, 022905 (2017). (Cited on page 71.)

[62] M. N. Bannerman *et al.*, Phys. Rev. E **84**, 011301 (2011). (Cited on pages 71 and 73.)

[63] A. Sack, M. Heckel, J. E. Kollmer, F. Zimber, and T. Pöschel, Phys. Rev. Lett. **111**, 018001 (2013). (Cited on pages 71, 72, 73 and 99.)

[64] J. E. Kollmer, M. . Tupy, M. Heckel, A. Sack, and T. Pöschel, Phys. Rev. Appl. **3**, 024007 (2015). (Cited on pages 71 and 74.)

[65] M. Noirhomme, E. Opsomer, N. Vandewalle, and F. Ludewig, Eur. Phys. J. E **38**, 15009 (2015). (Cited on pages 74 and 75.)

[66] J. M. Ottino and D. V. Khakhar, Annu. Rev. Fluid Mech. **32**, 55 (2000). (Cited on page 87.)

[67] C. Güttler, I. von Borstel, R. Schräpler, and J. Blum, Phys. Rev. E **87**, 044201 (2013). (Cited on page 87.)

[68] R. Mikkelsen, D. van der Meer, K. van der Weele, and D. Lohse, Phys. Rev. Lett. **89**, 214301 (2002). (Cited on page 87.)

[69] M. Hou, H. Tu, R. Liu, Y. Li, and K. Lu, Phys. Rev. Lett. **100**, 068001 (2008). (Cited on page 87.)

[70] R. Liu, Y. Li, and M. Hou, Phys. Rev. E **79**, 052301 (2009). (Cited on page 87.)

[71] M. Hou, Y. Li, R. Liu, Y. Zhang, and K. Lu, Phys. Status Solidi A **207**, 2739 (2010). (Cited on page 87.)